

ANALYSIS AND PERFORMANCE PREDICTIONS
OF EVACUATED TUBULAR SOLAR COLLECTORS
USING AIR AS THE WORKING FLUID

BY

MICHAEL B. EBERLEIN

A thesis submitted in partial fulfillment of the
requirements for the degree of

MASTER OF SCIENCE
(Mechanical Engineering)

at the

UNIVERSITY OF WISCONSIN-MADISON

1976

ACKNOWLEDGEMENTS

I would like to express my appreciation and gratitude to my advisors, Professors W. A. Beckman and J. A. Duffie, for their encouragement, guidance and support. I am grateful to all my fellow graduate students at the University of Wisconsin Solar Energy Laboratory for the helpful suggestions and criticisms that they have made, particularly those of Patrick Hughes and Howard Grunes.

The financial assistance of the Wisconsin Alumni Research Foundation and of the Energy Research and Development Administration under grant E(11-1) 2588 to the University of Wisconsin-Madison is also gratefully acknowledged.

LIST OF FIGURES

<u>Figure</u>	<u>Page</u>
1.1 O-I Collector Tube Assembly	2
1.2 Collector Array and Flow Paths	3
2.1.1 Angle Ω	8
2.3.1 End View of Collector Array	13
2.8.1 F_{dA-s}	23
2.8.2 F_{p-t} , View Factor from Backing Plate to All the Tubes	25
2.8.3 F_{dA-t} vs. Position	26
2.8.4 Ratio $(F_{dA-t})/F_{p-t}$	27
2.8.5 R_B' and R_D'	30
2.8.6 Effect of D_b on R_B'	31
3.1.1 Collector Tube Cross-Section	43
3.1.2 Thermal Network Representing an Operating Collector Tube Assembly	44
3.3.1 Collector Tube Loss Network	47
3.3.2 U_L , Loss Coefficient	53
3.4.1 Modes of Air Delivery	55
3.6.1 Collector Divided into N Segments	61
3.6.2 Thermal Network Representing Linear Collec- tor Model	61
3.7.1 Air Temperature Distributions Using Different Collector Models	69

<u>Figure</u>	<u>Page</u>
3.7.2 Absorber Tube Temperatures Using Different Collector Models	70
3.7.3 Comparison Temperature Distributions When Reversing Flow	71
3.8.1 Effect of Absorber Tube Emittance on Air Temperatures	74
3.8.2 Effect of Absorber Tube Solar Absorptance on Air Temperatures	75
4.2.1 Effect of Thermal Coupling When a Liquid is Used	87
4.2.2 Effect of Delivery Tube Properties on Air Temperatures	89
4.2.3 Effect of Delivery Tube Properties on Delivery Tube Temperatures	90
5.3.1 Thermal Network When Coupling is Neglected	106
5.5.1 Tube Pair Efficiency; $\dot{m} = 15.87$ kg/hr	114
5.5.2 Tube Pair Efficiency; $\dot{m} = 6.135$ kg/hr	115
5.5.3 Tube Pair Efficiency	116
6.1.1 General Procedure for Predicting Collector Array Performance	124
6.1.2 Procedure Used for TRNSYS Simulations	126
6.2.1 Typical Air Heated Solar System	129

<u>Figure</u>	<u>Page</u>
A.1.1 Celestial Sphere	137
A.1.2 Celestial Sphere as Seen From North Pole	137
A.1.3 Coordinate System	138
A.1.4 Angle Ψ	138
A1.5a,b Projected Path of Sun on a North-South Tilted Axis	140
A2.2a,b Temperature Distribution for Different Sets of Boundary Conditions	151

LIST OF TABLES

<u>Table</u>		<u>Page</u>
3.7.1	O-I Collector Tube Dimensions, Surface Properties, Other Typical Operating Conditions and Collector Parameters	67

TABLE OF CONTENTS

	Page
Acknowledgements	i
List of Figures	ii
List of Tables	v
1. Introduction	1
2. Incident Radiation on a Collector Array	
2.1 Angular Relationships	7
2.2 Components of Solar Radiation Received by Array	10
2.3 Direct Beam Radiation	12
2.4 Reflected Beam Radiation	14
2.5 Directly Intercepted Diffuse Radiation	15
2.6 Back Reflected Diffuse Radiation	17
2.7 Converting Total Radiation on Tilted Surface to Total Radiation Intercepted by the Tubes	18
2.8 View Factors and Simplifications	21
2.9 Solar Radiation Flux on a Single Tube	33
2.10 Diameters on Which to Base Radiation Calculations	35
2.11 Conclusions and Discussion	39

	Page
3. Thermal Analysis of a Single Collector Tube	
3.1 Nomenclature Used in Thermal Analysis	41
3.2 Assumptions Made in Modeling the Collector Tube Performance	45
3.3 U_L , Collector Tube Assembly Loss Coefficient	45
3.3.1 General Expression for U_L	46
3.3.2 Numerical Results and Simplifica- tions	50
3.4 Formulation of Energy Balances	54
3.5 General Solution Procedure Used For Thermal Analysis of a Collector Tube	58
3.6 Different Methods Used to Determine the Temperature Distributions in a Collector Tube	60
3.7 Typical Temperature Distribution Predicted by the Different Collector Models	66
3.8 Effects of Surface Properties of the Absorber Tube	72
4. Determination of Important Parameters Affecting Collector Tube Performance	76
4.1 Effect of Uncertainty of Convection Coef- ficients on Collector Tube Performance	78

	Page
4.2 Effects of Delivery Tube Material and Surface Properties	85
4.3 Effects of Mass Flow Rate and Delivery Tube Diameter	93
5. Simplified Models for Use in Solar System Simulations	
5.1 Comparison of Linear Model With Analytic Model	98
5.2 Effects of Neglecting Thermal Coupling Between the Two Flow Streams	99
5.3 F_R , Collector Heat Removal Factor	103
5.4 Performance Map of Collector Efficiency	109
5.5 Graphical Results	111
5.6 Summary and Conclusions About Collector Models	118
6. Solar System Simulations Using the O-I Collector Models	
6.1 Models Used in Simulations	123
6.2 Description of System Configuration and Simulation Results	127
7. Conclusions and Recommendations	132

	Page
Appendices	
1. Derivation of Angular Relationships for an Array of Tubular Collectors	136
2. Internal Heat Transfer	145
2.1 Reduction of Differential and Algebraic Equations for General Analytic Model	145
2.2 Solutions for Different Sets of Boundary Conditions	149
2.3 Convection and Radiation Conductances	153
Bibliography	156

1. INTRODUCTION

The primary purpose of this thesis is to investigate the thermal performance of the evacuated glass tubular collectors of the type currently being manufactured by Owens-Illinois, Inc. when air is used as the working fluid.

The all glass, selectively coated evacuated tubular collector presently manufactured by Owens-Illinois is of unique design and differs significantly in its operation from the conventional flat plate solar collectors frequently used for residential heating and cooling purposes. Figure 1.1 is a diagram of a single collector tube. The individual collector element consists of two concentric cylindrical glass tubes. The outer tube, or cover tube, is transparent; the inner tube or absorber tube has a selective coating on its outer surface. The cover tube and absorber tube are sealed together at one end with the annular space between the tube evacuated to eliminate convection losses from the absorber tube. The heat transfer medium, which can be either air or a liquid, is introduced into the collector tube by the use of another tube, the delivery tube, inserted inside the absorber tube. Figure 1.2 shows how the collector tubes are usually installed. The collector tube assemblies are placed in arrays above a reflecting backing surface with the tube axes parallel

O-I
COLLECTOR TUBE ASSEMBLY
(NOT TO SCALE)

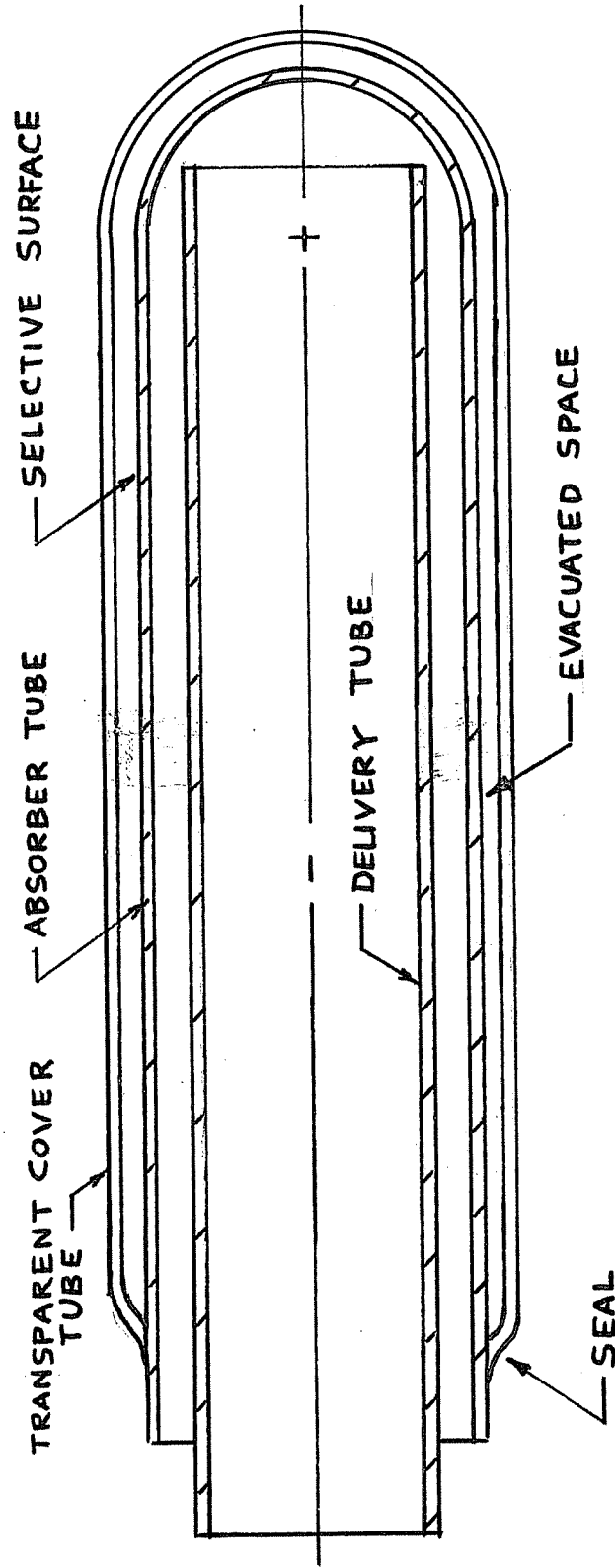


FIGURE 1.1

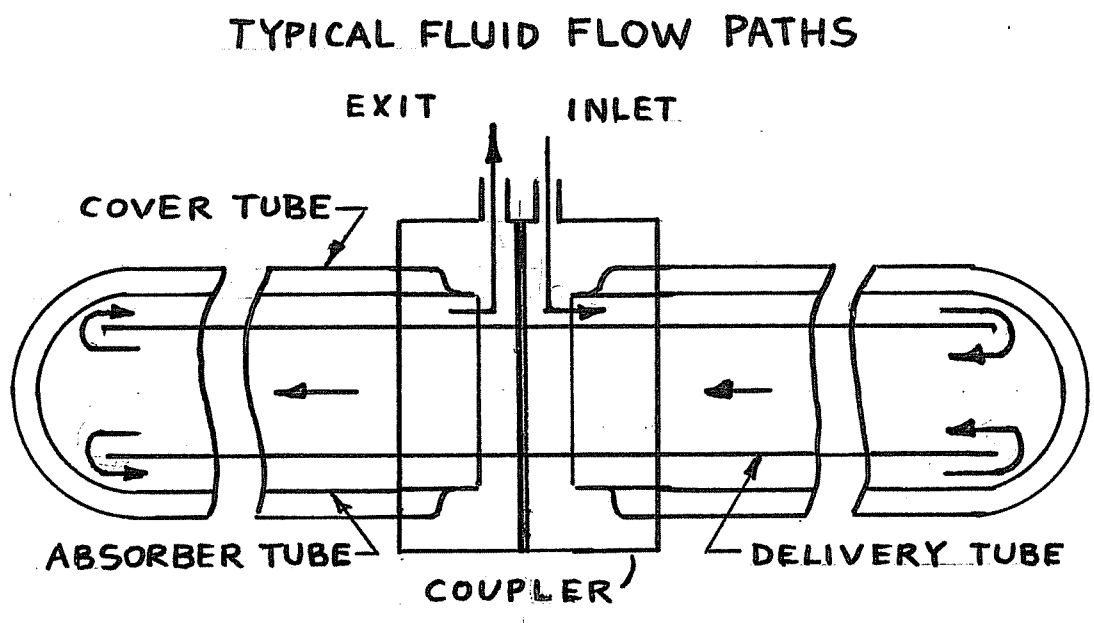
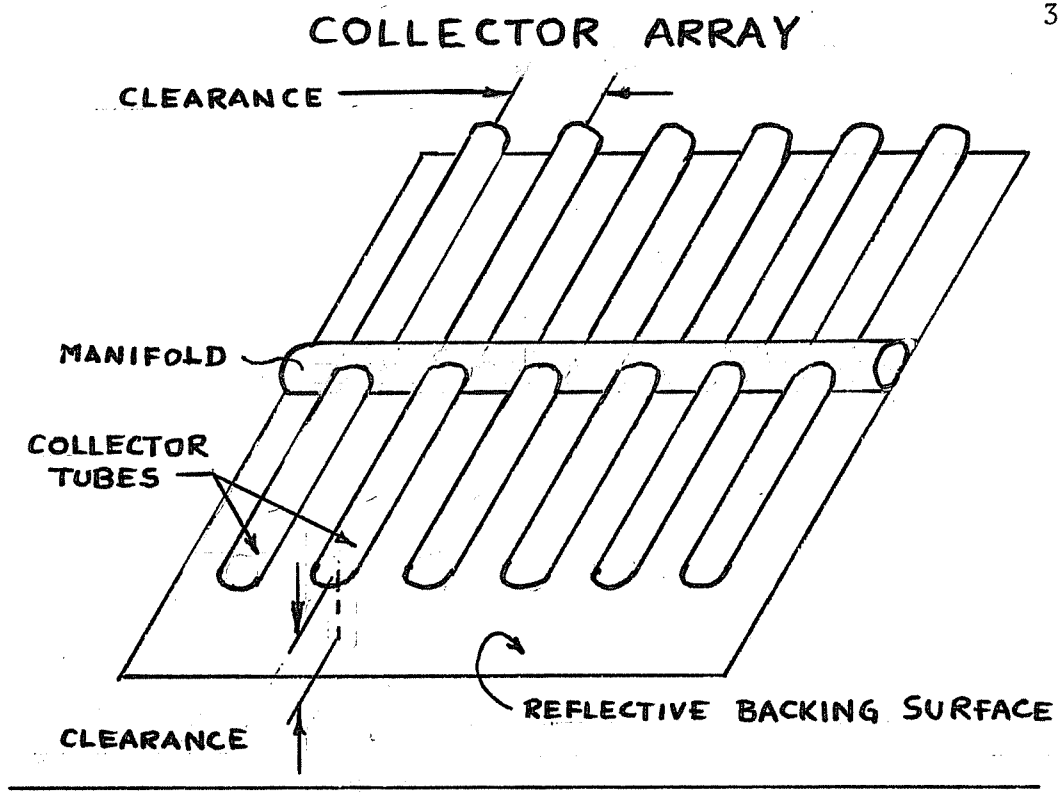


FIGURE 1.2

to each other and parallel to the surface. The collector tubes in a typical array are usually spaced apart with clearance between adjacent tubes and clearance above the backing surface. During collector array operation, solar radiation is received directly on the collector tubes, and additional radiation is also intercepted by the tubes after being reflected off the backing surface, particularly when the backing surface has a high reflectance for solar radiation. When a liquid is used as the working fluid, a single delivery tube is shared by two collector tubes that are butted together. The fluid is introduced into the annulus formed by the absorber tube and delivery tube, flows down to the end of one tube assembly, reverses directions and flows back through the delivery tube to the end of the other collector tube, again reverses direction and exits through the annulus in the second collector tube assembly.

Because this type of collector is quite new, very few design "rules of thumb" have been developed when air is used as the working fluid. Some of the possible design parameters that can affect collector array output and that will be investigated are:

1. Collector tube spacing in an array
2. Collector array orientation (i.e., collector backing surface tilt, and the tube orientation above the backing surface)

3. Methods of collector tube manifolding
4. Flow rates used in each collector tube
5. Diameter and material used for the delivery tube.

Additionally, because a numerical model of the collector array performance is needed for use in simulating the Arlington House, consideration must be given to finding simple models. This simple model is needed for long term simulations to decrease the computational effort required in predicting the performance of the total system. This requires looking closely at the internal heat transfer mechanisms in a collector tube assembly with the expectation of making simplifying assumptions about the heat transfer and bounding the possible error that results when these assumptions are made.

An analysis of the performance of a tubular collector array using a liquid as the heat transfer medium was done by Beekley and Mather [1]. Their work and the experimental results reported by Simon [2], base the collector array efficiency on the area of the backing surface above which the collector tubes are installed. The instantaneous efficiency, defined as the ratio of useful energy output of the entire array to the solar radiation on the projected backing surface area, changes as the sun's position in the sky changes during the day. Another definition of efficiency, the definition used in this work, is the ratio of the use-

ful energy output of the collector tube (or a series connected tube pair) to the total radiation incident upon the tube(s). With this new definition it is possible to separate the effects of the collector array geometry and array orientation, which determine the magnitude of the incident radiation that reaches each tube, from the thermal performance of a collector tube assembly. Separating the thermal performance from the incident radiation on each collector tube allows the independent treatment of many of the different design parameters on the total array performance that might otherwise be masked if the incident radiation and the thermal performance are investigated simultaneously, as was done in the liquid studies.

2. INCIDENT RADIATION ON A COLLECTOR ARRAY

2.1 Angular Relationships

The instantaneous solar radiation intercepted by an array of the tubular collectors mounted above a diffusely reflecting backing surface is a function of backing surface tilt, latitude, time of day, time of year, collector tube orientation, collector tube spacing, backing surface properties, and the instantaneous values of beam and diffuse radiation falling on the collector array.

It is possible to define a special incidence angle Ω , that includes the effects of declination, latitude, slope of the collector backing surface from horizontal, hour angle of the sun and rotation angle of the collector tubes from a north-south meridian projection on the collector array backing surface. Referring to Figure 2.1.1 it is seen that Ω is the projection of the sun's beam radiation measured from vertical in a plane normal to the longitudinal axes of the tubes when the tubes are parallel to the collector array backing surface. Ω is a fictitious incidence angle and is different from the actual angle of incidence of the beam radiation, θ_T , also shown in Figure 2.1.1.

It can be shown that for all orientations of collector tubes where the normal to the collector array backing surface is in the plane of the local north-south meridian (i.e., $\gamma = 0$, γ being the surface azimuth angle as defined

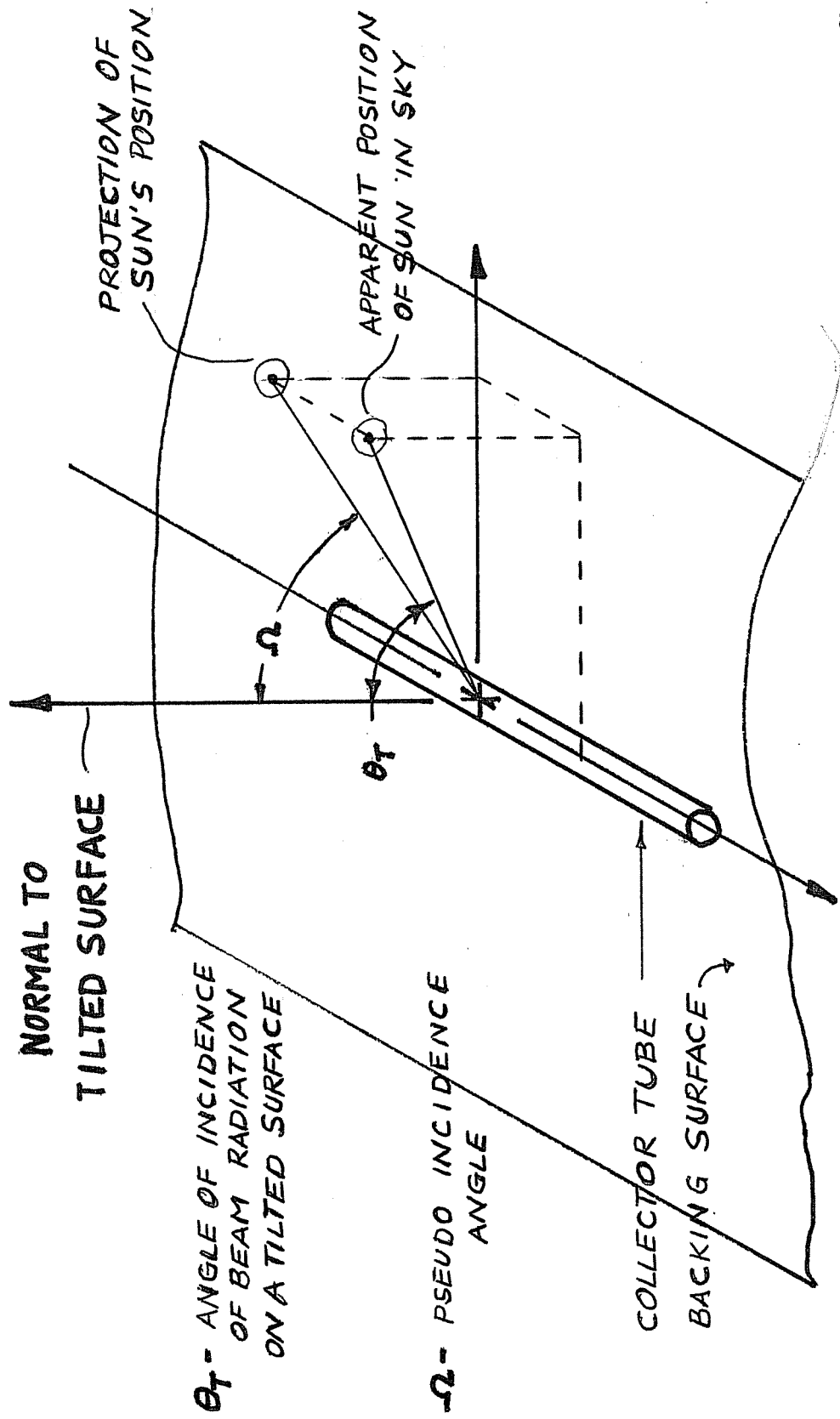


FIGURE 2.1.1

by Duffie and Beckman [3]):

$$\Omega = \tan^{-1} \left[\frac{x'}{y} \right] \quad 2.1.1$$

where $x' = \cos \delta \sin \omega \cos \Psi - \sin \Psi [\cos \delta \sin(\phi - s) \cos \omega - \cos(\phi - s) \sin \delta]$

$$y = \cos(\phi - s) \cos \delta \cos \omega + \sin(\delta - s) \sin \delta$$

δ = declination of the sun

ϕ = latitude of the collector array

s = slope of the collector backing surface from horizontal

ω = hour angle of the sun

Ψ = rotation angle of the tube axis measured counter-clockwise from the projection of the north-south meridian in the plane of the collector array backing surface (north = 0)

The relationships given in Eq 2.1.1 are derived in Appendix 1. The sign conventions for δ , s , ϕ , and ω are the same as used in Duffie and Beckman [3].

For an orientation of the tube axis along the north-south meridian projection, Ω becomes

$$\Omega = \tan^{-1} \left[\frac{\cos \delta \sin \omega}{\cos(\phi - s) \cos \delta \cos \omega + \sin(\phi - s) \sin \delta} \right] \quad 2.1.2$$

For an east-west orientation of the tube axis,

$$\Omega = \tan^{-1} \left[\frac{\cos(\phi - s) \sin \delta - \cos \delta \sin(\phi - s) \cos \omega}{\cos(\phi - s) \cos \delta \cos \omega + \sin(\phi - s) \sin \delta} \right] \quad 2.1.3$$

There are several advantages of using the angle Ω . This single angle determines the location of the illuminated "window" on the backing surface during the course of the day as the sun's apparent position in the sky changes. It will be shown that by knowing the angle Ω and the instantaneous beam and diffuse radiation falling on an unobstructed flat backing surface of the same size and orientation as the collector, it is possible to determine the total instantaneous radiation received by the collector tube array for any arbitrary tube spacing.

2.2 Components of Solar Radiation Received by a Collector Tube Array

An array of tubular collectors intercepts both beam and diffuse components of radiation; the circular symmetry of the collector tubes allows radiation to be absorbed around the entire periphery of the tube. When the collectors are installed in an array above a backing surface with a high reflectance for solar radiation, the portion of beam and diffuse radiation reflected off the backing surface and intercepted by the tubes can be a significant fraction of the total radiation absorbed by the collector tubes.

There are four different components of solar radiation that will be considered for the general cases where the

tubes are not close-packed:

1. Beam radiation directly intercepted by the tubes.
2. Beam radiation which passes between tubes and is reflected off the backing surface and is intercepted by the tubes.
3. Diffuse radiation from the sky and reflected from the ground that is directly intercepted by the tubes.
4. Diffuse radiation which passes between the tubes and is reflected off the backing screen and intercepted by the tubes.

For simplicity of analysis it will be assumed that the backing surface is an entirely diffuse reflector for solar radiation. It will also be assumed that the diffuse component of solar radiation that is available for collection is distributed uniformly across the "sky" as seen by the collector array. The tube array will be treated as if it were infinitely long and infinitely wide in comparison to a single tube diameter. By knowing the total radiation that hits the entire tube array the incident energy per tube can be found by dividing the total radiation by the number of tubes. In addition, angular dependence of the physical properties of the tube array, such as the transmittance of the glass cover tube, absorbtance of the absorber tube, reflectance of the backing screen and multiple

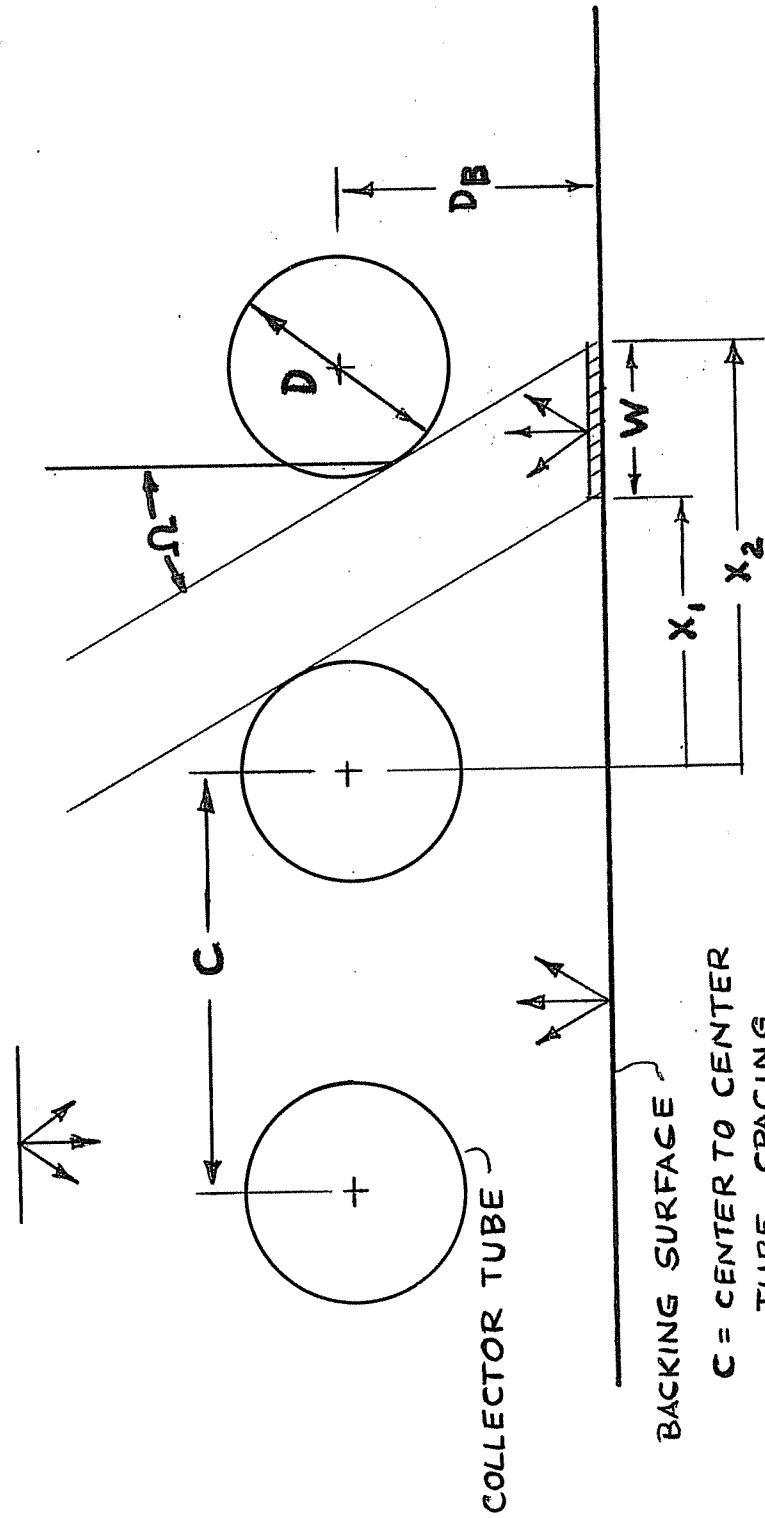
reflections of radiation components will be ignored. These are the same assumptions used by Beekley and Mather [1] and Simon [2].

2.3 Total Beam Radiation Directly Intercepted by Absorber Tubes

Using the terminology of Duffie and Beckman [3], H_B is the beam radiation intensity (energy/unit area) on a horizontal surface and R_B is the correction factor for converting beam radiation on a horizontal surface to beam radiation incident on a tilted surface. The beam radiation incident on a tilted surface is $H_B R_B$ and is incident at angle θ_T . It is convenient to define another quantity S_B where

$$S_B \cos \Omega \equiv H_B R_B \quad S_B = \frac{H_B R_B}{\cos \Omega}$$

S_B is then a fictitious solar flux in the same plane as angle Ω that gives the correct beam radiation intensity received by the tilted surface. This definition is made only for convenience as it allows both beam components to be specified in terms of the apparent incident angle Ω . Referring to Figure 2.3.1 it can be seen that the circular shape of the absorber surface presents a constant intercept area for beam radiation that is independent of sun position until



W = ILLUMINATED
STRIP WIDTH

FIGURE 2.3.1

COLLECTOR TUBE

C = CENTER TO CENTER
TUBE SPACING

D = TUBE DIAMETER

D_b = DISTANCE TO BACK

shading of one tube by its neighbor occurs. The total beam radiation intercepted by all the tubes is then:

$$S_B^{\text{DNL}} - \text{when no shading occurs} \quad 2.3.2a$$

$$S_B^{\text{CNL}} \cos \Omega - \text{when shading occurs} \quad 2.3.2b$$

When shading occurs, the beam radiation intercepted is the same as that intercepted by a flat plate of the same area as the backing surface of the tube array.

2.4 Total Beam Radiation Diffusely Reflected Off Backing Surface to the Tubes

For the times of the day when no shading of adjacent tubes occurs, some of the beam radiation passes between the tubes and strikes the backing surface, creating a uniformly illuminated strip of width W , and spanning the position coordinates from x_1 to x_2 (see Figure 2.3.1). Restricting the analysis at present to opaque cylinders with the sun at apparent incident angle Ω , if:

C = center-to-center cylinder separation

D = cylinder diameter

D_b = distance to backing surface measured from center of cylinder

then

$$W = C - \frac{D}{\cos\Omega} \quad 2.4.1$$

$$x_1 = \frac{D}{\cos\Omega} + D_b \tan\Omega \quad 2.4.2$$

$$x_2 = x_1 + W \quad 2.4.3$$

and defining

ρ_B = diffuse reflectance of the backing screen for
solar radiation

F_{w-t} = view factor from illuminated strip to all the
tubes

then the total beam radiation diffusely reflected off the
backing surface and intercepted by the tube is

$$S_D \cos\Omega W L N \rho_B F_{w-t} \quad 2.4.4$$

2.5 Total Diffuse Radiation Directly Intercepted by the Tube Array

Let S_D be the intensity of diffuse radiation assumed
uniformly distributed across the sky. The total diffuse
radiation directly intercepted by the tubes is $S_D A_s F_{s-t}$

where A_s = sky area

F_{s-t} = view factor from sky to the tubes

By reciprocity relationships:

$$A_s F_{s-t} = A_t F_{t-s}$$

where A_t = area of all tubes

F_{t-s} = view factor of one (or all) the tubes to the sky

Because each tube "sees" two other tubes, the sky and the backing surface, and assuming that the view factors from the tube to the sky and the tube to the backing surface are equal for a wide enough array we can write:

$$2F_{t-t} + 2F_{t-s} = 1$$

where F_{t-s} = view factor from one tube to the sky

$$F_{t-s} = \frac{1}{2} - F_{t-t}$$

F_{t-t} = view factor from one tube to another tube.

F_{t-t} can be evaluated directly using Hottel's crossed and uncrossed strings method [4]

$$F_{t-t} = [\sin^{-1}(\frac{D}{C}) + [(\frac{C}{D})^2 - 1]^{1/2} - \frac{C}{D}] / \pi \quad 2.5.1$$

then

$$F_{t-s} = \frac{1}{2} - \{ \sin^{-1}(\frac{D}{C}) + [(\frac{C}{D})^2 - 1]^{1/2} - \frac{C}{D} \} / \pi \quad 2.5.2$$

and the total diffuse radiation directly intercepted becomes

$$S_D \pi D N L F_{t-s} \quad 2.5.3$$

2.6 Total Diffuse Radiation Which Passes Between Tubes and is Reflected Off Backing Surface to Tubes

In general, the radiation intensity across a screen is not uniform when the tubes are diffusely illuminated from above. The total diffuse radiation reaching an incremental area dA on the backing surface is

$$S_D A_s dF_{s-dA} \quad 2.6.1$$

where A_s = sky area

dF_{s-dA} = differential view factor from sky to incremental area.

Using reciprocity relationships

$$A_s dF_{s-dA} = dA F_{dA-s}$$

where F_{dA-s} = view factor from incremental area on backing plate to the sky

because the incremental area "sees" only the sky and the tubes

$$1 - F_{dA-s} = F_{dA-t} = \text{view factor from incremental area on backing plate to all the tubes}$$

The total diffuse radiation which passes through the tubes and is reflected off the back to the tubes is

$$S_{D\rho_B} \int_{\text{back}} (F_{dA-s})(1-F_{dA-s})dA \quad 2.6.2$$

Because of equal tube spacing and view factor symmetry equation 2.6.2 can be written as

$$\text{Reflected diffuse} = S_{D\rho_B} NL \int_0^c (F_{dA-s})(1-F_{dA-s})dx \quad 2.6.3$$

2.7 Converting Total Radiation on a Tilted Surface to Total Radiation Intercepted by the Tubes

The total radiation received by all the collector tubes is the sum of the directly intercepted beam radiation, the beam reflected off the backing surface, the directly intercepted diffuse radiation and the diffuse radiation reflected off the backing surface.

Combining equations 2.3.2, 2.4.4, 2.5.3 and 2.6.3

$$S_{\text{TOTAL BEAM}} = S_B DLN + S_B \cos\Omega WLN \rho_B F_{w-t} \quad 2.7.1$$

$$S_{\text{TOTAL DIFFUSE}} = S_D \pi DNLF_{t-s} + S_D NL \rho_B \int_0^c (F_{dA-s})(1-F_{dA-s})dx \quad 2.7.2$$

The total beam radiation which hits an unobstructed flat plate of the same inclination and backing area as the tube array is $S_B \text{CNL} \cos \Omega$. The total diffuse radiation which hits an unobstructed flat plate of the same inclination and backing area as the tube array is $S_D \text{CNL}$. The ratio of the total beam radiation which is received by all the collector tubes to that received by an unobstructed flat plate of same inclination and back area as tube array is:

$$\frac{S_B \text{DLN} + S_B \cos \Omega \text{WLN} \rho_B F_{w-t}}{S_B \text{CNL} \cos \Omega} \quad \begin{array}{l} \text{(no shading)} \\ 2.7.3a \end{array}$$

When shading of adjacent tubes occurs, no beam radiation reaches the backing surface and the ratio becomes

$$\frac{S_B \text{CNL} \cos \Omega}{S_B \text{CNL} \cos \Omega} = 1 \quad \begin{array}{l} \text{(shading)} \\ 2.7.3b \end{array}$$

and similarly for the diffuse radiation the ratio becomes

$$\frac{S_D \pi \text{DNLF}_{t-s} + S_D \text{NL} \rho_B \int_0^c (F_{dA-s})(1 - F_{dA-s}) dx}{S_D \text{CNL}} \quad 2.7.4$$

It is convenient to define these two ratios as R_B' and R_D' , respectively:

R_B' \equiv total beam radiation received by the tubes
 total beam radiation incident upon an unobstructed flat plate of same backing area as array and having the same inclination as the array.

R_D' \equiv total diffuse radiation received by the tubes
 total diffuse radiation incident upon an unobstructed flat plate of same backing area as array and having the same inclination as array.

then:

$$R_B' = \frac{D + \rho_B \cos \Omega W F_{w-t}}{C \cos \Omega} \quad 2.7.5a$$

(if no shading occurs)

$$R_B' = 1 \quad (\text{when shading occurs}) \quad 2.7.5b$$

and

$$R_D' = \frac{\pi D F_{t-s} + \rho_B \int_0^c (F_{dA-s}) (1 - F_{dA-s}) dx}{C} \quad 2.7.6$$

It should be noted that when the assumption is made that the diffuse radiation is uniformly distributed across the sky, R_D' is a function only of tube array geometry and is independent of sun position and angle Ω .

2.8 View Factors and Simplifications

In order to determine the amounts of beam and diffuse radiation hitting the tubes the view factors F_{W-t} and F_{dA-s} are required. Although an analytic expression for F_{W-t} can be derived by direct application of Hottel's crossed-string method, it would require summing the view factors from an individual strip to all the tubes. Some of the tubes seen by the illuminated strip are partially obstructed by other tubes, while the view of some of the tubes is unobstructed. Calculating the view factors from a strip to the unobstructed tubes is relatively straight forward, but calculating the view factor to the partially obstructed tubes is considerably more difficult. However, F_{W-t} is the mean view factor of the area, W , to the tubes when the view factor F_{dA-t} is integrated along the strip width:

$$F_{W-t} = \frac{\int_{x_1}^{x_2} (F_{dA-t}) dx}{[x_2 - x_1]} \quad 2.8.1$$

and because $F_{dA-t} = 1 - F_{dA-s}$

$$F_{W-t} = \frac{1}{W} \int_{x_1}^{x_2} (1 - F_{dA-s}) dx \quad 2.8.2$$

The view factor, F_{dA-s} , can be obtained directly by applying Hottel's method of finding view factors from infinitesimal strips [4], a modification of the crossed and uncrossed

strings method. Although this method for evaluating F_{w-t} does not seem to be much of an improvement, because it requires an integration that usually must be done numerically rather than analytically, for many geometries of interest the view factor F_{dA-s} does not vary appreciably across the screen and F_{w-t} will be almost constant and independent of the illuminated strips position.

Figure 2.8.1 shows the view factor from a differential area on the backing screen to the sky, F_{dA-s} , for a $\frac{C}{D}$ ratio of 2.0 and different backing screen distances. It is interesting to note that as D_b , the distance from the backing screen increases, the variation in F_{dA-s} along the screen decreases and tends to approach a constant value. By implication, the variation of F_{dA-t} also decreases. Investigation of this view factor variation across the screen for different geometries shows the following:

$$\text{when } \frac{C}{D} \leq 2.0$$

and $\frac{D_b}{D} \geq 1.5$ the value of F_{dA-t} everywhere along the screen is quite close to the value of F_{p-t} , the view factor from the whole backing surface to all the tubes.

$$\text{when } \frac{C}{D} > 2.0$$

$$\frac{D_b}{C} > 0.75$$

F_{dA-S}

0.6

$\frac{C}{D} = 2.0$

0.5

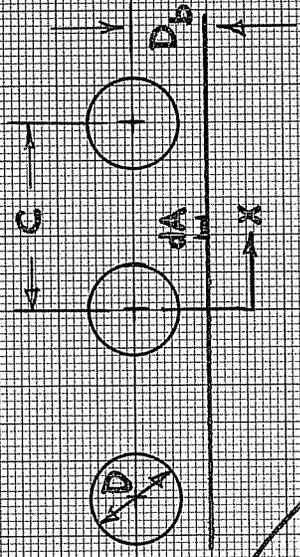
0.4

0.3

0.2

0.1

0.1
0.2
0.3



$\frac{D_b}{D} = 1.5$
 $\frac{D_b}{D} = 1.0$
 $\frac{D_b}{D} = 0.75$

0.9

0.8

0.7

0.6

0.5

0.4

0.3

0.2

0.1

0

$\frac{X}{C}$

1.0

FIGURE 2.8.1

F_{dA-t} again everywhere approaches the value of F_{p-t} .

From Hottel and Sarofim [4],

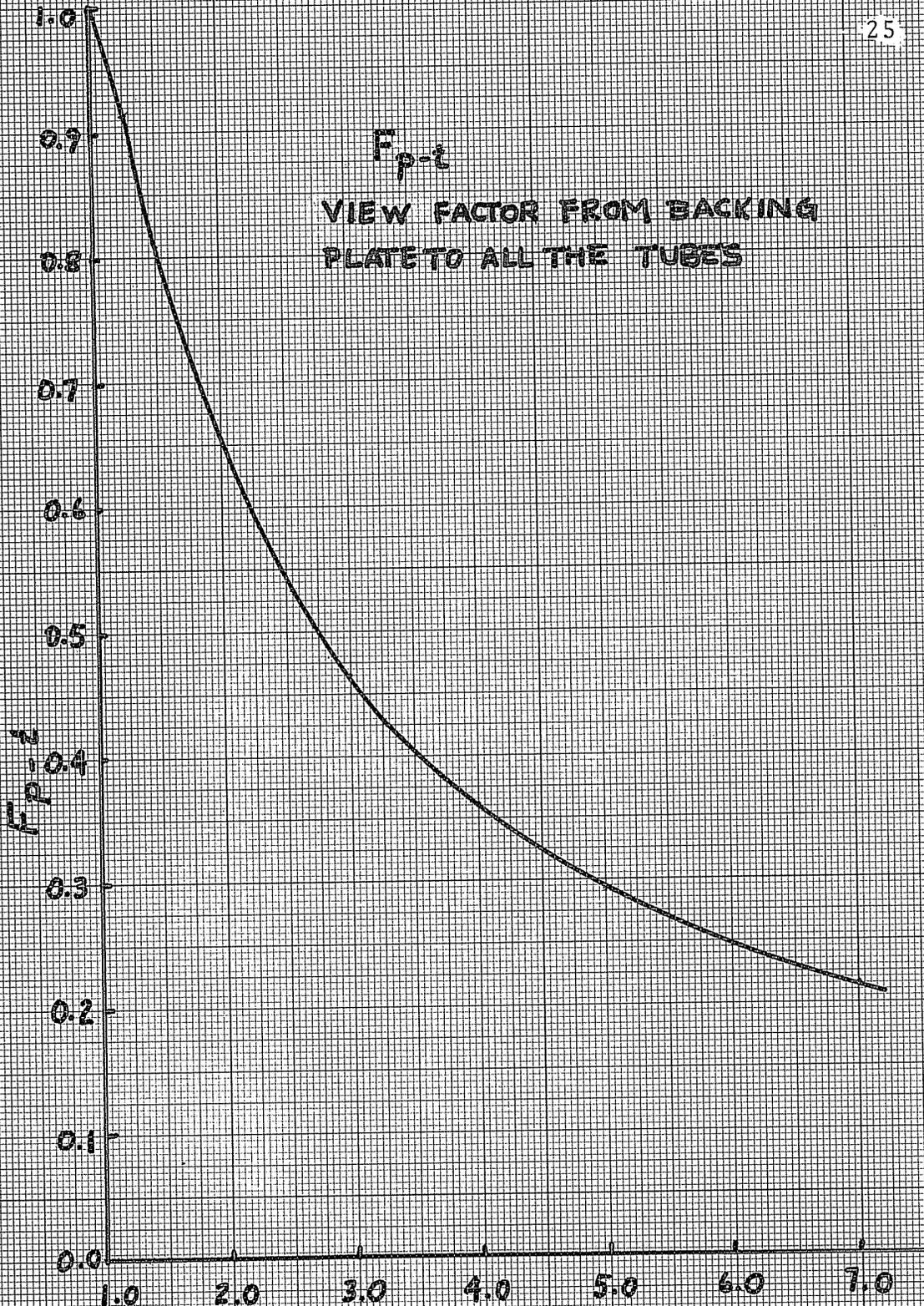
$$F_{p-t} = \frac{D}{C} \left[\pi/2 - \left(\sin^{-1} \left(\frac{D}{C} \right) + \left[\left(\frac{C}{D} \right)^2 - 1 \right]^{1/2} \frac{C}{D} \right) \right] \quad 2.8.3$$

Figure 2.8.2 shows F_{p-t} as a function of C/D . The general trend is as expected: the fraction of diffuse radiation leaving the backing surface and directly reaching the tubes decreases as C/D increases.

For a fixed distance of the absorber tubes to the back, the variation of the local view factor F_{dA-t} increases as the center-to-center distance is increased. Figures 2.8.3 and 2.8.4 show this variation. Figure 2.8.4 shows the ratio of the local view factor, F_{dA-t} to the view factor F_{p-t} , the view factor from the entire backing surface to all the tubes for different C/D ratios. It should be noted that the areas under all three curves in Figure 2.8.4 must be the same and correspond to

$$\frac{\int_0^1 F_{dA-t} d\left(\frac{x}{C}\right)}{F_{p-t}} = 1$$

This provides a good check on the accuracy of the method used for calculating the view factor F_{dA-s} , because the value of F_{p-t} can be arrived at by use of Eq. 2.8.3, a totally different application of Hottel's crossed and uncrossed string method.



F_{p-t}
VIEW FACTOR FROM BACKING
PLATE TO ALL THE TUBES

FIGURE 2.8.2

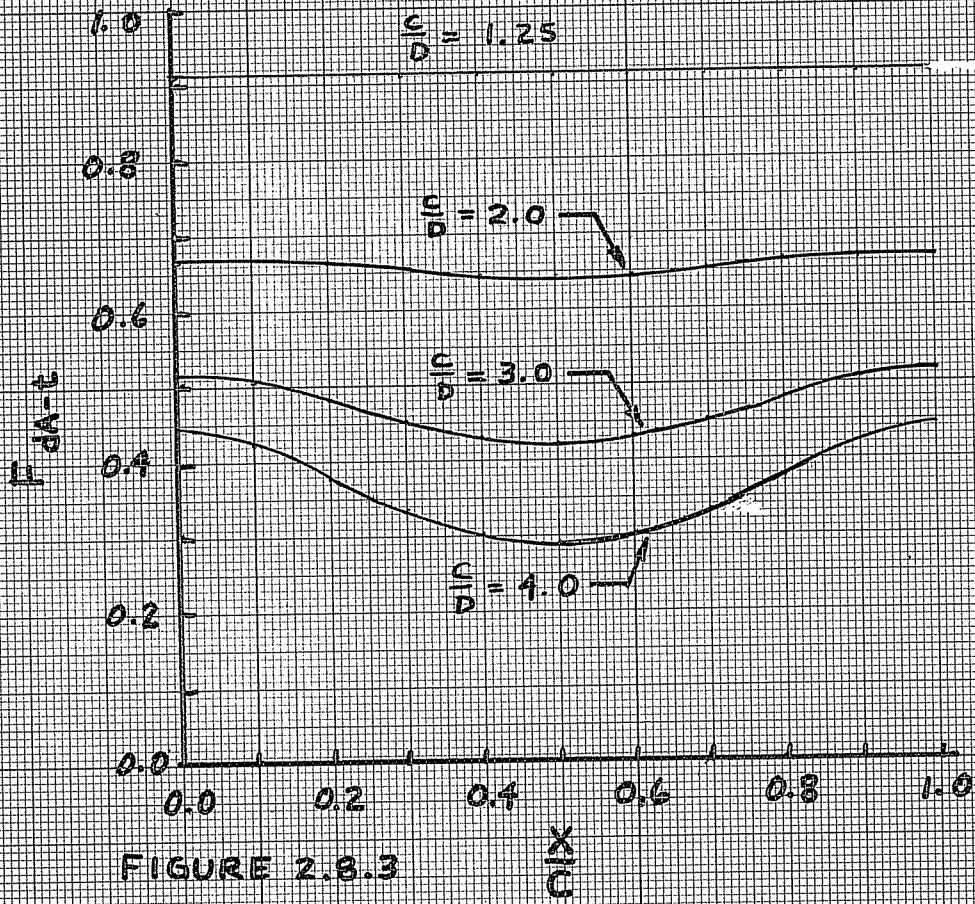
C/D

EUGENE DIETZGEN CO.
MADE IN U. S. A.

NO. 341-M DIETZGEN GRAPH PAPER
MILLIMETER

F_{dA-t} VS POSITION

$\frac{D_b}{D} = 1.5$



RATIO OF F_{QA-t} TO F_{P-t}

$$\frac{D_b}{D} = 1.5$$

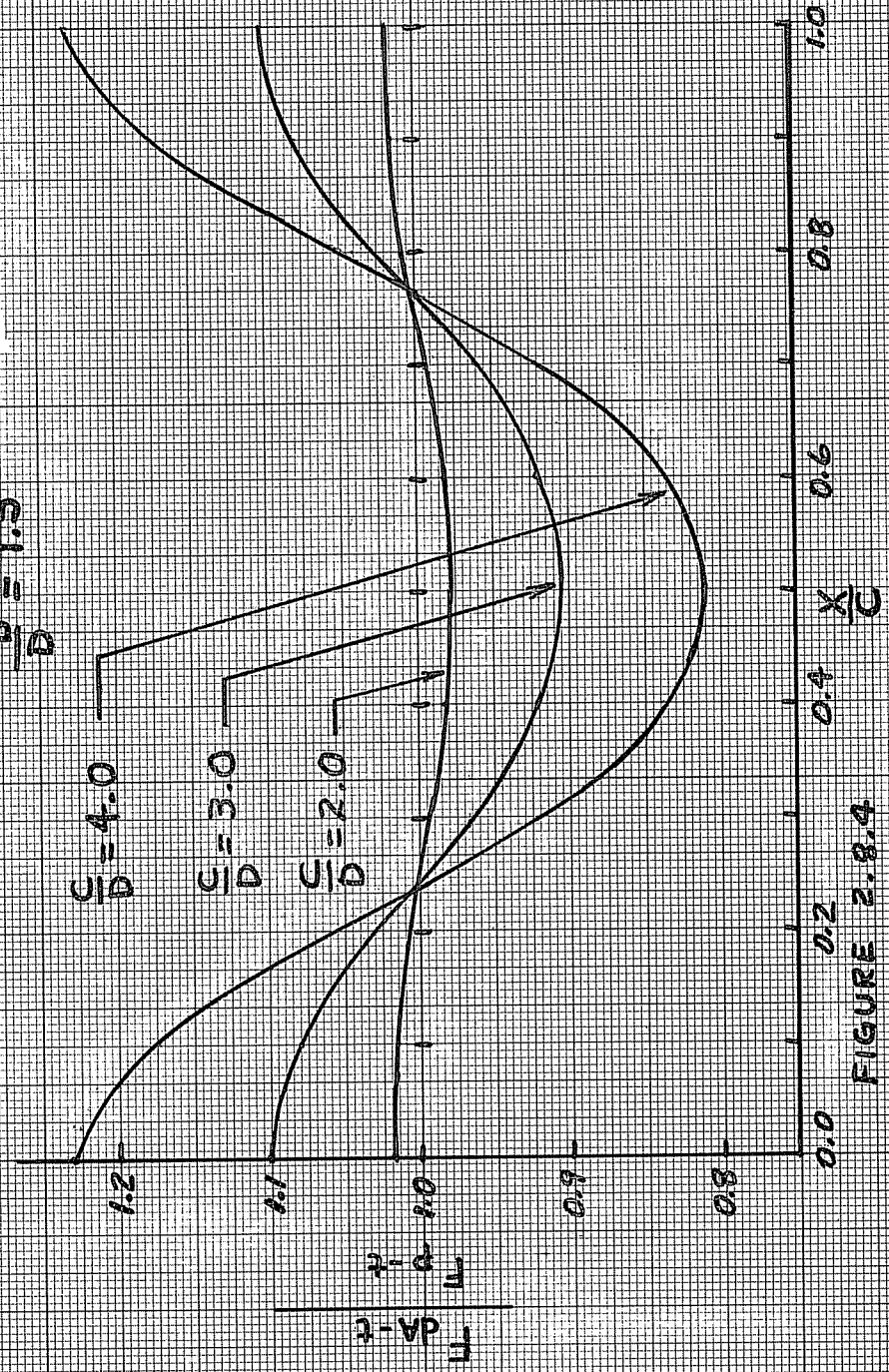


FIGURE 2.8.4

For the case of arbitrary tube geometry, the ratio R_B' is a function of the sun's position (angle Ω), which determines the location and width of the illuminated strip, and the magnitude of the local view factor F_{dA-t} integrated over the strip. R_D' is, however, independent of the sun's position (within the limits of the assumptions made), and is constant if the tube geometry is specified. For those tube spacings where the local view factor F_{dA-s} does not vary significantly with position on the backing surface, eqs. 2.7.5 and 2.7.6 can be simplified:

Replacing $\int_{x_1}^{x_2} (1 - F_{dA-s}) dx$ by $(W)(F_{p-t})$
and knowing

$$W = C - \frac{D}{\cos \Omega}$$

then

$$R_B' = \rho_B F_{p-t} \left[1 - \frac{D}{C \cos \Omega} \right] + \frac{D}{C \cos \Omega} \quad 2.8.4$$

2.7.6 can be modified in a similar fashion assuming

$$F_{t-s} = F_{t-p}; \quad \frac{A_p F_{p-t}}{A_T} = \frac{C}{\pi D} F_{p-t}$$

after rearrangement

$$R_D' = F_{p-t} [1 + \rho_B (1 - F_{p-t})] \quad 2.8.5$$

Equations 2.8.4 and 2.8.5 can be used without introducing significant error when

$$\frac{D_b}{D} \geq 1.5 \quad \text{and} \quad \frac{C}{D} \leq 2.0 \quad \text{or when}$$

$$\frac{D_b}{C} \geq 0.75 \quad \text{and} \quad \frac{C}{D} > 2.0$$

Figure 2.8.5 shows R_B' and R_D' with a fixed ratio $\frac{D_b}{D} = 1.5$ for different center-to center spacings and different angles Ω . For any specific tube spacing the value of R_B' is lowest when Ω is zero and increases with increasing Ω until R_B' becomes 1, at which time shading of adjacent tubes occurs and no direct beam radiation is received on the backing surface.

Figure 2.8.6 shows R_B' for a $\frac{C}{D}$ ratio of 5.0 with different distances from the backing surface, $\frac{D_b}{D}$, plotted against angle Ω . This graph illustrates several interesting points. Comparing the curves for $\frac{D_b}{D} = 0.5, 1.5$ and 4.0 , it is seen that for values of Ω less than 45° , decreasing the backing plate distance decreases the value of R_B' , thereby decreasing the total amount of beam radiation reaching the tubes. For any set of points where the angle Ω is constant, the strip width on the backing surface is also constant. The variation in R_B' values is then due entirely to the variation of the local view

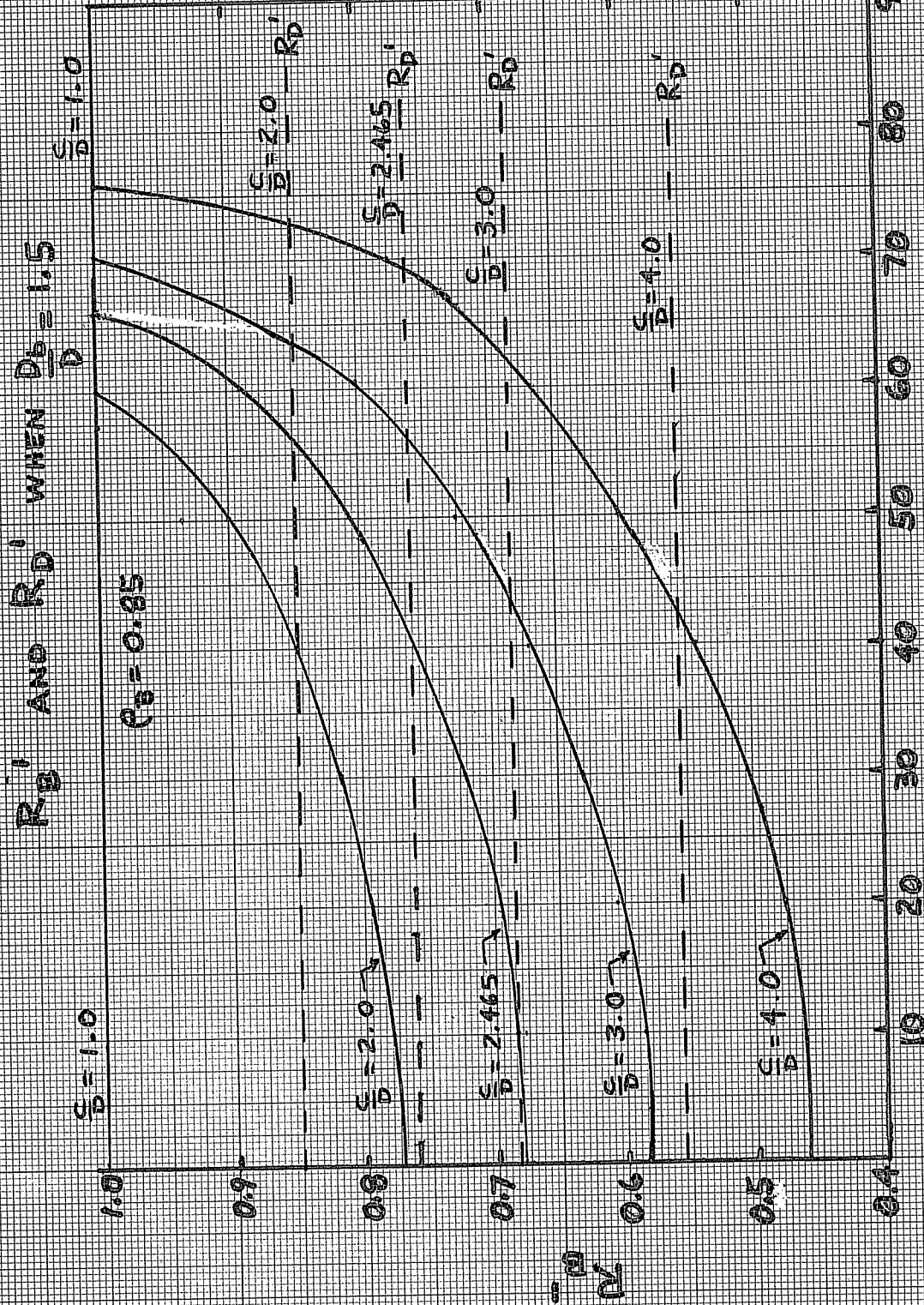


FIGURE 2.8.5 ANGLE ϕ , DEGREES

EFFECT OF DISTANCE FROM BACKING SCREEN (D_b) ON R_B'

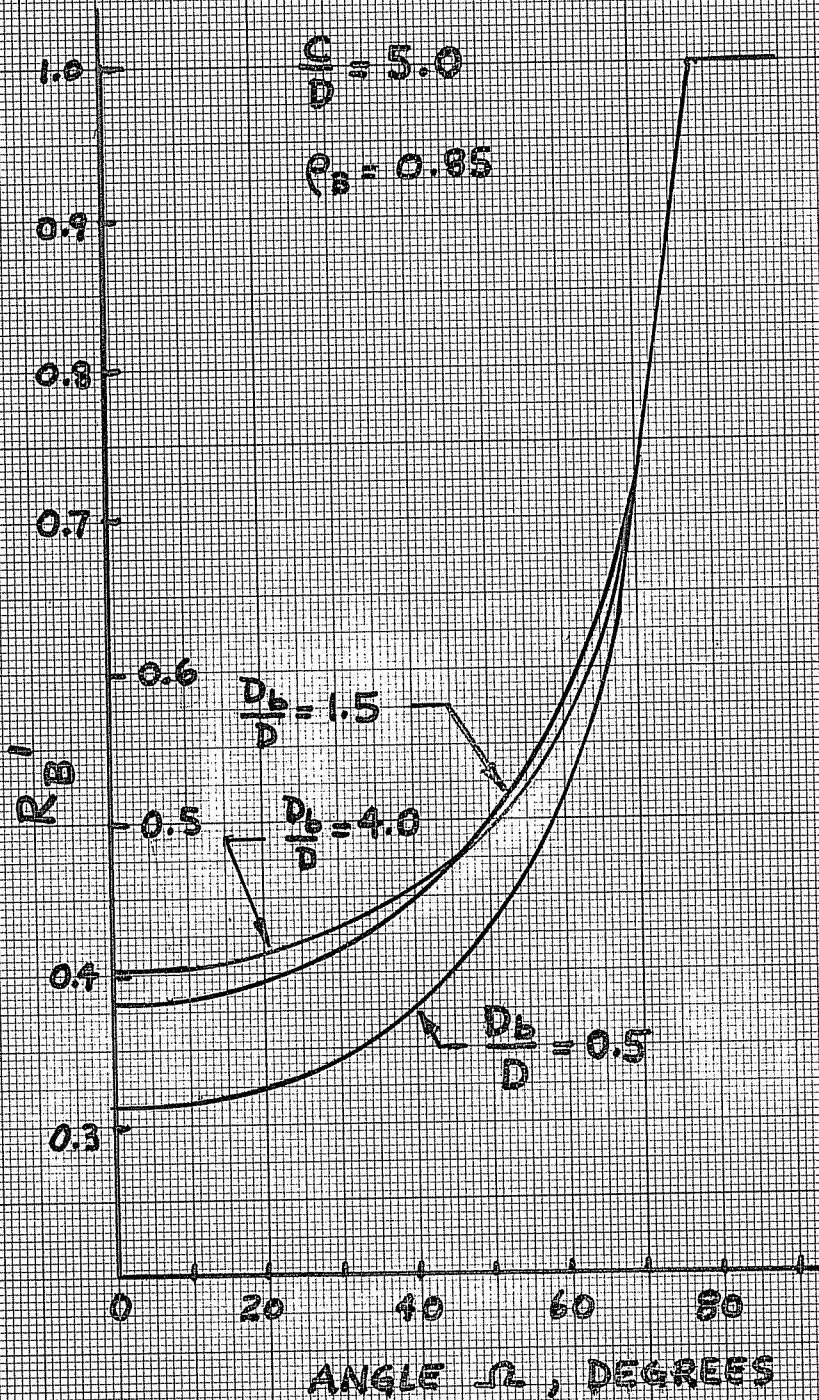


FIGURE 2.8.6

factor F_{dA-t} across the illuminated strip. Referring again to Figure 2.8.3, it can be seen that at angles Ω near zero, the illuminated strip is located between the tube centers where the local view factors F_{dA-t} and strip view factors F_{W-t} are the smallest. As Ω increases, the strip is translated sideways along the screen, and the strip view factor F_{W-t} increases as Ω increases. The ratio $\frac{D_b}{D} = 4.0$ corresponds to one of the tube spacings where the local view factor F_{dA-t} and the strip view factor, F_{W-t} , are essentially independent of strip position and constant. The characteristic shape of the R_B' curves for all tube spacings are similar to that when $\frac{D_b}{D} = 4.0$. For all tube spacings with constant view factors F_{W-t} along the screen, the variation of R_B' is due only to the change in size of the illuminated strip width W , with changing angle Ω .

2.9 Solar Radiation Flux on a Single Tube

The total radiation received by all the collector tubes is S_T , and is found from

$$S_T = [H_B R_B R_B' + H_D R R_D'] CNL \quad 2.9.1$$

where H_B is beam radiation flux on a horizontal surface
 R_B is angular conversion factor for converting beam radiation on a horizontal surface to beam radiation on a tilted surface

H_D is diffuse radiation on a horizontal surface
 and R is a correction factor for converting diffuse radiation on a horizontal surface to a tilted surface. This factor will take on different forms depending upon the distribution of diffuse radiation and to the extent which the ground reflectance is considered. (For the specific form of R see ref. 3)

If it is assumed that the solar radiation on a single tube is uniformly distributed around the perimeter, then we can define S_{eff} , the effective insolation on a single tube [energy/unit area] as:

$$S_{eff} = [H_B R_B R_B' + H_D R R_D'] \frac{C}{\pi D} \quad 2.9.2$$

Some general comments should be made about this equation. The solar flux received by a single tube in a collector array will be affected by the center-to-center tube separation distance, the distance the tubes are mounted above the backing surface, and the time distribution of the solar radiation incident upon the collector array (angle Ω). For a fixed distance of the collector tubes from the backing surface, S_{eff} will always increase as the tube separation increases. This increase does not depend upon angle Ω , but occurs because the decrease in the fraction of radiation that is reflected to each tube per unit of backing area (shown by the decrease in R_B' and R_D' with increasing tube separation for any angle Ω) is more than offset by the increase in total backing surface area that reflects beam and diffuse radiation to the tubes.

When the tube center-to-center distance is held constant, however, and the distance from the backing surface is varied, the changes in S_{eff} are dependent upon angle Ω (shown by the effect of the backing surface distance on R_B' in Figure 2.8.6). For collector arrays with the tubes oriented north-south, the maximum incident solar radiation on the backing surface occurs at the hours near solar noon (when the hour angle, ω , and the apparent incidence angle, Ω , are small). Spacing the tubes far enough above the

backing surface so that the view factor, F_{w-t} , does not vary appreciably across the backing surface, will increase R_B' for these hours, and will increase the fraction of the total radiation incident upon the array that is intercepted by the tubes. If it is desired to maximize the solar radiation received by a single tube for the times near solar noon, it is clear that this backing distance should be used. For tube orientations other than north-south, the effect of backing distance on the incident radiation per tube is a more complicated function of backing surface orientation and sun position, and it is not clear what the optimum spacing of the tubes from the back should be.

2.10 Diameters on Which to Base Radiation Calculations

All of the preceding comments have been based on consideration of opaque cylinders uniformly spaced above a diffusely reflecting surface. The actual collector tube currently being manufactured by Owens-Illinois has a transparent outer glass cover tube of 53 mm OD, and an opaque inner absorber tube of 43 mm OD. Basing the calculations on either the absorber tube diameter, the outer tube diameter, or a combination of both diameters is possible.

An approach that will yield conservative estimates of all four components of radiation [and the method apparently used by Beekley and Mather] is outlined below:

1. Base directly intercepted beam on absorber diameter.
2. Calculate the width of the illuminated strip by using the cover tube diameter. This will tend to underestimate the back reflected beam component.
3. Base the view factor F_{dA-s} on the cover tube diameter; this will tend to decrease the amount of diffuse radiation reaching the backing plate.
4. Base the view factor F_{dA-t} on the absorber tube diameter. This decreases both the back reflected beam and diffuse components.
5. Base view factor F_{t-s} on the absorber tube diameter. This will tend to decrease the diffuse radiation directly intercepted by the tubes.

Note that for this method F_{dA-s} is no longer equal to $1-F_{dA-t}$, as the view factors are based on different diameters and tube separations.

The equations for R_B' and R_D' can be rewritten based on these different diameters as follows:

$$R_B' \text{ CONSERVATIVE} = \frac{D_a + \rho_B \cos \Omega W_c F_{w-t}(a)}{C \cos \Omega} \quad 2.10.1$$

$$R_D' \text{ CONSERVATIVE} = \frac{\pi D_a F_{t-s}(a) + \rho_B \int_0^c (F_{dA-s})_c (F_{dA-t})_a dx}{C} \quad 2.10.2$$

where the subscripts a and c refer to the absorber diameter and cover tube diameter, respectively. If we consider the case where the cover tubes are separated by one tube spacing $\frac{C}{D_c} = 2.0$; and letting $\frac{D_b}{D_c} > 1.5$, $\Omega = 0$ and considering only beam radiation, then

$$\begin{array}{lll} \frac{D_c}{C} = 2.0 & \frac{D_a}{C} = 2.465 & \frac{D_a}{C} = 2.465 \\ R_B'{}_c = 0.779 & R_B'{}_a = 0.6855 & R_B' \text{ CONS} = .6411 \\ \frac{(S_{\text{eff}})_c}{H_b R_B} = .4959 & \frac{(S_{\text{eff}})_a}{H_b R_B} = .5376 & \frac{(S_{\text{eff}}) \text{ CONS}}{H_b R_B} = .5030 \end{array}$$

The maximum deviation in S_{eff} is 8.4% for this example. The conservative estimate based on an actual $\frac{D_a}{C}$ ratio of 2.465 is bounded by the two cases:

1. Where the flux on the absorber tube is assumed to be the same as the flux on an opaque tube of diameter equal to the cover tube, and
2. The flux on an opaque tube of diameter equal to the absorber tube when no cover tube is present.

This bounding of the beam radiation intercepted by the tubes applies to all general tube spacings, not just this example. In a similar manner, the conservative diffuse contributions can be shown to lie between the values predicted by using the cover tube diameter only or the absorber tube diameter only.

Because of the simple nature of the model used for calculating the effective insolation, it is not clear which diameter should be used. Ignoring multiple reflections of the solar radiation, the angular dependence of the absorptance of the absorber tube, the transmittance of the cover tube, the reflectance of the backing screen, and shading due to air ducts and manifolds could introduce errors considerably larger than those arising from using an incorrect diameter in the calculations of S_{eff} . In the absence of experimental data and tests, it seems to be a matter of arbitrary choice which diameter is used. It is probably wise to use relationships that give conservative results for the flux per tube, however.

2.11 Conclusions and Discussion

The influence of the distance from the backing surface and the center-to-center tube separation on the effective solar radiation received by a single tube have important implications for collector array design. For tubes oriented north-south, placing the tubes far enough from the backing surface so that the view factor from an area on the back to the tubes does not vary with position insures that the maximum reflected radiation will reach the tubes at those times of the day when the radiation incident upon the backing surface is a maximum. For east-west orientations, it is possible to adjust the seasonal variations in incident radiation by changing the distance from the backing surface. Spacing the tubes directly on the backing surface will decrease the magnitude of the radiation received per tube in the spring and fall and increase the magnitude in the summer and winter from the magnitudes that are received when the tubes are spaced with clearance above the backing surface. This might be desirable when the greatest loads are required in the summer and winter and the spring and fall performance is not as important. In general, the effect of the backing distance depends upon the collector backing surface tilt, the collector tube orientation on the backing surface, and will affect the hourly and seasonal magnitudes of the

solar radiation received by each tube. The optimum backing distance can be expected to change with different types of solar system applications.

The increase in S_{eff} as the ratio $\frac{C}{D}$ increases allows flexibility in system design. For applications where the available backing area is large, such as domestic hot water heating in residences, better thermal performance per tube can be expected at larger tube spacings. For applications where a large total solar input is required, such as heating and cooling of houses and buildings, the total load supplied by a collector array will increase as the tube separation decreases. This occurs because as the tube separation decreases, the number of tubes that can be put into a finite area increases faster than the decrease in S_{eff} per tube, hence the total array output increases.

Actual array designs will be dictated by economic considerations rather than thermal considerations. If the cost of manifolding or tube supports becomes a significant percentage of the total array cost, it is expected that the optimum tube spacing will be different from the spacings that give the best thermal performance.

3. THERMAL ANALYSIS OF A SINGLE COLLECTOR TUBE

3.1 Nomenclature Used in Thermal Analysis

Figure 3.1.1 shows a cross section of a single collector tube assembly with the delivery tube inserted.

Figure 3.1.2 shows the general thermal network representing the heat transfer that occurs in an operating collector tube assembly. The symbols shown in both figures are defined below:

- D_1 delivery tube outside diameter
- D_{3i} inside absorber tube diameter
- D_{3o} outside absorber tube diameter
- D_o outside glass cover tube diameter
- D_i inside glass cover tube diameter

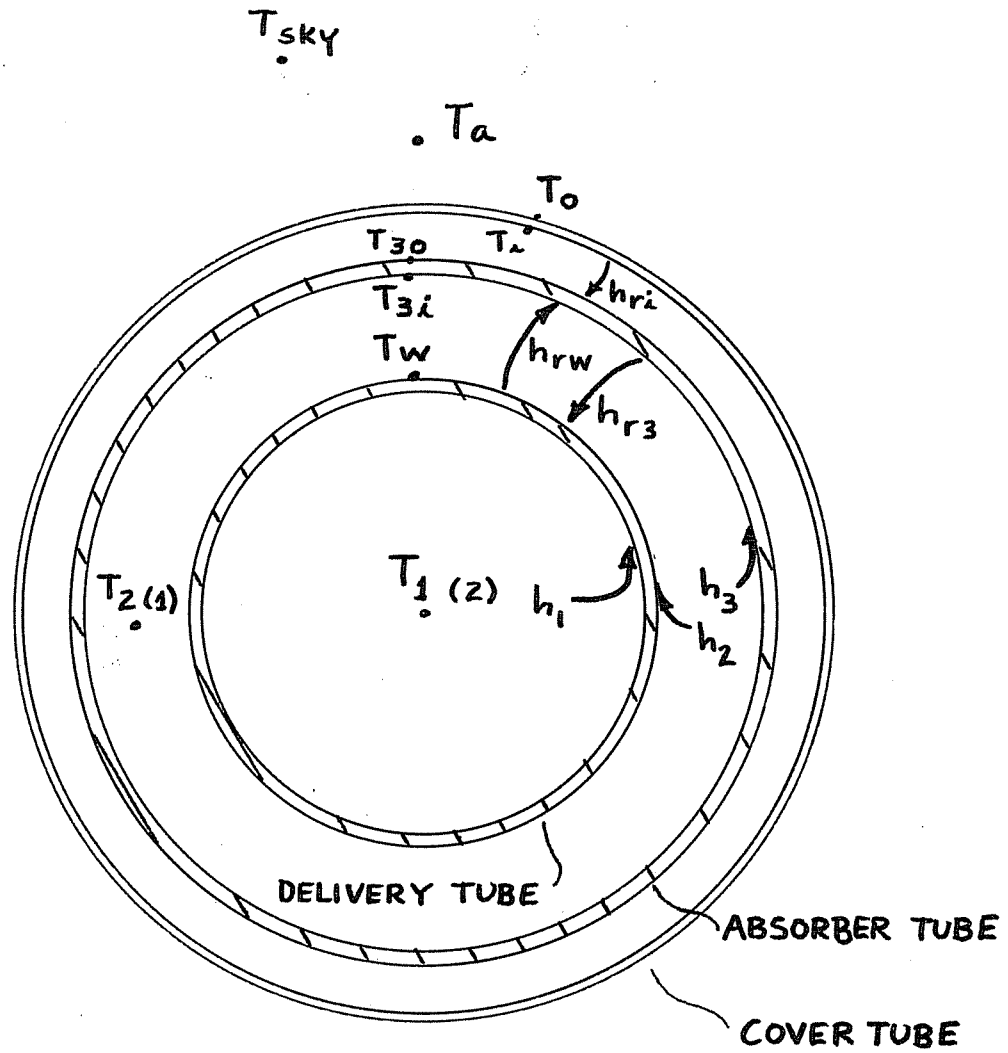
All perimeters and areas based on these diameters use the same subscripts, i.e. A_1 is the delivery tube outside surface area, P_1 is the perimeter.

- h_1 convection heat transfer coefficient from the air within the annulus to the inside surface of the delivery tube
- h_2 convection heat transfer coefficient from the air within the annulus to the outside surface of the delivery tube
- h_3 convection heat transfer coefficient from the air within the annulus to the inside surface of the absorber tube

- h_{rw} radiation heat transfer coefficient from the delivery tube to the absorber tube based on the delivery tube area A_1
- h_{ri} radiation coefficient from the inside surface of the cover tube to the outside surface of the absorber tube, based on D_i
- h_{r3} radiation coefficient from absorber tube to delivery tube based on absorber tube area, A_{3i}
- U_L overall loss coefficient of the collector tube assembly based on the outside absorber tube diameter, D_{30}
- U_1 overall heat transfer coefficient from the outside surface of the delivery tube, to the air within the delivery tube, based on D_1 .

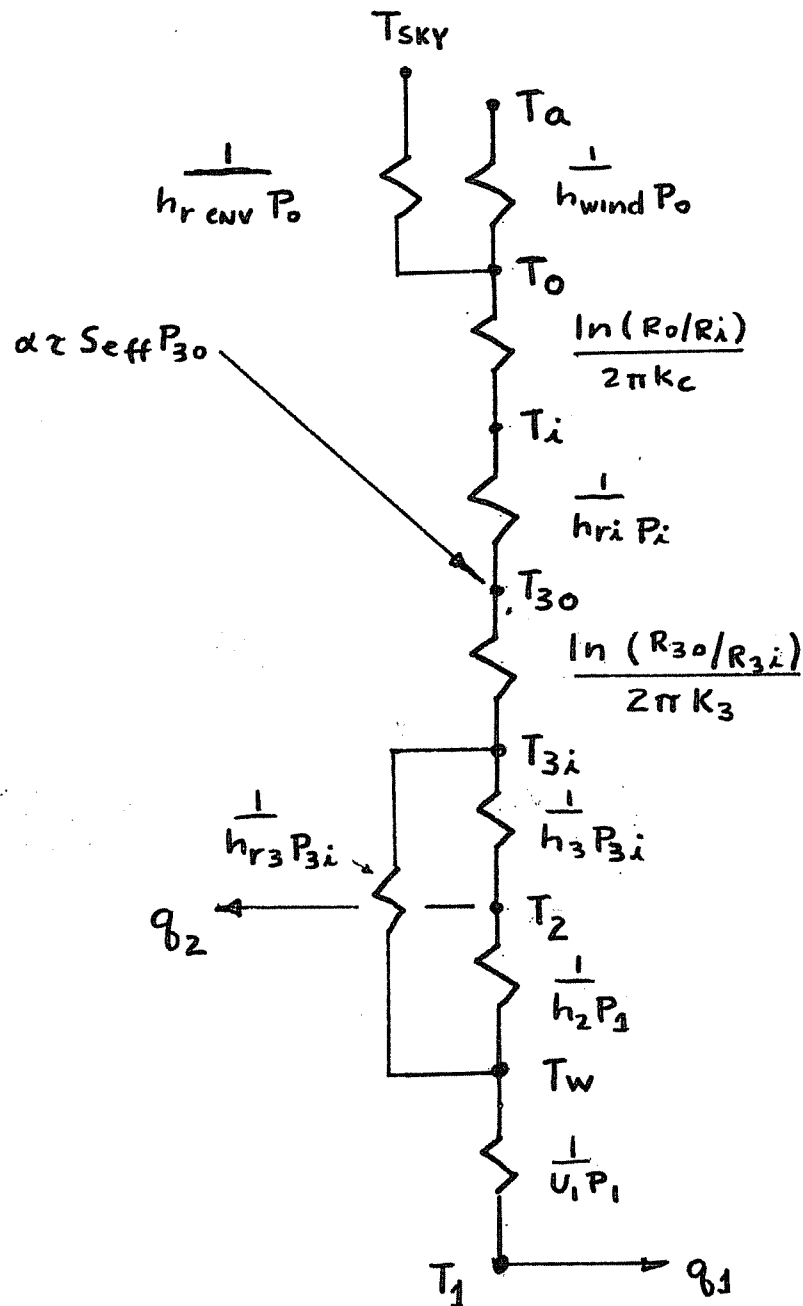
Temperatures:

- T_1 air temperature
- T_2 air temperature
- T_{3i} inside absorber tube temperature
- T_{30} outside absorber tube temperature
- T_w temperature of the delivery tube outer surface
- T_i temperature of cover tube inner surface
- T_o temperature of cover tube outer surface
- T_a ambient temperature
- T_{sky} equivalent sky temperature for radiation losses from cover tube.



COLLECTOR TUBE ASSEMBLY

FIGURE 3.1.1



THERMAL NETWORK REPRESENTING AN
OPERATING COLLECTOR TUBE ASSEMBLY

FIGURE 3.1.2

3.2 Assumptions Made in Modeling the Collector Tube Performance

In modeling the thermal performance of a single collector tube, some assumptions are made to simplify the analysis. These are:

1. Operation is steady state; the thermal capacitance effects of absorber tube, cover tube, delivery tube, and air within the collector tube assembly are neglected.
2. Longitudinal conduction along the absorber tube and delivery tube is negligible.
3. Steady state radial conduction occurs through the delivery tube walls.
4. The temperature gradient across the glass absorber tube is negligible ($T_{3o} = T_{3i} = T_3$).
5. The radiative heat transfer occurring between the absorber tube inner surface and the delivery tube, and the radiative transfer between the absorber tube outer surface and the cover tube can be modeled as occurring between gray, diffusely reflecting surfaces.
6. The convection heat transfer coefficients between the fluid and the inside surface of the absorber tube and between the fluid and the outside surface of the delivery tube are equal (i.e., $h_3 = h_2$, see

Fig. 3.1.1).

7. All heat transfer coefficients and physical properties are independent of length.
8. Absorption of solar radiation by the cover tube is negligible.
9. Solar radiation absorbed by the outer surface of the absorber tube is uniformly distributed around the tube perimeter.

Some of these assumptions, particularly those concerning the treatment of convection, will be examined in detail in later sections.

3.3 U_L , Collector Tube Assembly Loss Coefficient

3.3.1 General Expression for U_L

The collector tube currently being manufactured by Owens-Illinois has an evacuated annular space between the absorber tube and the transparent glass cover tube. It will be assumed that a total vacuum exists between the inner and outer tubes, and that no heat transfer by conduction occurs between the absorber tube and the cover tube at the tube ends. Then, the heat lost by the absorber tube outer surface to the cover tube is entirely by radiation.

Figure 3.3.1 shows the thermal network used in solving for the steady state heat loss by a constant temperature absorber tube. The two known temperatures are T_3 and T_a , the absorber tube temperature and the ambient temperature. It is assumed for simplicity that the equivalent sky temperature for radiation losses from the outer glass cover is the same as the ambient temperature.

Energy balances at the inside and outside surfaces of the cover tube yield the following equations:

$$h_{ri}(T_3 - T_i) + \frac{2 k_c (T_o - T_i)}{D_i \ln(D_o/D_i)} = 0 \quad 3.3.1$$

Inside glass cover surface

$$U_T(T_a - T_o) + \frac{2 k_c (T_i - T_o)}{D_o \ln(D_o/D_i)} = 0 \quad 3.3.2$$

Outside glass cover surface

where $U_T = h_{wind} + h_{r env}$

h_{wind} = convection coefficient due to wind acting
on the outside cover tube surface

$$h_{r env} = \epsilon_o \sigma (T_a^2 + T_o^2)(T_a + T_o)$$

σ = Stephan Boltzman constant

k_c = thermal conductivity of the cover tube

The radiation coefficient is given by

$$h_{ri} = \frac{\sigma(T_3^2 + T_i^2)(T_3 + T_i)}{\frac{D_i}{D_{30}} \left[\frac{1 - \epsilon_3}{\epsilon_3} \right] + \frac{1}{F_{i3}} + \frac{1 - \epsilon_i}{\epsilon_i}} \quad 3.3.3$$

where ϵ_3 is the long wave emittance of the absorber tube selective surface

$\epsilon_i = \epsilon_o$ emittance of inner and outer glass cover surfaces

F_{i3} view factor from the inside cover tube surface to the absorber tube

T_a , T_o , T_i and T_3 are absolute temperatures.

Because of the assumption of steady state heat losses the energy lost by the absorber tube to the inner cover is equal to the energy lost by the absorber tube to ambient. These losses can be expressed as

$$h_{ri} A_i (T_3 - T_i) = U_L A_{30} (T_3 - T_a)$$

and

$$U_L = \frac{h_{ri} A_i (T_3 - T_i)}{A_{30} (T_3 - T_a)} \quad 3.3.4$$

3.3.2 Numerical Results and Resulting Simplifications

Eqs. 3.3.1 and 3.3.2 can be solved easily for the inner and outer glass cover temperatures if the magnitudes of the different conductances are known. The values of the radiation conductances h_{ri} and $h_{r\ env}$ are temperature dependent, however, so an iterative procedure is required. The solution procedure used was to guess an initial temperature for the inner and outer glass cover temperatures, evaluate the radiation conductances and solve 3.3.1 and 3.3.2 for an improved estimate of the inner and outer glass temperatures. The iteration was repeated until the inner and outer cover temperatures were within a specified tolerance for 2 successive iterations. 3.3.1 and 3.3.2 were solved for the cover tube temperatures and U_L calculated by use of eq. 3.3.4 for the following sets of independently varying conditions:

1. The temperature difference ($T_3 - T_a$) varied from 10°C to 300°C
2. T_3 varied from 0°C to 200°C
3. Windspeed varied from 0 m/sec to 50 m/sec

The values used for collector tube dimensions, absorber tube and glass cover emittances are the same as the currently manufactured O-I collector tube. These values are:

$$\epsilon_i = \epsilon_o = 0.90$$

$$\epsilon_3 = 0.07$$

$$D_i = 0.053 \text{ m}$$

$$D_o = 0.049 \text{ m}$$

$$D_{3o} = 0.043 \text{ m}$$

$$k_c = 1.05 \text{ W/m}^\circ\text{C}$$

$$h_{\text{wind}} = 5.7 + 3.8 V \text{ (W/m}^2\text{-}^\circ\text{C)} \quad V=\text{velocity, m/sec}$$

This h_{wind} correlation from Duffie and Beckman [3] is for flat surfaces, but it will be shown that the overall loss coefficient U_L is quite insensitive to the magnitude of this coefficient.

When the network was solved using these values, the resulting temperatures for the inside and outside of the glass cover tube closely duplicated those values reported by Beekley and Mather [1]. For the worst case when $(T_3 - T_{\text{amb}})$ is 300°C and T_3 is 200°C , there is less than a 2.5% difference in the value of U_L for a wind speed of 0 m/sec and a windspeed of 50 m/sec. For the 50 m/sec wind speed, the inside cover surface temperature is only slightly above ambient. The variation of U_L due to fluctuations of wind speed decreases as the temperature level of the absorber tube drops. Because the emittance of the absorber tube is very low, the largest resistance to heat transfer is the radiation path from the absorber surface to the inside glass cover surface.

It can be seen that by assuming the inner glass cover surface is at the ambient temperature, eq. 3.3.4 can be written as

$$U_L = \frac{h_{ri} D_i}{D_{3o}} \quad 3.3.5$$

This assumption, suggested by Beekley et al., will give slightly conservative estimates for U_L for all levels of collector operation and will be used exclusively, as it simplifies the evaluation of the loss coefficient and only introduces small error. The collector tube is then assumed to be totally insensitive to wind speed, with all losses occurring by radiation from the absorber tube to the cover tube inside surface at ambient temperature.

Figure 3.3.2 shows U_L as a function of T_3 and $(T_3 - T_{amb})$ for a wide range of operating temperatures. U_L is variable, and depends upon the operating conditions. However, the magnitude of the loss coefficient is quite low when compared to the loss coefficient of a conventional flat plate collector using air as the working fluid.

EUGENE DIETZGEN CO.
MADE IN U. S. A.

NO. 341-M DIETZGEN GRAPH PAPER
MILLIMETER

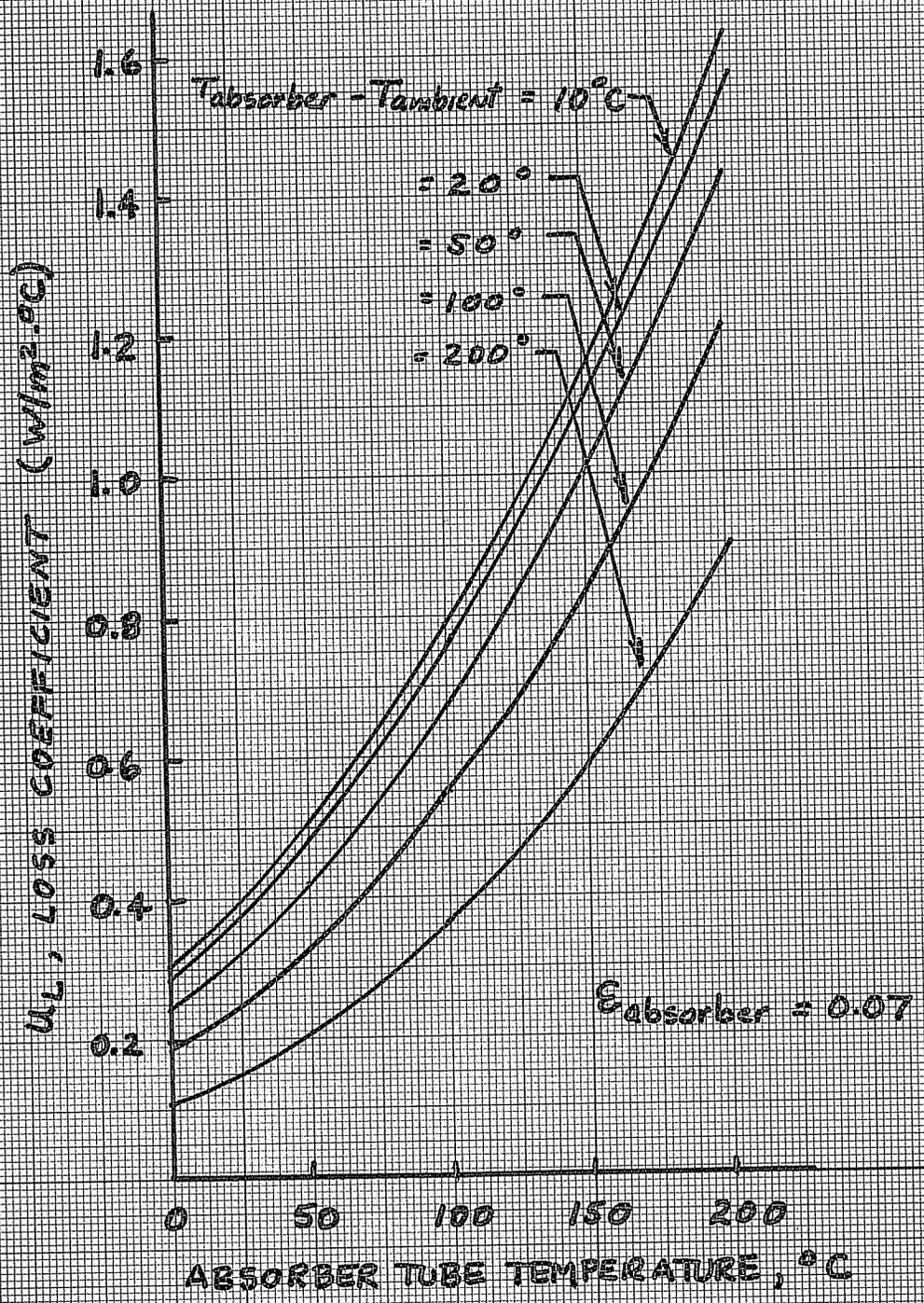


FIGURE 3.3.2

3.4 Formulation of Energy Balances

The usual manner of circulating air through a collector tube assembly is to insert a delivery tube of suitable size inside the collector tube. Air can then be forced either in the delivery tube and out the annulus, or forced in the annulus and out the delivery tube. Although for most operating conditions the useful energy is closely the same for either mode of operation, the internal temperature distributions can be quite different. The two modes of delivery will be modeled separately.

Figure 3.4.1 shows the coordinate system used in the formulation of the energy balances. The origin of the x coordinate is taken at the turn-around point of the collector tube. The mode where the air enters the delivery tube and exits through the annulus will be called Case 1. Case 2 is the delivery mode where the air enters the annulus and exits the delivery tube. It should be noted that in both cases the "cold" stream is labeled T_1 and the "hot" stream which exits the collector tube is T_2 . Energy balances are done on four different systems within the collector assembly:

1. On the absorber tube
2. On the delivery tube
3. On the air inside the delivery tube

MODES OF AIR DELIVERY

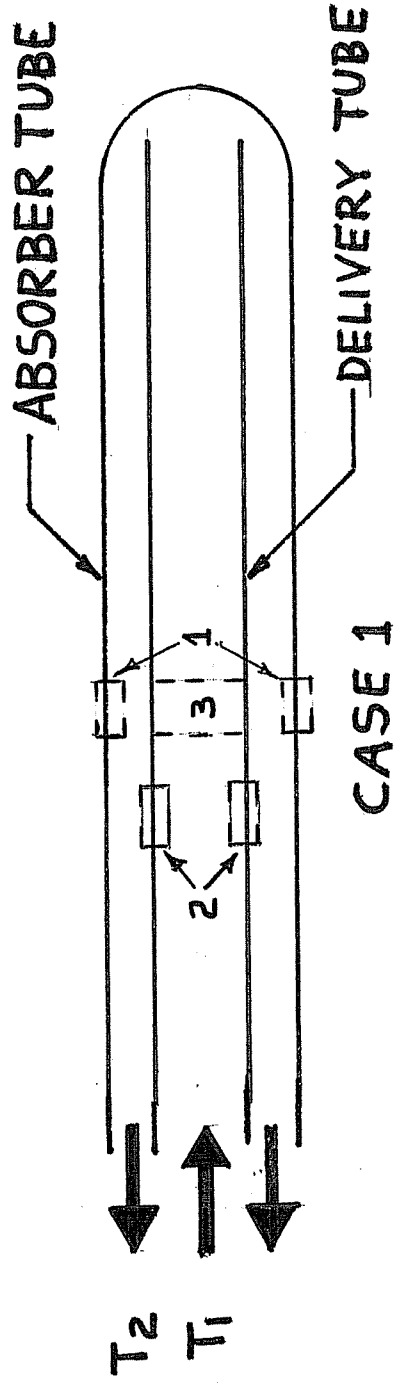
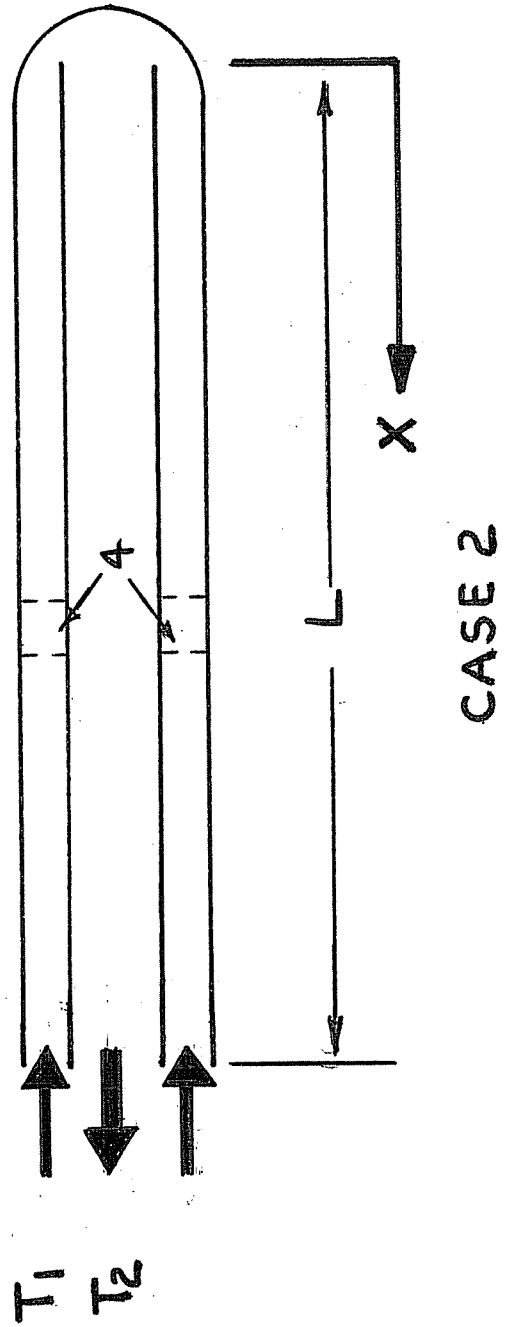


FIGURE 3.4.1



4. On the air inside the annulus formed by the absorber tube and delivery tube

The locations of these systems are also shown in Figure 3.4.1.

An energy balance on the absorber tube at some position x gives for case 1

$$\alpha \tau S_{\text{eff}} \frac{D_{30}}{D_{3i}} + U_L \frac{D_{30}}{D_{3i}} (T_a - T_3) + h_{r3} (T_w - T_3) = 0 \quad 3.4.1a$$

This equation can be rewritten without the diameter ratio, $\frac{D_{30}}{D_{3i}}$, in the terms containing U_L and S_{eff} by defining new

values of U_L and S_{eff} that are $\frac{D_{30}}{D_{3i}}$ times their actual values as predicted by equations 3.3.5 and 2.9.2. These new definitions are proposed for algebraic convenience, and will be used for the remainder of this work. Then,

$$\alpha \tau S_{\text{eff}} + U_L (T_a - T_3) + h_3 (T_2 - T_3) + h_{r3} (T_w - T_3) = 0 \quad 3.4.1b$$

The energy balance on the delivery tube for case 1 gives:

$$h_2 (T_2 - T_w) + h_{rw} (T_3 - T_w) + U_L (T_1 - T_w) = 0 \quad 3.4.2$$

An energy balance on the air inside the delivery tube for case 1 yields:

$$-m c_p \frac{dT_1}{dx} + U_L P_1 (T_1 - T_w) = 0 \quad 3.4.3$$

Similarly, an energy balance on the air in the annulus for case 1 yields

$$\dot{m}c_p \frac{dT_2}{dx} + h_3P_3(T_2 - T_3) + h_2P_1(T_2 - T_w) = 0 \quad 3.4.4$$

The equations for case 2 are derived in the same manner. For case 2, the labels T_1 and T_2 are interchanged in the energy balances with corresponding changes in the signs of the derivatives because of the different flow direction. The four equations for case 2 are,

Absorber tube:

$$\alpha\tau S_{\text{eff}} + U_L(T_2 - T_3) + h_3(T_1 - T_3) + h_{r3}(T_w - T_3) = 0 \quad 3.4.5$$

Delivery tube:

$$h_2(T_1 - T_w) + h_{rw}(T_3 - T_w) + U_1(T_2 - T_w) = 0 \quad 3.4.6$$

Air in delivery tube:

$$\dot{m}c_p \frac{dT_2}{dx} + U_1P_1(T_2 - T_w) = 0 \quad 3.4.7$$

Air in annulus:

$$-\dot{m}c_p \frac{dT_2}{dx} + h_3P_3(T_1 - T_3) + h_2P_1(T_1 - T_w) = 0 \quad 3.4.8$$

For both case 1 and case 2 we have 4 equations relating 4 unknown temperatures: T_1 , T_2 , T_w and T_3 . Two equations are linear algebraic equations and two are linear first order differential equations. An analytic solution for the equations for cases 1 and 2 for two sets of boundary

conditions is found in Appendices 2.1 and 2.2. The general solutions for the temperature distributions of T_1 and T_2 for the entire collector tube or any finite length segment of the collector tube are of the form:

$$T_1 = M_1 e^{m_1 x} + M_2 e^{m_2 x} + g_1 \quad \text{A-2.2.1}$$

$$T_2 = M_1 \frac{(m_1 + e_1)}{e_2} e^{m_1 x} + M_2 \frac{(m_2 + e_1)}{e_2} e^{m_2 x} + g_2 \quad \text{A-2.2.2}$$

3.5 General Solution Procedure Used for Thermal Analysis of a Collector Tube

Determining the useful energy gain of a single collector tube requires predicting the outlet temperature of the collector when the operating conditions are known. Equations A-2.2.1 and A-2.2.2 allow the treatment of internal flow in the collector tube annulus and delivery tube to include the effects of developing flow (allowing the local convection conductance to vary with length) and any ratio of heat fluxes on the inner and outer surfaces of the annulus formed by the absorber tube and delivery tube, if desired.

Because the radiation exchange between the delivery tube and inside surface of the absorber tube can be significant, particularly at low flow rates, an iterative solution procedure is needed if a precise value for the useful

energy gain from the collector tube is required. One possible procedure is outlined below:

1. Guess temperatures for which radiation exchange are based for the absorber tube, \hat{T}_3 and the delivery tube outside surface, \hat{T}_w . This allows evaluation of U_L and the h_r 's. (See Appendix A-2.3)
2. Knowing the air flow rate and collector tube internal geometry, the convection coefficients h_1 , h_2 , and h_3 are evaluated using suitable correlations.
3. Using the analytic solutions for T_1 and T_2 given in Appendix A-2, the values of the local fluid temperatures, and the local absorber tube and delivery tube temperatures can be evaluated at different positions along the tube length.
4. An outlet air temperature is predicted.
5. Mean or average bulk fluid temperatures can be determined and used for correction of the fluid properties (if desired).
6. \hat{T}_3 and \hat{T}_w can be found and used to improve estimates of U_L and h_{rw} .

7. The procedure is repeated until the outlet temperature of the air is within a specified tolerance for two successive iterations.

3.6 Different Methods Used for Determining the Temperature Distribution in a Collector Tube

The general solution procedure outlined in 3.5 can be modified in a number of ways depending upon the extent that it is necessary to specify the convection coefficients h_1 , h_2 and h_3 . If h_1 , h_2 and h_3 are constant with length, the entire fluid temperature distribution can be predicted at one time using the solutions for the entire tube length given in Appendix 2, and using the iteration scheme given in the last section.

A method for including the variation with length of the local convection conductances h_1 , h_2 and h_3 is shown diagrammatically in Figure 3.6.1 and outlined below:

1. The collector tube is divided into N equal length segments.
2. Equations A-2.2.1 and A-2.2.2 are used to evaluate the fluid temperatures in each segment. For segment N , the segment with the flow turn-around, the coefficients M_1 and M_2 are evaluated using

COLLECTOR IS DIVIDED INTO
N EQUAL LENGTH SEGMENTS

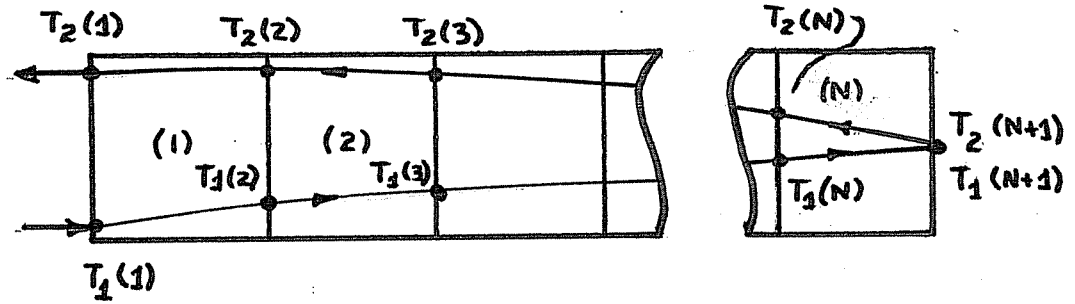


FIGURE 3.6.1

THERMAL NETWORK REPRESENTING
LINEAR COLLECTOR MODEL

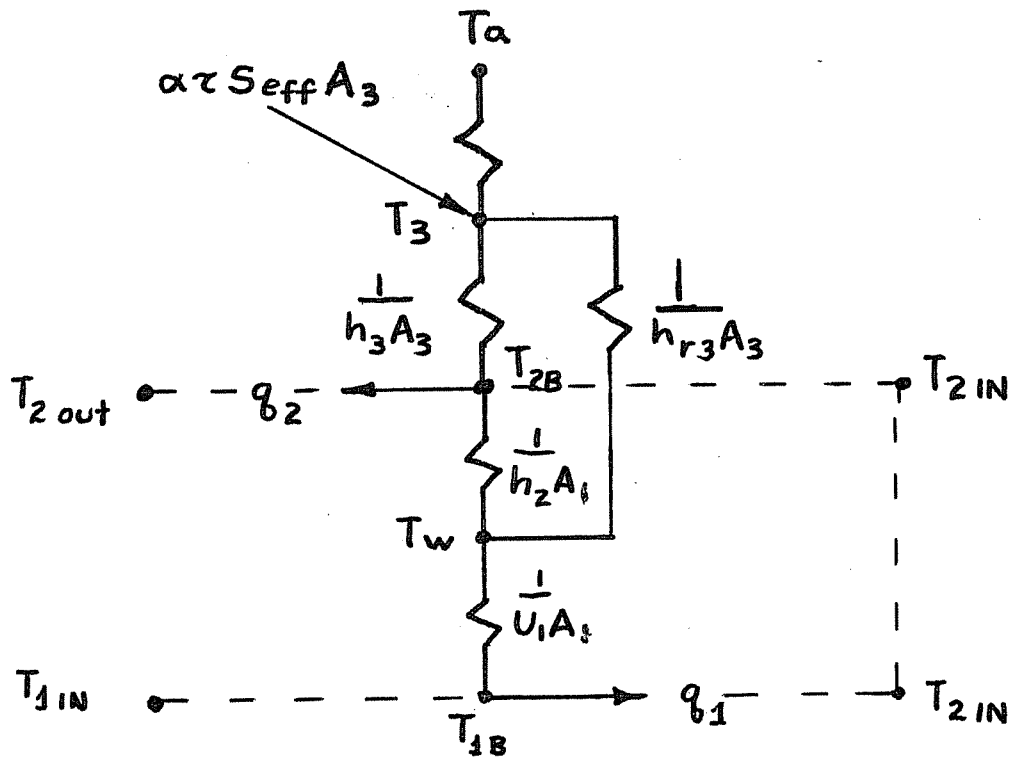


FIGURE 3.6.2

A-2.2.5 and A-2.2.6. For all other segments the coefficients M_1 and M_2 are evaluated using A-2.2.9 and A-2.2.10.

3. The convection coefficients in each segment are considered constant with length, but variable from segment to segment.
4. Solving for the collector tube outlet temperature requires a series of iterative and sequential temperature evaluations.
 - a. Initialize the lower fluid temperature distribution [$T_1(1)$ through $T_1(N)$] to some starting value.
 - b. Starting at the turn-around end (segment N), successively predict the hot outlet temperatures [$T_2(i)$] from each segment using the initial guesses of the lower inlet temperature to the segment.
 - c. Using the new top temperature distribution, and the known inlet temperature, start from segment 1 and recalculate the lower fluid temperature profile.
 - d. Repeat the calculation for the top fluid temperature distribution and compare the outlet temperature with the first prediction; if within

tolerance, stop. If not, repeat the entire process until the outlet temperature converges acceptably.

The variation of the convection coefficients with the length can be handled in this manner, but the procedure is awkward to use for the general case where laminar or turbulent flow occurs in the delivery tube or annulus because it assumes the variation of the local convective conductances is known. This method has been used for single cases where the local heat transfer coefficients are assumed to decrease with distance from the tube and annulus entrances in some arbitrary fashion.

A third method involving the solution of only linear algebraic equations was used to model the thermal performance of a collector tube assembly. It uses additional assumptions about the internal heat transfer that are different than those used in the more general analytic model. These assumptions are:

1. The absorber tube and delivery tube are at constant temperatures T_3 and T_w , respectively.
2. The temperature distributions of the air within the annulus and delivery tube are linear with length.
3. All heat transfer by convection in the delivery tube is modeled as occurring between the delivery

tube outside surface T_w and the average air bulk temperature T_{1B} , which is defined as the arithmetic average of the inlet and exit temperature of the air within the delivery tube.

4. Convection heat transfer in the annulus occurs between the average bulk air temperature T_{2B} and the absorber temperature T_3 and the delivery tube outside temperature T_w .

The difference between this linear model and the other models developed earlier is the size of the control volume that the energy balance is made upon. This method can be expected to give good agreement with the more general models when the temperature profiles of the fluid and tube surfaces do not exhibit extreme deviations from linearity. It is analogous to the use of an arithmetic average temperature difference in place of a log-mean temperature difference as used in heat exchanger calculations. Figure 3.6.2 shows the thermal network representing this model.

Energy balances on the delivery tube, absorber tube, the air inside the annulus, and the air in the delivery tube yield four equations:

$$h_2(T_{2B} - T_w) + h_{rw}(T_3 - T_w) + U_1(T_{1B} - T_w) = 0 \quad 3.6.1$$

$$\alpha \tau S_{\text{eff}} + U_L(T_a - T_3) + h_3(T_{2B} - T_3) + h_{r3}(T_w - T_3) = 0 \quad 3.6.2$$

$$\dot{m}c_p(T_{2 \text{ out}} - T_{2 \text{ in}}) + h_3 P_3 L(T_{2B} - T_3) + h_2 P_1 L(T_{2B} - T_w) = 0 \quad 3.6.3$$

$$\dot{m}c_p(T_{2 \text{ in}} - T_{1 \text{ in}}) + U_1 P_1 L(T_{1B} - T_w) = 0 \quad 3.6.4$$

T_{1B} and T_{2B} are defined by

$$T_{1B} = \frac{T_{1 \text{ in}} + T_{2 \text{ in}}}{2} \quad 3.6.5$$

$$T_{2B} = \frac{T_{2 \text{ in}} + T_{2 \text{ out}}}{2} \quad 3.6.6$$

There are six linear algebraic equations and 6 unknown temperatures. The equations can be solved and the useful energy gain predicted for any specified set of operating conditions by a variety of methods. Because it was of some interest to compare the temperatures predicted by the linear model with the temperature distributions of the more complicated models, a computer subroutine was used to solve directly for the unknown temperatures. No attempt was made to simplify the resulting equations to a more convenient form for hand calculation.

3.7 Typical Temperature Distributions Predicted by the Different Collector Models

Figure 3.7.1 shows the predicted air temperatures using three different models as a function of position in the collector tube for a typical set of operating conditions. The figure shows the air temperature distributions for case 1, where the air enters the delivery tube and exits through the annulus. The three different methods used were the linear model and the two variations of the general analytic model. One variation considers the entire collector tube and assumes the convection coefficients h_1 , h_2 and h_3 constant with length. The other model divides the collector in a number of equal length segments and assumes h_1 , h_2 and h_3 constant with length within each segment but variable from segment to segment. Table 3.7.1 shows the values used for the collector tube dimensions and operating parameters. The dimensions are the same as the currently manufactured Owens-Illinois collector tube reported by Beekley and Mather [1].

The forced convection heat transfer correlations used for each model were:

1. Analytic Model -- entire collector tube length.

For both laminar and turbulent flow, it was assumed that the hydrodynamic and thermal boundary layers

Table 3.7.1

O-I Collector Tube Dimensions and Surface Properties

(From Ref. 1)

Cover Tube Outside Diameter:	53 mm
Cover Tube Inside Diameter:	49 mm
Absorber Tube Outside Diameter:	43 mm
Absorber Tube Inside Diameter:	39 mm
Selective Surface Properties:	$\alpha=0.85$; $\epsilon=0.07$
Collector Tube Length:	1.067 m
Cover Tube Transmittance:	$\tau=0.92$
Absorber Tube Inner Surface, Emittance	$\epsilon=0.90$

Other Typical Operating Conditions
and Collector Parameters

Delivery tube OD:	23 mm
Delivery tube ID:	21.43 mm
Delivery tube properties: (galvanized steel)	$k = 47.6 \text{ W/m}^\circ\text{C}$ $\epsilon = 0.23$
Flow Rate through Collector:	$\dot{m} = 8.18 \text{ kg/hr}$
Incident Solar Radiation:	$S_{\text{eff}} = 650 \text{ W/m}^2\text{ }^\circ\text{C}$
Ambient Temperature:	10°C
Inlet Temperature:	30°C

were fully developed. For laminar flow, the relationship from Kays [5] for constant temperature conditions for flow between flat plates with one side heated was used; $Nu = 4.9$. For turbulent flow the relationship given in Duffie and Beckman [3], $Nu = 0.0158 Re^{0.8}$, for turbulent flow between flat plates with one side heated was used. (The applicability of these correlations is discussed in Section 4.1.)

2. Linear Model --

$$\text{Laminar: } Nu = 4.9$$

$$\text{Turbulent: } Nu = 0.0158 Re^{0.8}$$

3. Analytical Model -- the collector tube was broken into segments. The variation of heat transfer with length was assumed to follow the approximate equation from Kreith [6] for turbulent flow of gases and liquids in short circular tubes.

$$\frac{h_L}{h} = 1 + (D/L)^{0.7} \quad \text{when } 2 < L/D < 20$$

$$\frac{h_L}{h} = 1 + 6(D/L) \quad \text{when } 20 < L/D < 60$$

where h_L is the average unit conductance to a tube of finite length L and h is the conductance of an infinitely long tube.

AIR TEMPERATURE DISTRIBUTIONS IN A
SINGLE COLLECTOR TUBE USING DIFFERENT
COLLECTOR MODELS

— CONVECTION COEFFICIENTS VARY
WITH DISTANCE

- - - CONVECTION COEFFICIENTS ARE
CONSTANT

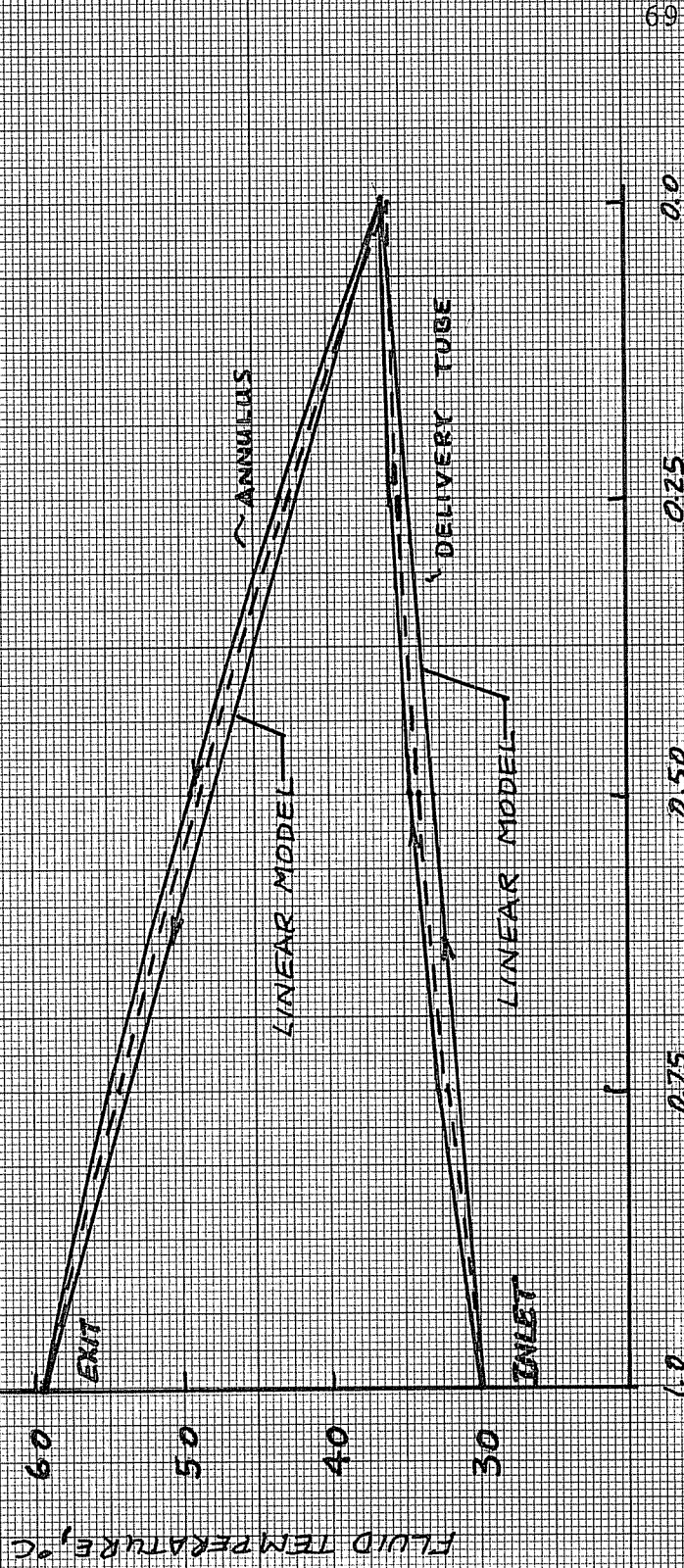


FIGURE 3.7.1 X (L), DISTANCE FROM TURN-AROUND

ABSORBER TUBE TEMPERATURES
USING DIFFERENT COLLECTOR
MODELS

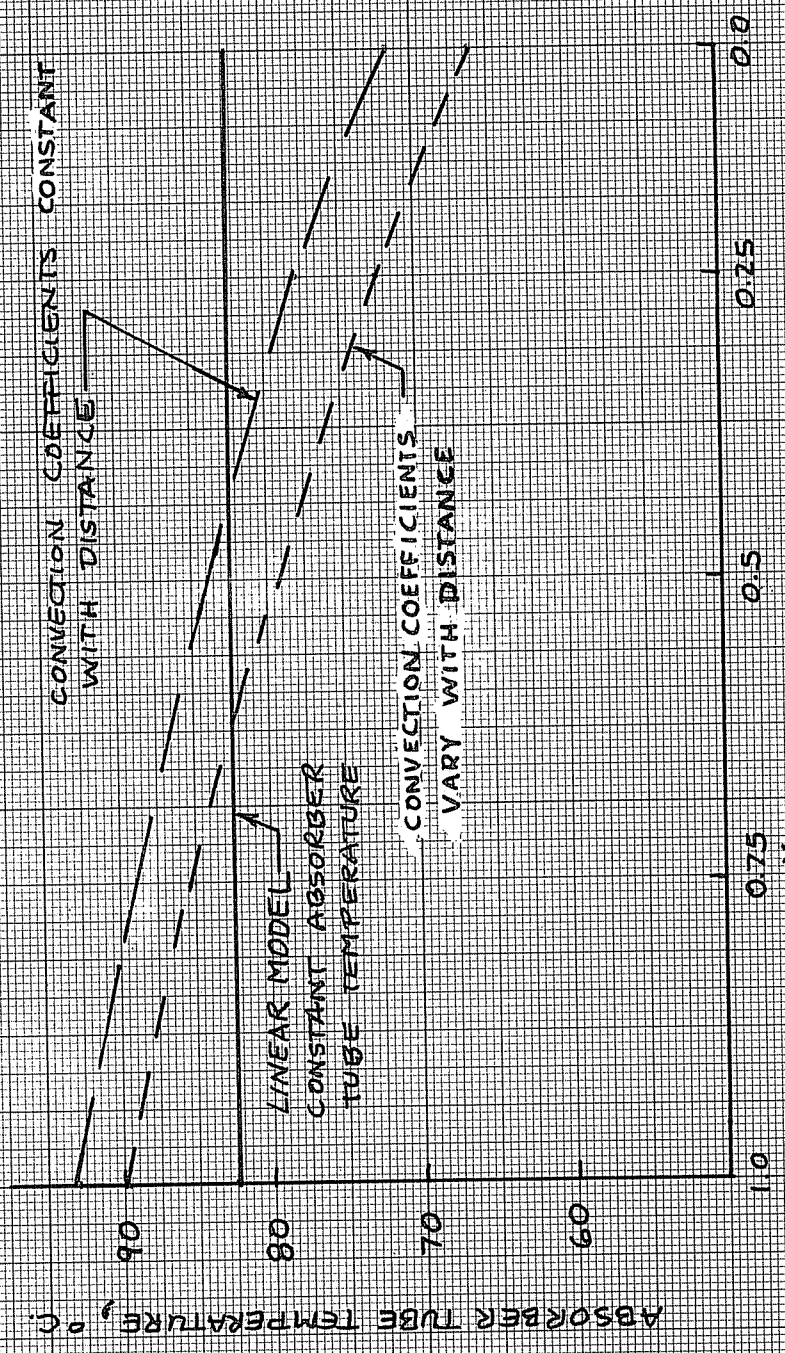


FIGURE 3.7.2 $\frac{X}{L}$, DISTANCE FROM TURNAROUND END

Figure 3.8.1 shows the air temperature distribution for a single collector tube with different absorber tube emittances. The collector dimensions and operating conditions are the same as in Table 3.7.1. It can easily be seen that changes in the value of the emittance have significant effects upon the useful energy gain from the collector tube assembly. Changing the emittance successively from 0.07 to 0.15, 0.30, and 0.92 reduces the useful energy gain 8.5%, 19.9% and 43.4%, respectively.

Figure 3.8.2 shows the effects of changes in the absorber tube absorptance on the air temperature when the long wave emittance is held constant at 0.07. For this specific set of flow conditions, the ratio of the useful energy gain to the useful gain of a tube with nominal absorptance of 0.85 is approximately equal to the ratio of the absorptances for the two cases.

These examples represent only a few sets of possible designs and operating conditions of an evacuated tubular collector, but they point out the performance increase that will be realized by an absorber tube with a low emittance and high absorptance. They also show that accurately determining the actual absorptance and emittance of the absorber tube is necessary for accurate predictions of the useful energy gain from a collector tube assembly.

EFFECT OF ABSORBER TUBE EMITTANCE ON AIR TEMPERATURES

- $\epsilon = 0.07$; $\alpha \tau = .782$
- $\epsilon = 0.15$; $\alpha \tau = .782$
- $\epsilon = 0.30$; $\alpha \tau = .782$
- $\epsilon = 0.42$; $\alpha \tau = .846$ (NON SELECTIVE)

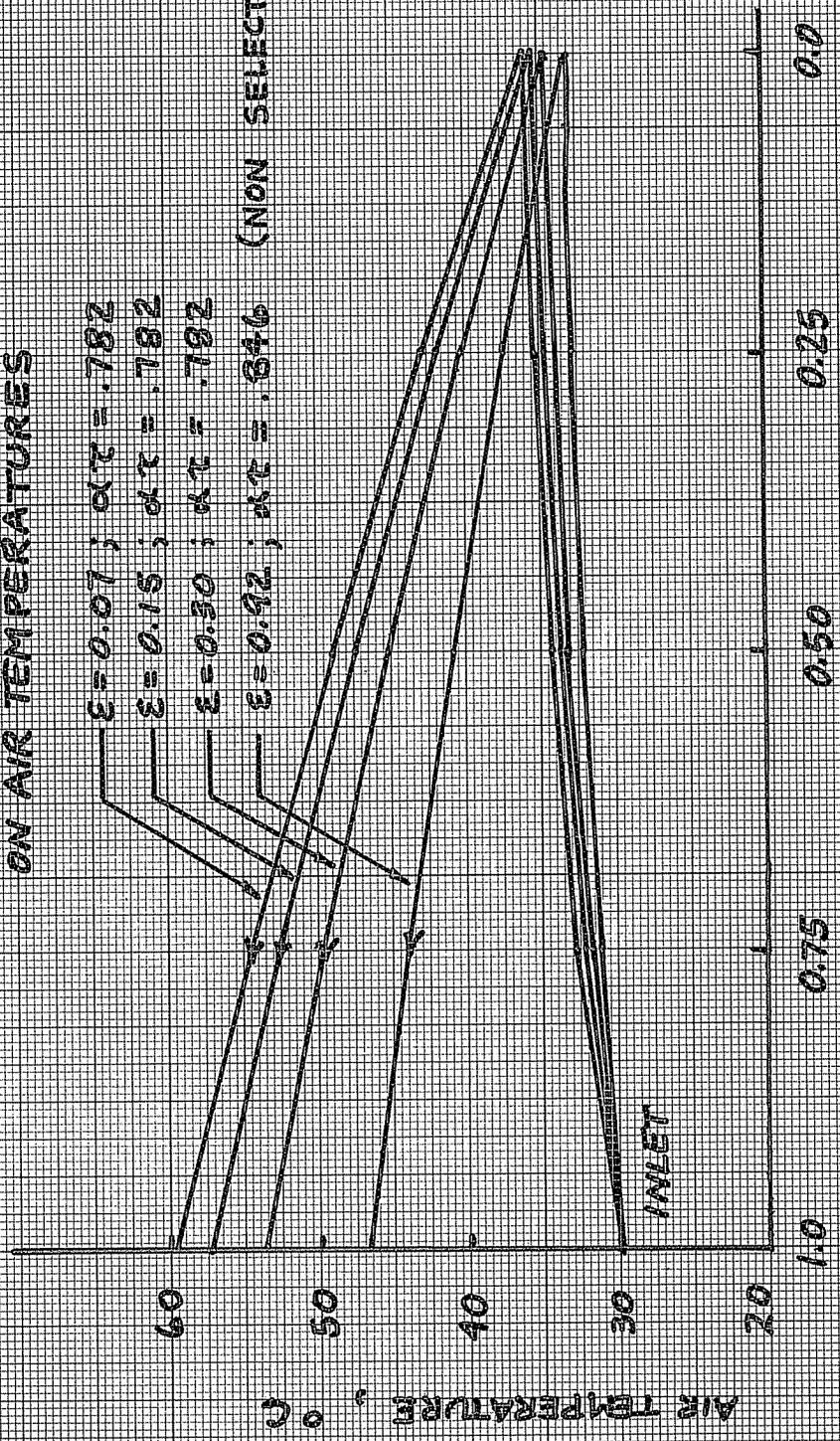


FIGURE 3.8.1 $\frac{X}{L}$, DISTANCE

EFFECT OF ABSORBER TUBE SOLAR ABSORPTANCE ON AIR TEMPERATURES

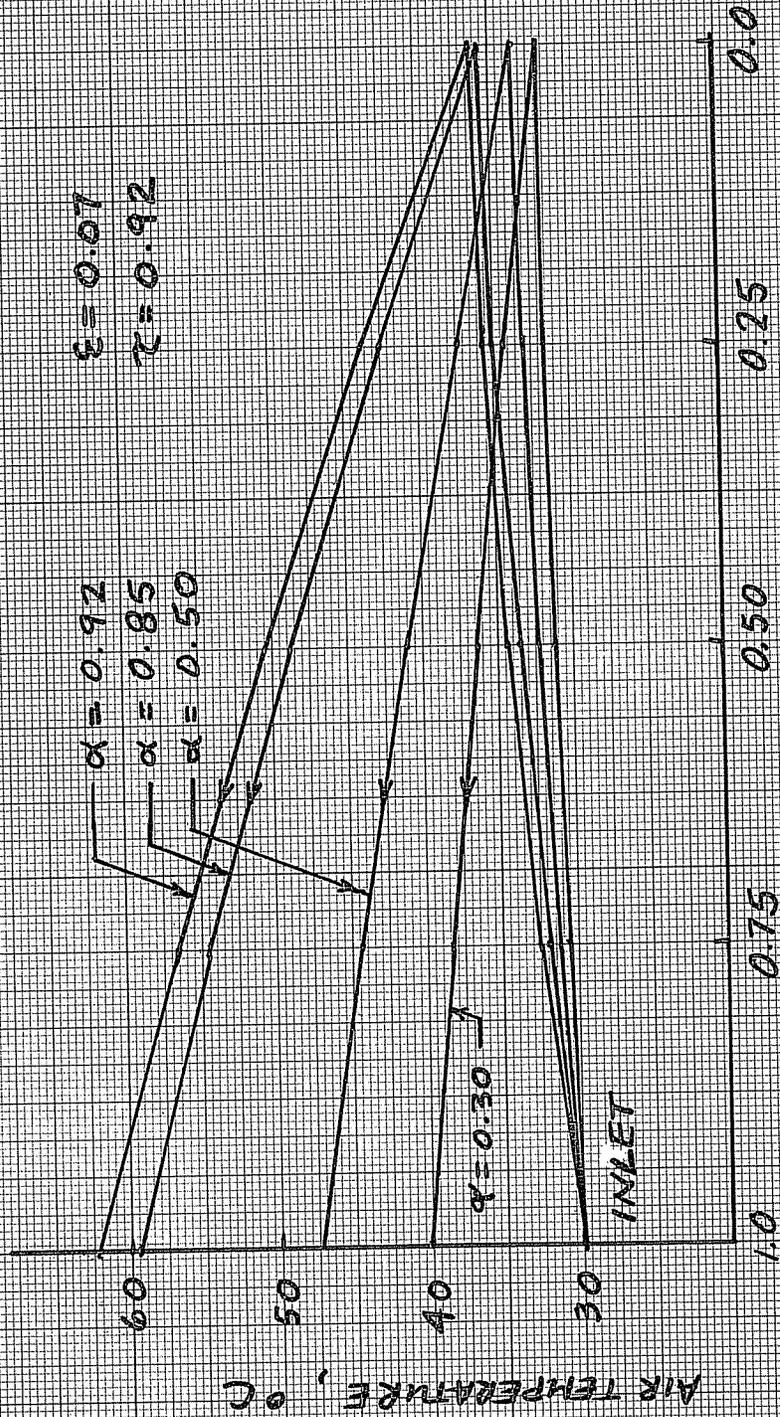


FIGURE 3.8.2 $\frac{X}{L}$, DISTANCE

4. DETERMINATION OF IMPORTANT PARAMETERS AFFECTING COLLECTOR TUBE PERFORMANCE

There are many variations of internal collector tube assembly and collector array operation that might have a significant effect upon the thermal performance of the collector arrays. Because collectors of this type are comparatively new, very few practical rules of thumb have been developed to optimize collector array performance, particularly when air is used as the working fluid. Some of the internal parameters that might be expected to have an important effect upon the collector tube output are:

1. Mass flow rate through each collector tube assembly.
2. Size of delivery tube (diameter).
3. Physical and surface properties of the delivery tube; thermal conductivity and long wave emittance.

For a fixed set of operating conditions, the inlet temperature, ambient temperature and incident solar radiation on the tube are specified. Because the losses from the absorber tube are radiative, it is apparent that the largest useful energy gain from a single collector tube will occur when the absorber tube is at the lowest possible temperature allowed by its internal construction and

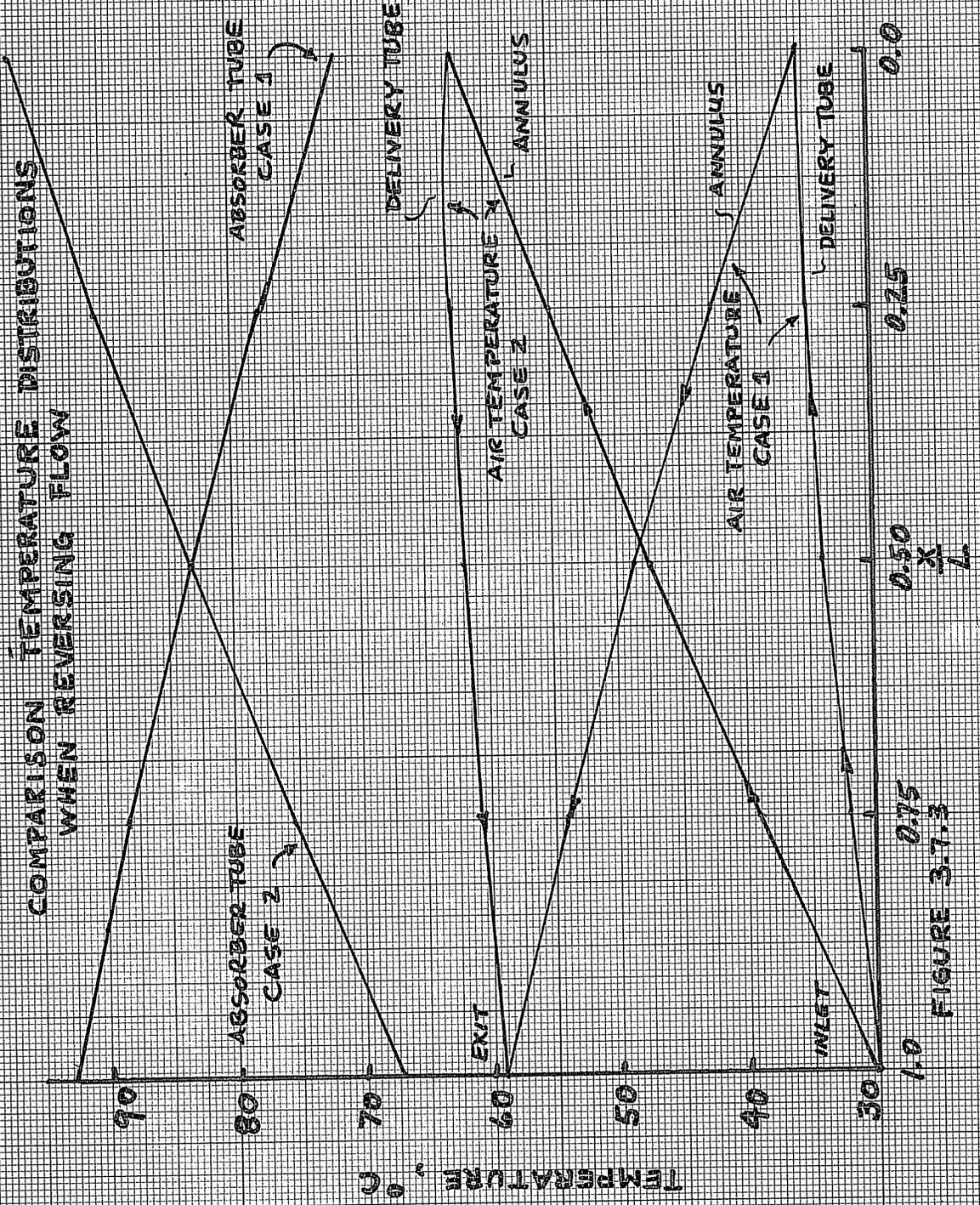


FIGURE 3.7.3

Figure 3.7.2 shows the absorber tube temperatures predicted by the three models. Comparing Figures 3.7.1 and 3.7.2, it can be seen that although the absorber tube temperatures vary with the different methods used, the difference in useful energy gain for this set of operating conditions is very small.

Figure 3.7.3 shows the predicted temperature distributions for case 1 and case 2 when the flow paths are reversed. The air temperatures and absorber temperatures are shown.

The collector dimensions and operating parameters are the same as in Table 3.7.1. The model assumes that the convection coefficients h_1 , h_2 and h_3 are independent of length.

3.8 Effects of the Surface Properties of the Absorber Tube

All of the useful energy that is supplied by an operating collector tube is incident on the absorber tube and transferred to the air stream by a combination of different heat transfer mechanisms. It was considered worthwhile to investigate briefly what effect changes in the values of the absorber tube solar absorptance and long wave emittance would have on the useful energy gain of the collector tube for some specific sets of operating conditions.

operation. The internal heat transfer in the tube is a combination of convection from the absorber and delivery tube to the air, radiation from the absorber tube to the delivery tube, and combined conduction and convection through the delivery tube to the air inside the tube. It is expected that changing the mass flow rate, the diameter of the delivery tube, and the material from which the delivery tube is made will change the temperature gradients inside the collector and affect the useful energy output.

A rigorous treatment and explanation of all possible variations of these three parameters over all the operating conditions that are likely to be encountered in a working solar system would be extremely difficult. When air is used as the working fluid, the allowable flow rates through the tubes will be determined by the pressure drops down the inlet and exit manifolds connecting the different collector tubes. Because one purpose of this study was to arrive at a reasonable model for predicting the performance of Owens-Illinois evacuated tubular collectors for inclusion on the Arlington House Project, calculations of the effects of these internal parameter changes were based on the dimensions and physical properties of the currently manufactured O-I collector tubes as reported by Beekley et al. [1]. The range of mass flow rates investigated repre-

sents the current estimates by Grunes [7] of the allowable flow rates that are compatible with manifold designs consistent with the physical limitations and heating requirements of the Arlington House. For a complete description of the Arlington House project, see Hughes [8].

4.1 Effect of Uncertainty of Convection Coefficients on Collector Tube Performance

Heat transfer by convection in the collector tube assembly occurs both in the delivery tube and in the annulus formed by the delivery tube and absorber tube. The heat transfer correlations used for determining the convection conductances should logically be based upon correlations developed for circular tubes and concentric circular annuli. Analytic solutions for flow through circular tubes and for flow through concentric circular annuli are available for both laminar and turbulent flow. For fully developed laminar flow in circular tubes, Kays [5] and Kays and London [9] give Nusselt number correlations for the cases of constant heat rate per unit of tube length and for constant wall temperature. For fully developed turbulent flow in circular tubes, Kreith [6] gives several different Nusselt number correlations and Kays and London have graphical correlations for the case of constant heat

rate per unit of tube length. For flow between concentric circular annuli, Lundberg, Reynolds and Kays [10] consider hydrodynamically fully established laminar flow with constant and variable wall temperatures and heat fluxes. Kays and Leung [11] present experimental data and graphical solutions for hydrodynamically developed turbulent flow in annular passages with arbitrarily prescribed heat flux. Most of the solutions for the annulus are presented either in graphical or tabular form, and are not very convenient for use when investigating the effects of changing flow rate and delivery tube size on the collector tube thermal performance over a wide variation of collector operating conditions. To explicitly handle the non-equal heat fluxes on the inner and outer surfaces of the annulus, in the manner as presented by Kays [5], it is necessary to know the ratio of heat fluxes on both surfaces, the single heated surface Nusselt numbers Nu_{ii} and Nu_{oo} , and the influence coefficients θ_i and θ_o . The following equations from Kays [5] relate these quantities:

$$Nu_i = \frac{Nu_{ii}}{1 - (q_o''/q_i'')\theta_i} \quad 4.1.4$$

$$Nu_o = \frac{Nu_{oo}}{1 - (q_i''/q_o'')\theta_o} \quad 4.1.2$$

where

$$q_i'' = h_2(T_w - T_m) \quad 4.1.3$$

$$q_o'' = h_3(T_3 - T_m) \quad 4.1.4$$

and

$$Nu_i = \frac{h_2 D_H}{k} \quad \text{and} \quad Nu_o = \frac{h_3 D_H}{k} \quad 4.1.5$$

where T_m is the mean fluid temperature in the annulus

D_H is the hydraulic diameter of the annulus

($D_H = \text{Outer diameter} - \text{inner diameter}$)

Because the heat flux ratios are usually unknown inside the collector assembly they must be iteratively solved for. Considering the convection coefficients h_2 and h_3 separately complicates the solution for the useful energy output. Conceptually this can be easily incorporated into the general iteration scheme outlined in Section 3.5 by evaluating the mean absorber and delivery tube temperatures, after solving for the fluid temperature distribution using suitable initial estimates for the coefficients, h_2 and h_3 . The ratios of the heat fluxes on each surface can be found from 4.1.3 and 4.1.4; improved estimates of Nu_i and Nu_o can be obtained by using 4.1.1 and 4.1.2, and new estimates of h_2 and h_3 are found by using eq. 4.1.5. The fluid temperature distributions are recalculated using the new values

for h_2 and h_3 , and the entire process is repeated until outlet temperature convergence is obtained. Practically, however, using this method is inconvenient because either laminar or turbulent flow can occur in the annulus, and correlations for Nu_{ii} , Nu_{oo} , θ_i and θ_o are usually available only in graphical form for specific radius ratios of the inner and outer tubes, and for specific Reynolds numbers. Obtaining the values for any possible flow rate or delivery tube diameter of interest becomes quite difficult then.

The sensitivity of the useful energy gain of a collector to the magnitudes of the heat transfer coefficients h_1 , h_2 and h_3 was investigated over a wide range of collector operating conditions for different mass flow rates through the collector assembly. The collector dimensions used were the same as given in Table 3.7.1. The operating conditions and internal collector parameters investigated were:

Collector inlet temperature:	17°C to 117°C
Ambient temperature:	-30°C to +40°C
Incident solar radiation, S_{eff} :	25 W/m ² to 1000 W/m ²
Selective surface:	$\epsilon = 0.07$
Delivery tube:	OD = 0.0230 m
	ID = 0.02143 m

Delivery tube characteristics: $k=47.6 \text{ W/m}^{\circ}\text{C}$; $\epsilon=0.23$

$k=1.0 \text{ W/m}^{\circ}\text{C}$; $\epsilon=0.90$

Mass flow rates: 2, 4, 8, 12 kg/hr

The method used to calculate the collector performance assumed that the heat transfer coefficients h_1 , h_2 and h_3 were constant with length and that h_2 and h_3 were equal.

The heat transfer correlations used were:

Laminar Flow; $Nu = 4.9$ 4.1.7

Turbulent Flow; $Nu = 0.0158 Re^{0.8}$ 4.1.8

Each different heat transfer coefficient was varied by 50% from the values predicted by the above equation (i.e., if $h_1=10 \text{ W/m}^2\text{C}$, then $h_1=15 \text{ W/m}^2\text{C}$ was also used) and the useful energy gains calculated and compared. For all cases and operating conditions, this wide variation in the magnitude of the heat transfer coefficient produced only small changes in the useful energy gain from the collector. When the useful energy gains from the high and low estimates were compared to the original calculations using the simplified relationships above, the following maximum deviations in useful energy gain were obtained.

1. $\dot{m} = 2 \text{ kg/hr}$; delivery tube $k=47.6 \text{ W/m}^{\circ}\text{C}$

(galvanized steel) $\epsilon=0.23$

the maximum increase in useful energy gain when the heat transfer coefficients were 50% high was

1%, the maximum decrease when the coefficients were

problem of determining the useful energy output of the collector tube assembly. The effect of the boundary layer development at the tube entrances is to give heat transfer rates higher than would occur if fully developed flow was present. In general, it is advisable to use conservative estimates for the heat transfer coefficients h_1 , h_2 and h_3 , as this will tend to underestimate the collector assembly's useful energy output.

The collector model that is used for the remainder of this work assumes that the heat transfer coefficients h_1 , h_2 and h_3 are independent of length, and that $h_2=h_3$. The heat transfer correlations used are:

$$\text{Laminar flow: } Nu = 4.9$$

$$\text{Turbulent Flow: } Nu = 0.0158 Re^{0.8}$$

These correlations and collector model are used because they are the simplest to evaluate, and the results are not expected to be significantly different from the results obtained if a much more complex model is used to calculate the useful energy output of a collector tube. The actual deviations in useful energy output from using these correlations is not expected to be as large as shown in the examples.

4.2 Effects of Delivery Tube Material and Surface Properties

The composition and surface properties of the delivery tube affect the internal heat transfer in two ways:

1. The higher the thermal conductivity of the delivery tube, the greater the thermal coupling between the two flow streams.
2. The radiation heat transfer between the absorber tube and delivery tube is controlled by the emittance of the delivery tube because the absorber tube inner surface is glass and has a high emittance.

Beekley and Mather [1] define a thermal coupling parameter, λ_1 , in their analysis of the O-I collectors using a liquid as the heat transfer medium. This parameter accounts for the effect of the heat transfer to the delivery tube fluid from the fluid in the annulus and its effect on the performance of the collector. When liquids are used, the effect of this thermal coupling is to elevate the fluid temperature in the annulus and delivery tube higher than it would be if the delivery tube were perfectly insulated. Because all heat transferred from the absorber tube to the tube interior is by convection to the liquid, the

increase in fluid temperature in the annulus means that the absorber tube is operating at a correspondingly higher temperature, and the useful energy gain is reduced.

Figure 4.2.1 is a qualitative graph, similar to that of Beekley et al [1] showing the effects of thermal coupling when a liquid is used in a collector tube under typical operating conditions. The solid lines are the liquid temperatures as functions of length for a high and low flow rate. The dashed lines indicate the temperature distributions to be expected if the delivery tube is perfectly insulated. The magnitude of the useful energy reduction when coupling occurs depends upon the specific operating conditions, but is, in general, small because of the low emittance of the selective surface and evacuated cover systems.

When air is used as the working medium there is an additional heat transfer mechanism between the absorber tube inner surface and the delivery tube that is not present when a liquid is used. During collector operation, heat is removed from the absorber tube by a combination of radiation to the delivery tube and convection to the air within the annulus. Thermal coupling between the flow streams also occurs when air is used, but the overall effect on the final absorber tube temperature is fundamentally different because the mechanisms of convection and radiation

EFFECT OF THERMAL COUPLING WHEN A LIQUID IS USED AS THE HEAT TRANSFER MEDIUM

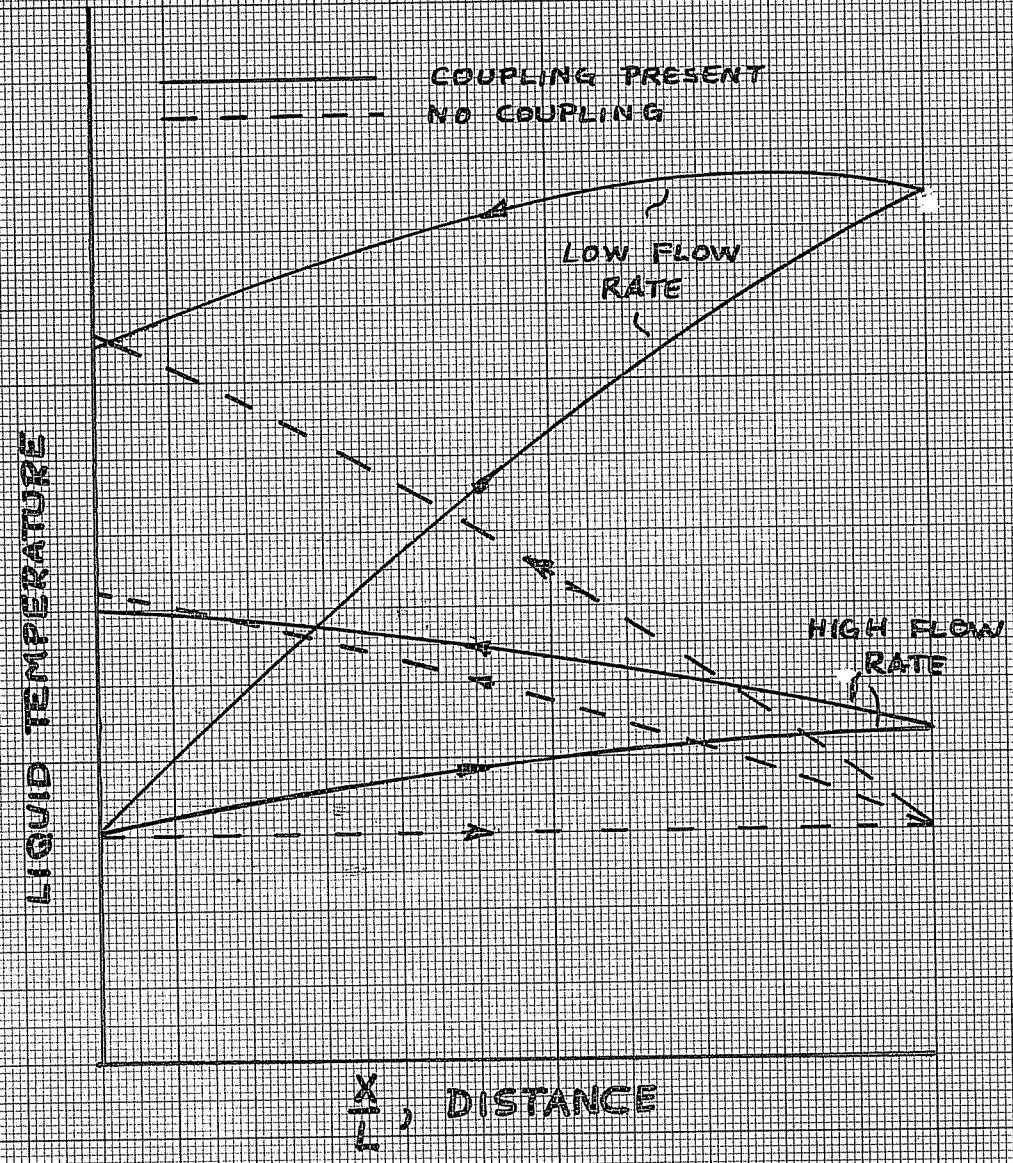


FIGURE 4.2.1

EUGENE DIETZGEN CO.
MADE IN U. S. A.

NO. 341-M DIETZGEN GRAPH PAPER
MILLIMETER

tend to offset each other. When the flow rate is high, the film coefficients between the air in the annulus and the absorber and delivery tubes are also comparatively high and the temperature differences between the absorber tube and delivery tube are low, thus decreasing the radiation transfer between the two tubes. If the flow rates are low, the convection coefficients are low, the temperature differences between the two tubes would be expected to rise and the radiation transfer between the two tubes would increase. Because both mechanisms occur simultaneously, the overall effect of the flow rate dependence of thermal coupling and its effect on the final temperature of the absorber tube depends upon the radiation properties of the delivery tube. The higher the emittance of the delivery tube, the larger the possible radiation transfer between the surfaces for a given set of operating conditions. The emittance of the delivery tube can then be expected to have an effect on the internal temperature distributions within the collector tube assembly.

Figures 4.2.2 and 4.2.3 show the effects of changing the properties of the delivery tube on the air temperature distribution and the delivery tube temperatures. The collector dimensions and operating conditions are the same as given in Table 3.7.1. Three types of delivery tubes are used, having the same outside and inside diameters, but

EFFECT OF DELIVERY TUBE PROPERTIES
ON AIR TEMPERATURES

- $k = 47.6 \text{ W/m}^\circ\text{C}; \epsilon = 0.23$
- - - $k = 47.6; \epsilon = 0.90$
- $k = 0.001; \epsilon = 0.90$

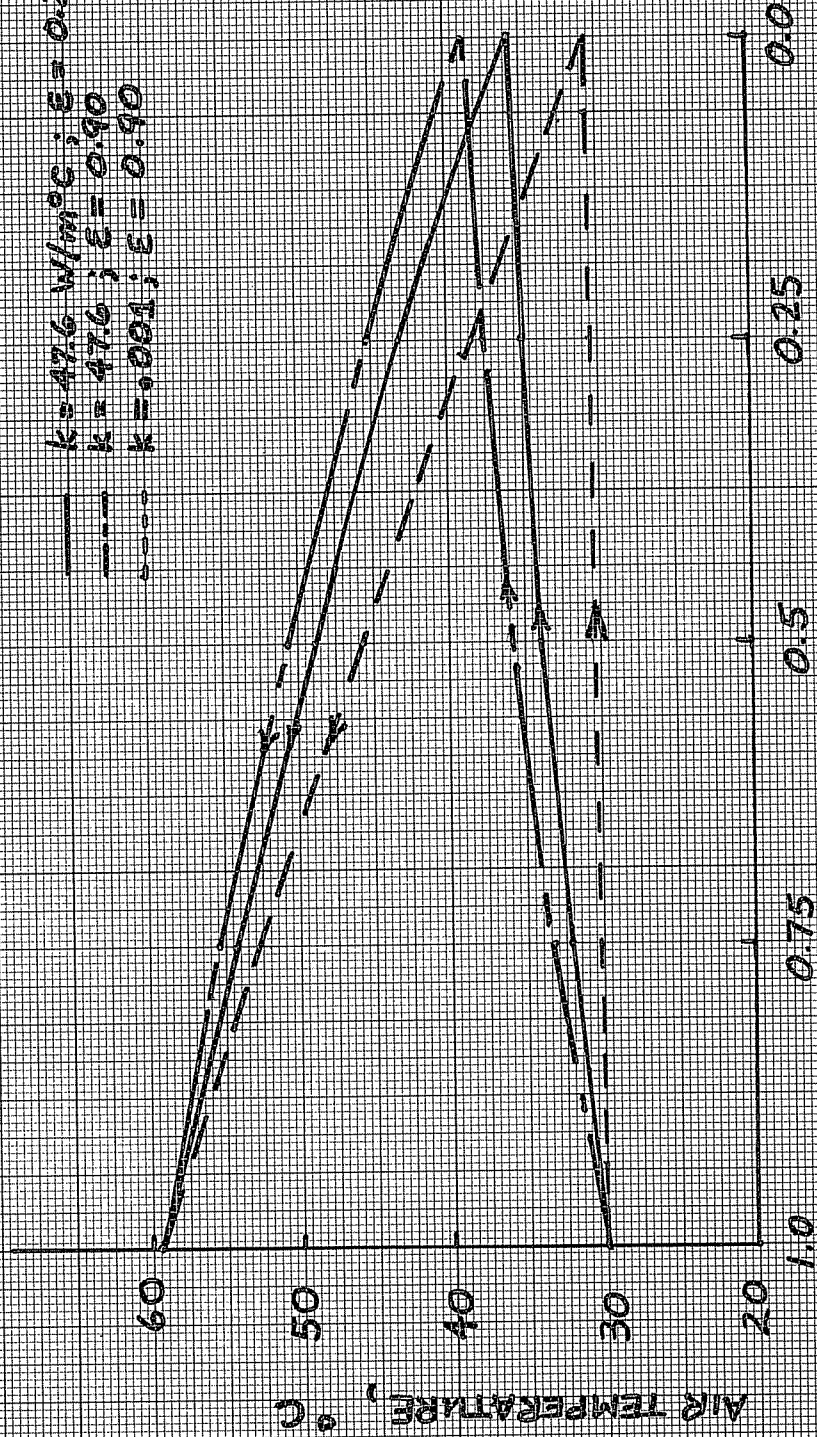


FIGURE 4.2.2 $\frac{X}{L}$, DISTANCE

EFFECT OF DELIVERY TUBE PROPERTIES ON DELIVERY TUBE TEMPERATURES

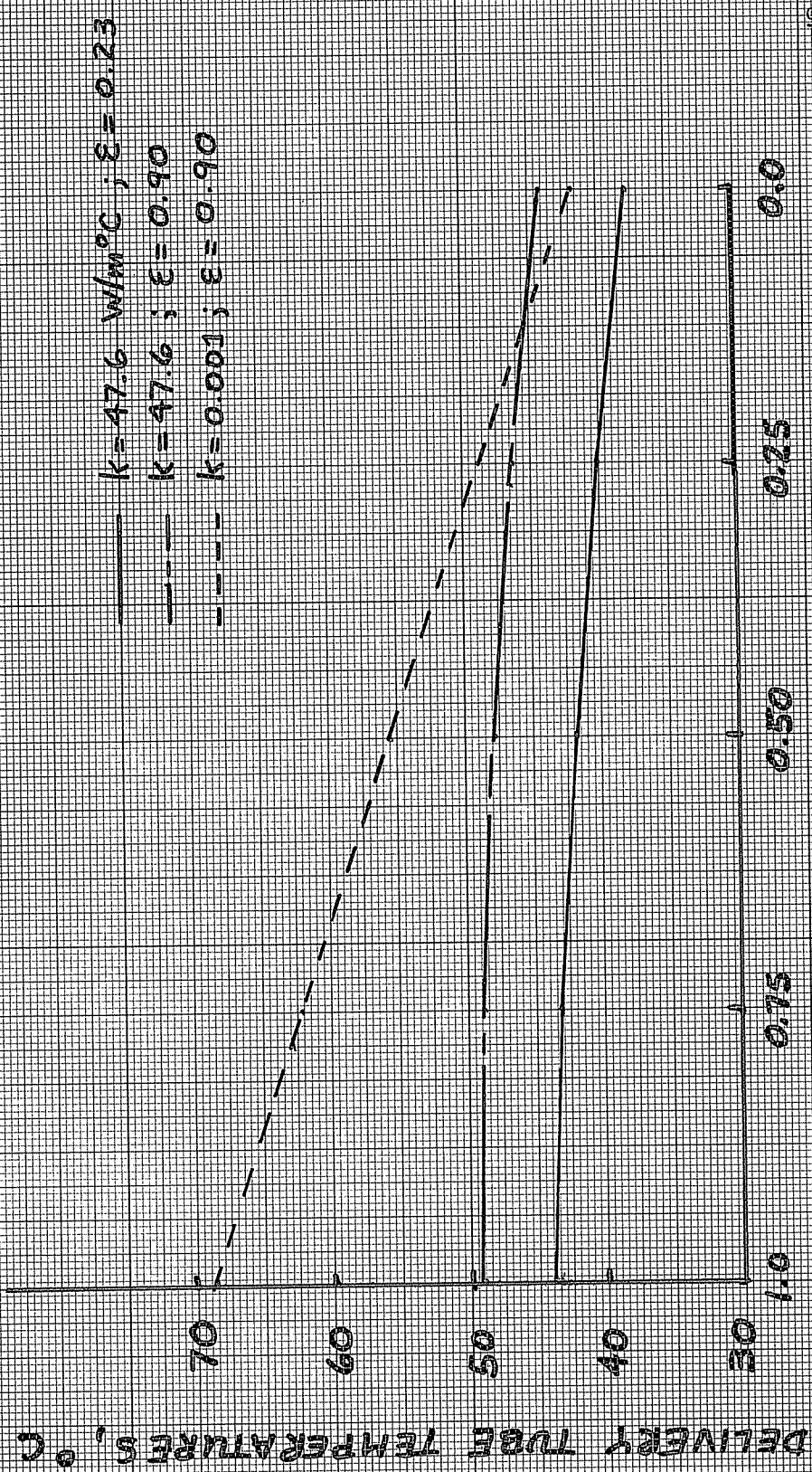


FIGURE 4-2.3 $\frac{X}{C}$, DISTANCE

differing in their thermal conductivities and emittances.

The tubes used were:

1. thermal conductivity, $k=47.6 \text{ W/m}^\circ\text{C}$; emittance $\epsilon=0.23$. This corresponds to a galvanized steel delivery tube.
2. $k=47.6 \text{ W/m}^\circ\text{C}$; $\epsilon=0.90$. This corresponds to a steel delivery tube painted with an absorbing black paint.
3. $k=.001 \text{ W/m}^\circ\text{C}$; $\epsilon=0.90$. An unknown material simulating a very good thermal insulator having a high emittance.

The differences in air temperatures as shown in Figure 4.2.2 are significant for all three cases. The difference between the steel tube with emittance of 0.23 and the steel tube with an emittance of 0.90 is due entirely to the different magnitudes of the radiation exchange between the absorber tube and delivery tube. Figures 4.2.2 and 4.2.3 show that both the delivery tube temperature and the air temperatures in the annulus are higher for the tube with $k=47.6$; $\epsilon=0.9$ than for the tube with $k=47.6$; $\epsilon=0.23$. The mean absorber tube temperature (not shown) is slightly lower for the high emittance steel tube case than for the tubes with the low emittance. Consequently, the useful energy gain for the high emittance steel tube is slightly

higher than for the low emittance steel delivery tube. The delivery tube with $k=0.001$; $\epsilon=0.9$ has the highest delivery tube temperature and the lowest absorber tube temperature, and as a result, a useful energy output fractionally higher than the other two cases. The point to be made is that increasing the delivery tube emittance can be expected to increase the delivery tube temperatures and fluid temperatures above those if the delivery tube had a low emittance. Unlike a liquid, however, the increase in fluid temperature in the annulus is accompanied by a reduction in the mean absorber tube temperature, resulting in a slightly higher useful energy output from the tube.

Because of the opposite effects of convection and radiation between the delivery tube and the absorber tube, no single parameter analogous to Beekley and Mather's thermal coupling parameter has been found at present. The combined effects are included in the equations for the fluid temperature distributions given by Eq. A-2.2.1 and A-2.2.2, however.

It is interesting to note that the useful energy gain of all three collector tube assemblies is almost identical for this set of conditions. It was expected that a high emittance delivery tube would give slightly better thermal performance under most circumstances than a low emittance tube. The magnitude of the useful energy increase, however, when investigated over a wide range of flow rates and

operating conditions, was fairly small. The useful energy increase was never greater than 2.5% for a tube with emittance of 0.90 when compared to a tube with emittance of 0.23; this occurred at low flow rates and high radiation and inlet temperature levels. For other cases, this increase was typically under 1%. This small variation is caused primarily by the low emittance of the absorber tube selective surface and the evacuated cover tube system, which allows the internal temperatures in the collector tube assembly to change significantly while affecting the useful energy output only slightly.

4.3 Effects of Mass Flow Rate and Delivery Tube Diameter on Collector Tube Performance

Changing the air flow rate and delivery tube diameter can be expected to have important effects on the useful energy gain from the collector tube assembly. For a given set of operating conditions, increasing the mass flow rate will decrease the overall temperature level of the collector for two reasons. First, increases in flow rates mean corresponding increases in fluid velocities resulting in higher heat transfer coefficients between the air and the absorber tube. Second, thermal coupling between the two flow streams is dependent upon the magnitude of the resis-

tance to heat transfer through the delivery tube wall. As the flow rate is increased, the finite resistance of the delivery tube becomes more limiting in the overall effect of coupling between the two streams.

The diameter of the delivery tube will have an effect upon the thermal performance. As the outer diameter of the delivery tube is increased, the cross sectional area of the annulus decreases and the air velocities increase. This will affect the convection coefficients between the air in the annulus and the absorber tube as well as increase the area for heat transfer by radiation from the absorber tube and convection from the fluid in the annulus. The overall effect of increasing the delivery tube outer diameter is expected to increase the useful energy output of the collector tube.

The effects of mass flow rate and delivery tube diameter were numerically investigated over the following range of collector operating conditions:

Ambient temperature: -30°C to $+40^{\circ}\text{C}$

Inlet temperature: 17°C to 117°C

S_{eff} , incident solar radiation: 25 W/m^2 to 1000 W/m^2

Selective surface emittance: $\epsilon = 0.07$

Two collector tube assemblies were connected in series where the outlet stream from one tube was the inlet stream to the next tube. For the cases where the mass flow rate was

varied the delivery tube was galvanized steel ($k=47.6$, $\epsilon=0.23$) with an OD of 0.0243 m and ID of 0.02143 m. For this delivery tube, the useful energy gains were calculated for flow rates of 2, 4, 8 and 12 kg/hr, and the reductions in useful gain referenced to the largest flow rate of 12 kg/hr. These results are summarized below:

$\dot{m} = 8$ kg/hr - tube pair - minimum output reduction approximately 2%; maximum reduction 7%, occurring at large inlet-ambient temperature differences and high solar radiation levels.

$\dot{m} = 4$ kg/hr - minimum reduction of 6% occurring at small temperature differences; maximum reduction 16% occurring at large temperature differences

$\dot{m} = 2$ kg/hr - minimum reduction of 11% occurring at small temperature differences; maximum reduction over 30% occurring at high temperature differences and high radiation levels.

The effect of delivery tube diameter was investigated over the same range of operating conditions but with four different sized delivery tubes.

Delivery Tube 1. .0350 m OD, .03343 m ID

Delivery Tube 2. .0300 m OD, .02843 m ID

Delivery Tube 3. .0230 m OD, .02143 m ID

Delivery Tube 4. .0150 m OD, .01343 m ID

Flow Rate: 8 kg/hr - tube pair

Delivery Tube Properties:

$k = 47.6 \text{ W/m}^\circ\text{C}; \epsilon = 0.23$ (galvanized steel)

$k = 1.05 \text{ W/m}^\circ\text{C}; \epsilon = 0.90$ (glass)

The magnitudes of the changes of the useful output due to delivery tube size are not as significant as the output reductions caused by decreasing the flow rate. The largest diameter delivery tube outperformed the smaller tubes in all instances:

Tube 2 - typical useful energy reduction	1.5%
Tube 3 - typical reduction	2.5% - 3.0%
Tube 4 - typical reduction	3% - 5%

The change in useful energy gain due to the surface emittance of the delivery tube was quite small, generally less than 1% for all tube sizes and ranges of inlet temperature, ambient temperature and incident solar radiation. The delivery tube was thin enough so that the resistance to heat transfer through the tube, for either glass or steel, was always small enough so that appreciable thermal coupling between flow streams took place. The differences in output due to the changes in thermal conductivity were less significant than the changes caused by the surface emittance of the delivery tube on the useful energy gain.

The results showing the numerical effects of changes in flow rate and delivery tube size should probably be viewed qualitatively rather than quantitatively because actual flow rate and delivery tube selections will be determined by the particular manifold design used for distribution of the air to all the collector tubes in an array. The manifold design is in turn dependent upon architectural and economic considerations.

5. SIMPLIFIED MODELS FOR USE IN SOLAR SYSTEM SIMULATIONS

A solar collector array consisting of many evacuated tubular collectors is only one component that can be used in a typical solar heating or cooling system. Numerically predicting the long term performance of the entire solar system is frequently desired as it offers one direct way of evaluating and comparing the advantages and disadvantages of one system design with another. Solar collectors operate over wide ranges of outdoor conditions; large daily and seasonal variations of ambient temperature and solar radiation occur that will affect the performance. Different system configurations will also affect the useful energy gain of the collector. A simplified numerical model of an evacuated tubular collector array for use in long term solar system simulations is desirable because it can significantly reduce the computations necessary to obtain reasonably accurate estimates of the overall system performance.

Simplified models of the collector tube performance can be of two different forms. One type of model can result from making simplifying assumptions about the internal heat transfer mechanisms. Another type of numerical simplification is to use graphical or multidimensional interpolation approaches to determine the collector performance when needed.

5.1 Comparison of Linear Model with Analytic Model

The linear model of a single collector tube assembly, as formulated in Section 3.6, gives excellent agreement when compared with the more general model, for a wide variation of collector operating conditions. The linear model was checked with the analytic model for the following ranges of conditions:

Ambient temperature:	-30°C to +40°C
Collector inlet temperature:	17°C to 117°C
Incident Solar Radiation:	25 W/m ² to 1000 W/m ²
Mass flow rates:	8,4,2 kg/hr - tube
Delivery tube size:	0.0230 m OD 0.02143 m ID
Delivery tube properties:	steel tube, low emittance
Methods of manifolding:	single tube, two tubes in series

The comparisons over this range of operating conditions and internal parameters show that the linear model differs from the analytic model by less than 2%. The maximum deviations occurred at the slower flow rates (2 kg/hr - tube) and at very high solar radiation levels. For the higher flow rates (4 and 8 kg/hr - tube) the deviation was always less than 1% for all operating conditions.

The linear model can then be used in place of the analytic model to predict the collector tube assembly's

useful energy output without introducing significant error. It can directly account for the thermal coupling between the two flow streams as does the analytic model. The chief disadvantage of this method is that although it offers some computational simplicity it still requires an iterative solution to improve initial estimates of the absorber tube and delivery tube temperatures.

5.2 Effects of Neglecting Thermal Coupling Between the Two Flow Streams

The effects of thermal coupling between the flow stream in the annulus and the flow stream in the delivery tube were explained in Section 4.2. It was noted for one example that although the internal temperature profiles were quite different when thermal coupling occurred from the profiles when no coupling was present, the useful energy gain was almost the same. It was considered worthwhile to investigate under what conditions the thermal coupling between the flow streams can be neglected, and to determine the magnitude of the error that neglecting the coupling will cause.

Although no single parameter has been found to explain the effects of the coupling, some general observations can be made. For any set of collector tube operating conditions (fixed internal geometry, with ambient temperature,

inlet temperature, and incident solar radiation known), the adverse effect of thermal coupling between the flow streams will increase as the mass flow rate decreases. The radiation transfer between the delivery tube and absorber tube increases as the flow rate decreases and tends to offset this adverse effect. Because a collector with a perfectly insulated delivery tube with a high emittance can be expected to have the best thermal performance for a given set of operating conditions, a "worst case" for thermal coupling is, by implication, a delivery tube with a high thermal conductivity and a relatively low emittance.

Numerical comparisons were made for the thermally coupled and uncoupled flow streams for the ranges of immediate interest for use in the Arlington House simulations.

The ranges of operating conditions used were:

Ambient temperature:	-30°C to +40°C
Inlet temperature:	17°C to 117°C
Incident solar radiation:	25 W/m ² to 1000 W/m ²
Mass flow rates:	2,8,12 kg/hr - tube
Delivery tube size:	.0230 m OD, .02143 m ID
Delivery tube properties:	k=47.6 W/m°C; ε = 0.23
Method of manifolding:	two tubes in series
Absorber surface emittance:	ε = 0.07

The decrease in useful energy gain for the thermally coupled streams were:

$\dot{m} = 2$ kg/hr - tube; maximum performance decrease approximately 6%, occurring at high radiation levels and high inlet temperatures

$\dot{m} = 8$ kg/hr - tube; maximum performance decrease less than 0.5% for all operating conditions

$\dot{m} = 12$ kg/hr - tube; maximum performance decrease 0.4% for all operating conditions

These results show that the effect of thermal coupling increases as the flow rate decreases, but at high enough flow rates the effect of the coupling on the overall thermal performance is almost negligible. This is due to the low value of the emittance of the selective surface of the absorber tube. Since all the losses are assumed to be radiative, elevating the mean fluid temperature in the annulus through the effect of thermal coupling above its mean temperature if coupling were not present decreases the useful energy output of the tube only slightly.

When the effect of thermal coupling is not significant on the collector useful energy output, the collector can be modeled as having an insulated delivery tube with flow passing only through the annulus between the absorber tube and the delivery tube. Modeling the collector performance in this manner will give internal temperature distributions that are different than those found if coupling is considered, but give the correct useful energy output.

5.3 F_R , Collector Heat Removal Factor

A convenient algebraic relationship for expressing the useful energy gain for a conventional flat plate collector as used in Duffie and Beckman [3] is:

$$Q_u = A_c F_R [S - U_L (T_{in} - T_{amb})] \quad 5.3.1$$

where A_c is the collector area

S is the solar radiation absorbed by the absorber plate

U_L is the collector loss coefficient

T_{in} is the collector inlet temperature

T_{amb} is the ambient temperature

F_R is a factor which relates the useful energy gain of a collector to the useful energy gain if the whole collector surface were at the fluid inlet temperature

It is possible to put the useful energy gain from an evacuated glass tubular collector array in a similar form

$$Q_u = A_t N_t F_R [\alpha \tau S_{eff} - U_L (T_{in} - T_{amb})] \quad 5.3.2$$

where N_t is the number of collector tube assemblies connected in parallel through each of which a uniform mass flow rate passes

A_t is the total absorber tube surface area of all collector tube assemblies in any series connected branch of the collector array

U_L is the collector loss coefficient based on mean absorber temperature of the tubes connected in series.

Because the useful energy gain of the collector array is

$$Q_u = N_t \dot{m} c_p (T_{out} - T_{in}) \quad 5.3.3$$

where T_{out} is the outlet temperature of each series connected assembly of collector tubes

\dot{m} is the mass flow rate

T_{in} is the inlet temperature to each series connected assembly of tubes

then

$$F_R = \frac{\dot{m} c_p (T_{out} - T_{in})}{A_t [\alpha \tau S_{eff} - U_L (T_{in} - T_{amb})]} \quad 5.3.4$$

When there is more than one collector tube connected in series (the outlet of one collector tube is the inlet to another tube assembly) the temperature T_{out} can be formed by successive evaluations of eq. 3.4.10. For long term simulations, this method is not particularly convenient, as an iterative procedure is required to accurately determine the outlet temperature from each collector tube

assembly.

It was shown that the effect of the thermal coupling over a wide variation of operating conditions was quite small for collectors with high enough flow rates. Modeling the collector tubes as having flow only through the annulus formed by the absorber tube and delivery tube is analogous to modeling a conventional flat plate air heater where the air flows between the absorber plate and an insulated backing plate. Except for corrections made for the circular geometry, this flow situation can be modeled exactly as done by Duffie and Beckman [3]. Their procedure will be outlined briefly. The thermal network for this case is shown in Figure 5.3.1.

1. Energy balances are made on the absorber tube and on the air within the annulus and expressions for the local useful energy gain, q_u , are obtained. The resulting equations are

$$q_u = U_3(T_3 - T_f) \quad 5.3.5$$

$$\alpha \tau S_{\text{eff}} - U_L(T_3 - T_a) - q_u = 0 \quad 5.3.6$$

where U_3 is the overall heat transfer coefficient from the fluid to the absorber tube based on the absorber tube area

THERMAL NETWORK WHEN
COUPLING IS NEGLECTED

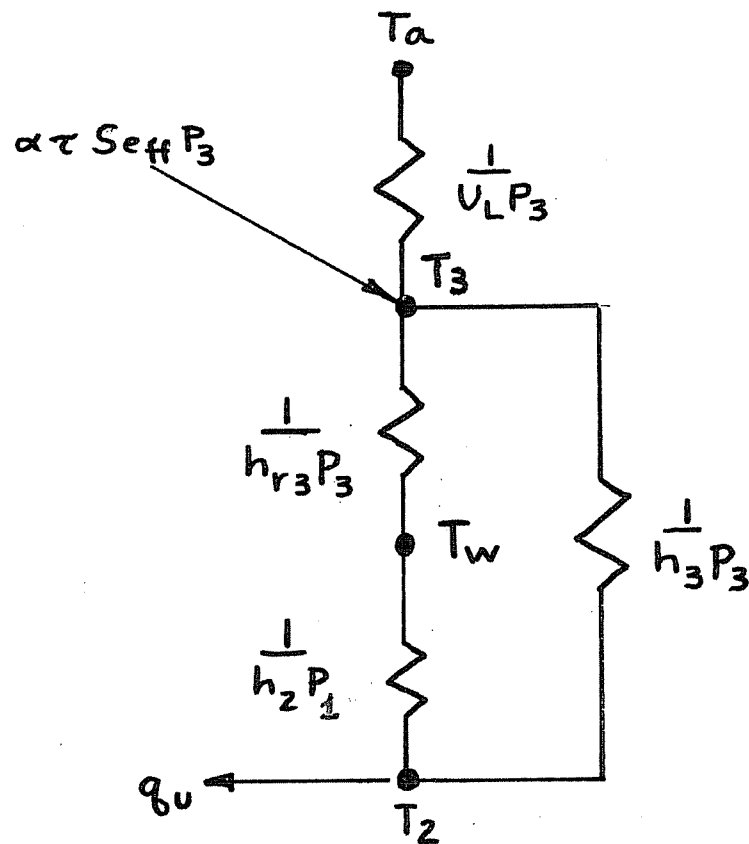


FIGURE 5.3.1

$$U_3 = h_3 + \frac{1}{\frac{1}{h_{r3}} + \frac{D_3}{h_2 D_1}} \quad 5.3.7$$

2. The local useful energy can be expressed as

$$q_u = F' [\alpha \tau S_{\text{eff}} - U_L (T_f - T_a)] \quad 5.3.8$$

where F' , the tube efficiency factor, is

$$F' = \frac{1}{1 + \frac{U_L}{U_3}} \quad 5.3.9$$

3. Now, F_R , the collector heat removal factor can be written as

$$F_R = \frac{\dot{m} c_p}{U_L A_t} [1 - e^{-[U_L F' A_t / \dot{m} c_p]}] \quad 5.3.10$$

4. For collector tube assemblies using air, U_L and F' are functions of temperatures. F' depends upon the convection coefficients and the surface temperatures and emittances of the delivery tube and absorber tube. Using suitable initial guesses for the average absorber and delivery tube temperatures, evaluating U_L , F' , and F_R , the outlet temperature can be calculated

$$T_{\text{out}} = T_{\text{in}} + \frac{A_t F_R [\alpha \tau S_{\text{eff}} - U_L (T_{\text{in}} - T_{\text{amb}})]}{\dot{m} c_p} \quad 5.3.11$$

5. The initial estimates of the absorber and delivery tube temperatures are improved by finding the mean fluid temperature using the relationship derived by Klein [12]

$$T_{f,\text{mean}} = T_{\text{in}} + \frac{Q_u/A_t}{U_L F_R} \left[1 - \frac{F_R}{F^+}\right] \quad 5.3.12$$

The mean absorber tube temperature is found:

$$T_{3,\text{mean}} = \frac{Q_u}{U_3 A_3} + T_{f,\text{mean}} \quad 5.3.13$$

and the mean delivery tube temperature is found from an energy balance on the delivery tube

$$T_{w,\text{mean}} = \frac{h_2 T_{f,\text{mean}} + h_{r3} \frac{D_1}{3 D_3} T_{3,\text{mean}}}{h_2 + h_{r3} \frac{D_1}{D_3}} \quad 5.3.14$$

Using the new estimates of T_w and T_3 , the outlet temperature of the collector is recalculated. The iteration process can be repeated until suitable convergence of the outlet temperature is obtained.

This method allows the flow inside a number of series-connected collector tubes to be treated as if the flow occurred inside a single tube, the length of the single equivalent tube being equal to the sum of the lengths of the separate tubes. When water is used as the heat transfer medium, and the effect of thermal coupling between the two flow streams is unimportant, this method can also be

used to predict the useful energy output. For this case, with no radiation exchange between the absorber tube and delivery tube, the series connected tubes can also be modeled as a single equivalent tube. Because the delivery tube can be considered to be insulated, it is at the same temperature as the local fluid temperature, and it is not necessary to solve for the delivery tube temperature.

5.4 Performance Map of Collector Efficiency

The numerical model of the collector tube assembly can be complex enough so that evaluation of the thermal performance for every changing set of inlet conditions seriously increases the number of computations in long term simulations of system performance.

A multi-dimensional "performance map" using interpolation can be used to good advantage in such a situation. The performance map separates the predictions of the collector array from the rest of the system simulation by calculating the useful energy gain of the collector assembly at discrete points over the range of the expected operating conditions of each independent variable. For the evacuated glass tubular collector with fixed geometry and known flow rate, the three variables that affect the useful

energy gain of the collector are inlet temperature, ambient temperature and solar radiation incident upon the collector tube. The efficiency of the collector tube assembly is calculated at selected values of inlet temperature to the collector, ambient temperature, and solar radiation, and these discrete efficiency values are stored in a three dimensional array and saved for later use. The collector output can be calculated for any combination of inlet temperature, ambient temperature, and incident solar radiation, when needed, by interpolation from this array.

The accuracy of the performance map in predicting the collector efficiency as compared to the actual model is controlled by both the number of discrete values used in constructing the performance map, and the degree of the interpolating polynomials used to calculate the efficiency from the array. The method used for all calculations to date has been three dimensional interpolation using quadratic interpolating polynomials. The interval spacing used was small enough so that the performance map introduced an error of collector efficiency of 0.5% or less for the range of inlet temperatures, ambient temperatures, or solar radiation levels considered.

The performance map can be used with a collector model of whatever degree of complexity is thought necessary and easily handle any method of collector array flow manifolding.

The initial calculation of the efficiency array can be done externally to the simulation program, and the useful output can be determined for any given set of inlet conditions when needed without requiring iteration.

5.5 Graphical Methods

A convenient graphical method for representing the thermal performance of either a single tube assembly or a number of series connected tube assemblies can be obtained when the collector tube efficiency, η , is plotted against the variable $T_{in}^3(T_{in}-T_a)/S_{eff}$, where T_{in} and T_a are absolute temperatures. If the useful energy output per unit of absorber area of the collector tube assemblies is put into the same form as used for a flat plate collector,

$$q_u = F_R[\alpha\tau S_{eff} - U_L(T_{in}-T_a)] \quad 5.5.1$$

dividing by S_{eff} ,

$$\eta = \frac{q_u}{S_{eff}} = \alpha\tau F_R - \frac{U_L F_R (T_{in}-T_a)}{S_{eff}} \quad 5.5.2$$

With flat plate collectors with a fixed flow rate, the efficiency is frequently plotted against the variable $(T_{in}-T_a)/S_{eff}$. If a straight line is drawn through the measured or calculated points, the intercept of the graph

is interpreted as being equal to $\alpha \tau F_R$ and the slope of the line as being equal to $-U_L F_R$. Because the losses from evacuated tubular collectors are entirely radiative, the collector assembly efficiency depends upon not only the temperature difference between the inlet air and the ambient temperature, but also on the temperature level of the collector assembly. When the predicted efficiency of an evacuated tubular collector is plotted against $(T_{in} - T_a)/S_{eff}$, as is done for a flat plate collector, the resulting graph shows considerable scatter and no unique curve is obtainable. When the efficiency is graphed versus $T_{in}^3 (T_{in} - T_a)/S_{eff}$, in an attempt to account for the temperature level dependence of the collector losses by estimating U_L with T_{in}^3 , the resulting graph exhibits considerably less scatter than before. Figures 5.5.1 and 5.5.2 show graphs of η vs $T_{in}^3 (T_{in} - T_a)/S_{eff}$ for a pair of series connected collector tubes with flow rates of 15.9 kg/hr and 6.14 kg/hr. The predicted points are indicated, showing the degree of scatter present. Figure 5.5.3 shows straight line fits to the predicted values of efficiency for flow rates of 15.9, 8.18 and 6.14 kg/hr. The figures show that the curves can be represented reasonably well with a single straight line.

For all graphs, the operating conditions varied from

Inlet temperature:	-17°C to 117°C
Ambient temperature:	-30°C to +40°C
Incident solar radiation:	100 W/m ² to 650 W/m ²
Collector dimensions:	given in Table 3.7.1

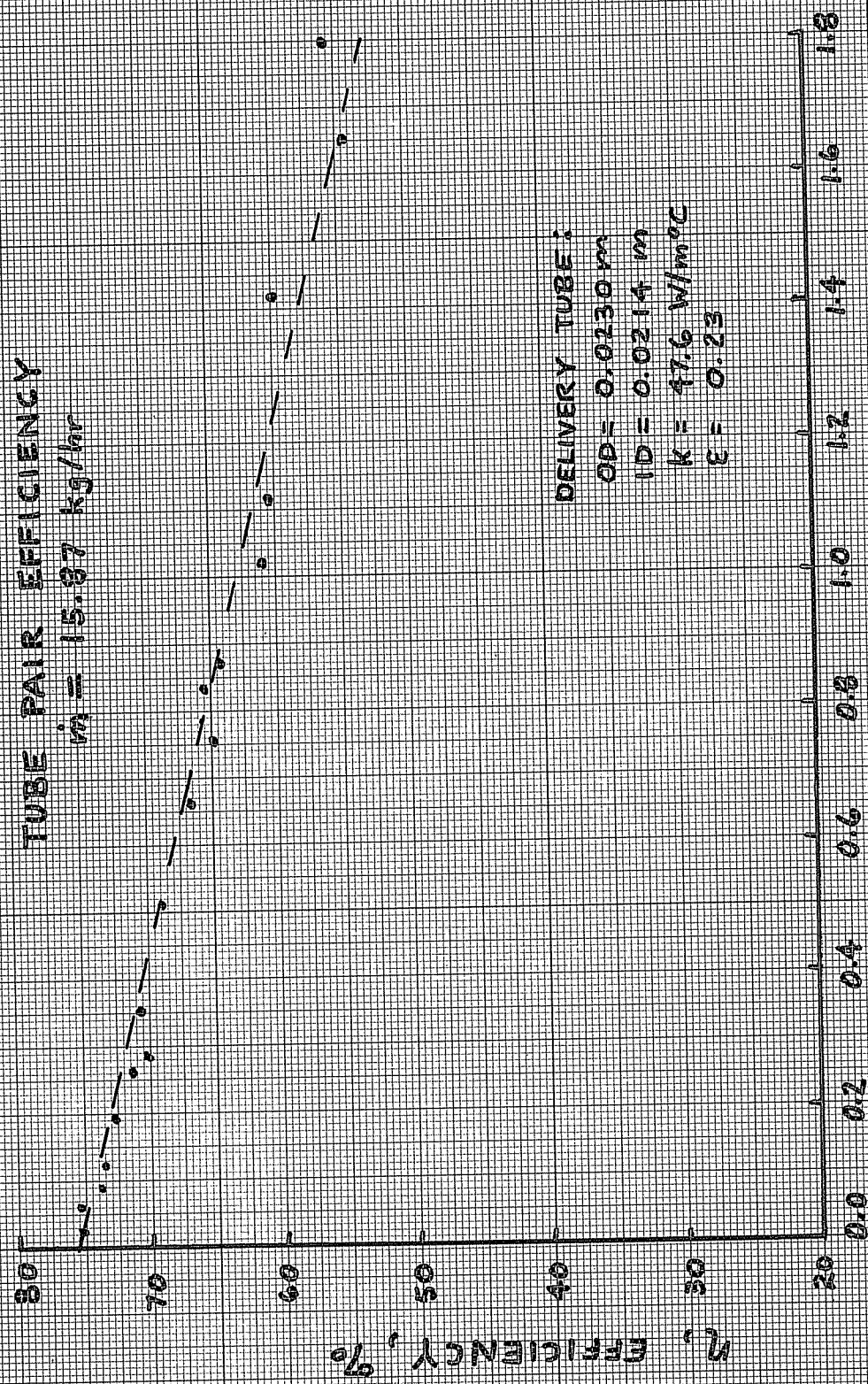
If equation 5.5.2 is written as

$$\eta = \alpha\tau F_R - \left(\frac{U_L F_R}{T_{in}^3}\right) (T_{in}^3 \frac{(T_{in} - T_a)}{S_{eff}}) \quad 5.5.3$$

it is clear that if a straight line is used to represent the predicted values, the intercept of the graph is $\alpha\tau F_R$, and the slope becomes $\frac{-U_L F_R}{T_{in}^3}$. Referring to Figure 5.5.3,

it is seen that for a flow rate of 15.8 kg/hr the intercept corresponding to $\alpha\tau F_R$ is 0.755. Because the $\alpha\tau$ product is assumed to be 0.782, this implies that $F_R = 0.965$. When the flow rate is 6.14 kg/hr, F_R is approximately equal to 0.88. It can also be seen from Figure 5.5.3 that a collector tube assembly behaves in a manner similar to a flat plate collector when the operating inputs are changed:

1. When the flow rate decreases, the collector efficiency decreases.
2. As the inlet temperature increases, the efficiency decreases.



DELIVERY TUBE:
 $OD = 0.0230 \text{ m}$
 $ID = 0.0214 \text{ m}$
 $k = 47.6 \text{ W/m}^2\text{C}$
 $\epsilon = 0.23$

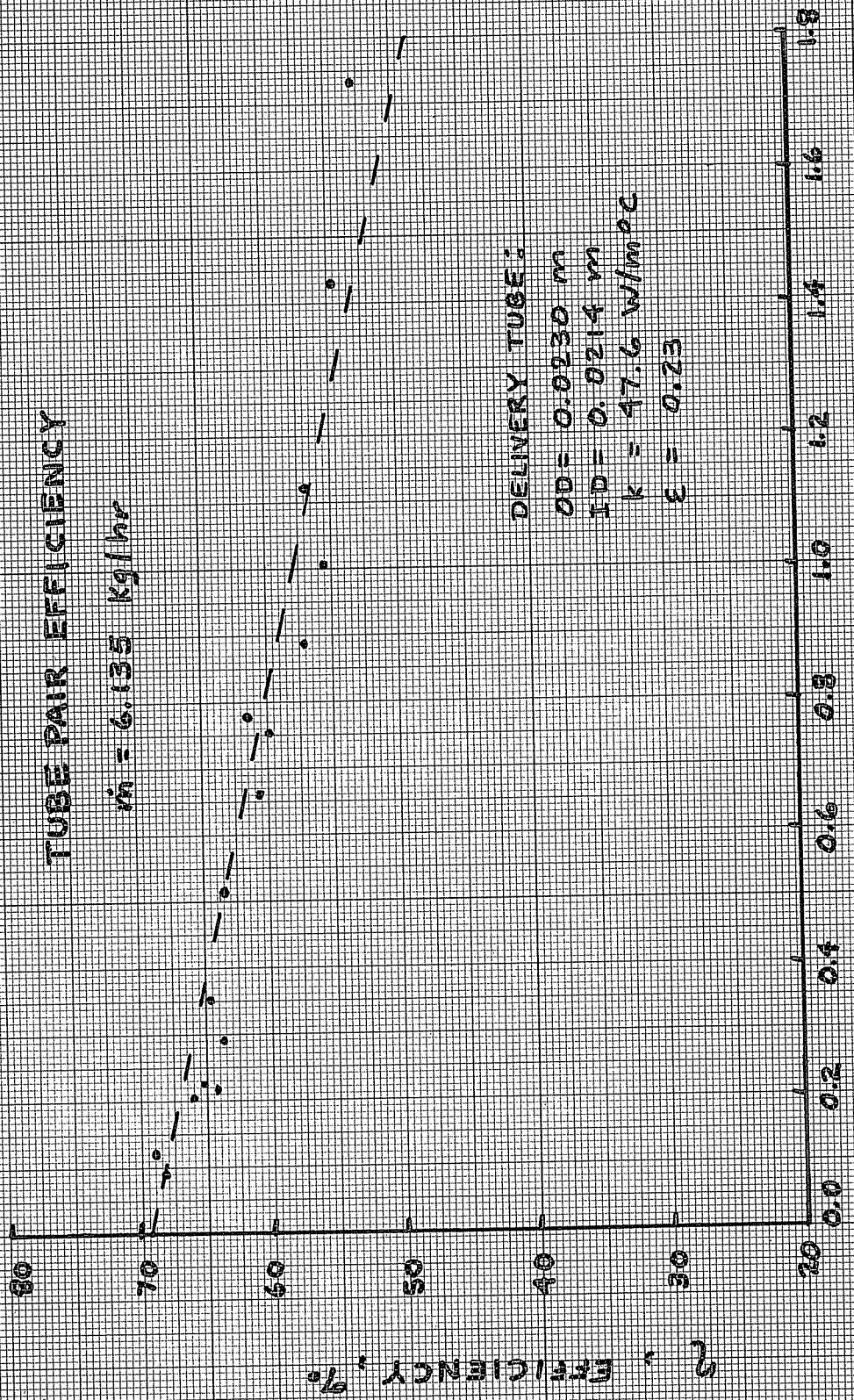
F14

$$\frac{T_{in}^3 (T_{in} - T_a)}{S_{eff}} \times 10^{-7} \text{ } \frac{\text{K}^4 \text{ m}^2}{\text{W}}$$

FIGURE 5.5.1

TUBE PAIR EFFICIENCY

$\dot{m} = 6.135 \text{ Kg/hr}$



DELIVERY TUBE:
OD = 0.0230 m
ID = 0.0214 m
k = 47.6 W/m°C
ε = 0.23

$$\frac{T_{in}^3 (T_{in} - T_a)}{S_{eff}} \times 10^{-3}, \frac{K^4 m^2}{W}$$

FIGURE 5.5.2

TUBE PAIR EFFICIENCY

vs $\frac{T_{in}^3(T_{in}-T_a)}{S_{eff}}$

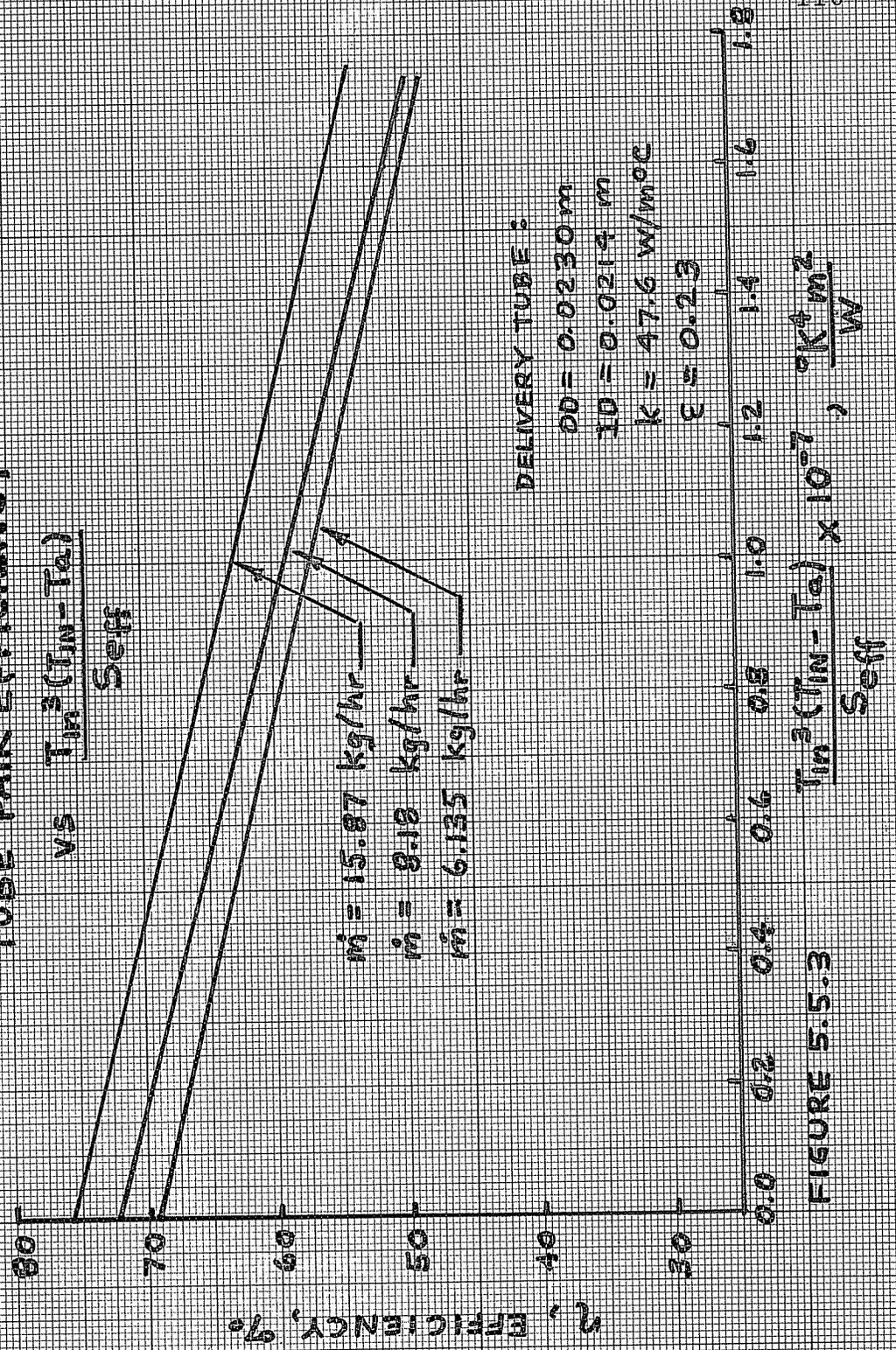


FIGURE 5.5.3

3. As the ambient temperature decreases, the efficiency decreases.
4. As the incident solar radiation decreases, the collector efficiency decreases.

This graphical method offers a convenient way of quickly determining the thermal performance of the collector tube assemblies when the inlet temperature, ambient temperature, and solar radiation are known. This correlation is not exact, however. At high flow rates (15 kg/hr) all the values of efficiency are usually within 1.5% at any given value of $T_{in}^3(T_{in}-T_{amb})/S_{eff}$. At low flow rates, when the temperature rise through the collector is high, this correlation gives greater scatter in efficiency values for single values of $T_{in}^3(T_{in}-T_{amb})/S_{eff}$.

This method can also be used for solar system simulations. The relationship for efficiency can be curve fitted, and the efficiency quickly calculated when the operating conditions are specified.

5.6 Summary and Conclusions about Collector Models for Use in Solar System Simulations

1. Simplifications used in predicting the thermal performance of the evacuated collector tubes are of two distinct forms:

- a. Simplifications resulting from assumptions about the internal heat transfer within the collector tube assemblies.
- b. Numerical simplifications that allow determination of the collector tube output without requiring an iterative solution procedure.

2. The following models have been developed to explicitly handle both the flow stream reversal found in O-I collector tubes and the radiation exchange that takes place between the absorber tube and the delivery tube.

- a. General Analytic Model -- Equations given in Appendix 2.1 and 2.2. This model can account for flow reversal in the tube, i.e. Case 1 or Case 2. It has been observed that for most flow rates and operating conditions, the difference in useful energy output because of flow direction reversal is insignificant; much less than 1% difference in useful energy gain. It is not necessary to model these cases separately when only the magnitude of

the useful energy gain is required.

Developing flow in both flow passages and non-equal heat fluxes on the two annulus surfaces can be accounted for. In practice, this should be unnecessary because the evacuated cover tube and low emittance of the absorber tube keep the losses to such a low level that large uncertainties in the values of the convection coefficients generate much smaller uncertainties in the magnitude of the useful energy gains. The method requires an iterative procedure.

- b. Linear Model -- Equations given in Section 3.6. This model gives excellent agreement when compared to the more general analytic model for most flow rates and operating conditions. This model introduces some error when the internal temperature gradients in the collector tube assembly exhibit extreme deviations from linearity, especially at low flow rates when the thermal coupling between the two flow streams is most pronounced. It also requires an iterative solution procedure.

3. The following conclusions are drawn about the internal heat transfer that occurs within the collector tube

assembly.

- a. Variations in the surface emittance of the delivery tube can significantly change the internal temperature distributions in the collector tube. The changes do not, however, have an important effect upon the useful energy output of the tube. Performance of a collector tube assembly is fractionally better for a delivery tube with a high emittance than a tube with a low emittance.
- b. For thin walled delivery tubes, the effect of the delivery tube conductivity on the useful energy output of the collector tube can be less significant than the effects of large changes in the delivery tube emittance.
- c. Thermal coupling between the flow streams changes the internal temperature distributions in the collector tube from those that would occur if coupling were not present. The effect upon the useful energy gain from the collector is small at higher flow rates. Neglecting the thermal coupling allows the collector tube assembly to be modeled as if the flow passed only through the annulus, with the delivery tube insulated.

4. An additional model of the collector tube can be proposed if both thermal coupling and the radiation exchange between the absorber tube and delivery tube are ignored. Both mechanisms become less important as the flow rate increases. The same model can then be used to predict the performance of the collector tubes using either air or a liquid as the heat transfer medium. This model has not been numerically investigated for the evacuated tubular collector, but it is expected that it will give good agreement with the more general models.

5. The performance map approach can be used with any model desired if extensive computations are required to determine the useful energy output for every changing set of inlet conditions. It is particularly advantageous for long term simulations when an iterative solution for the performance of the collector tubes is excessively time consuming.

6. The graphical approach can be used if the error in efficiency calculations is acceptable. It is used for a single flow rate and the correlations become worse at lower flow rates.

7. The final decision about which model will be used to simulate the performance of the collector tube assemblies depends upon what the model is needed for. For long term simulations, a model that requires no iteration is probably

the best. Either the performance map or the graphical method can be used. The graphical method is quick but can introduce error; the performance map approach is accurate but somewhat slower.

6. SOLAR SYSTEM SIMULATIONS USING THE O-I COLLECTOR MODEL

6.1 Models Used in Simulations

When a model of the evacuated tubular collector is used in a simulation program, such as TRNSYS [14], the collector model is referenced at time intervals where the predicted useful energy gain for a specified set of operating conditions is required by the main program. For most solar system simulations, the only time-dependent inputs that affect collector array operation are the solar radiation components incident on the array backing surface, the collector tube inlet temperature, the ambient temperature, and the current value of solar time (which specifies the declination, and sun hour angle).

The following general procedure, shown schematically in Figure 6.1.1, is used to predict the useful energy output of an operating array of tubular collectors. It is compatible with any specific model used for determining the radiation received by a single tube or any model used for determining the thermal performance of a single tube or several series-connected collector tubes.

1. The radiation received by a single tube is determined. This is done by computing
 - a. Angle Ω ; requires knowing the collector tilt, latitude, tube rotation angle, solar time (declination, hour angle), tube separation, tube

GENERAL PROCEDURE FOR
PREDICTING COLLECTOR ARRAY
PERFORMANCE

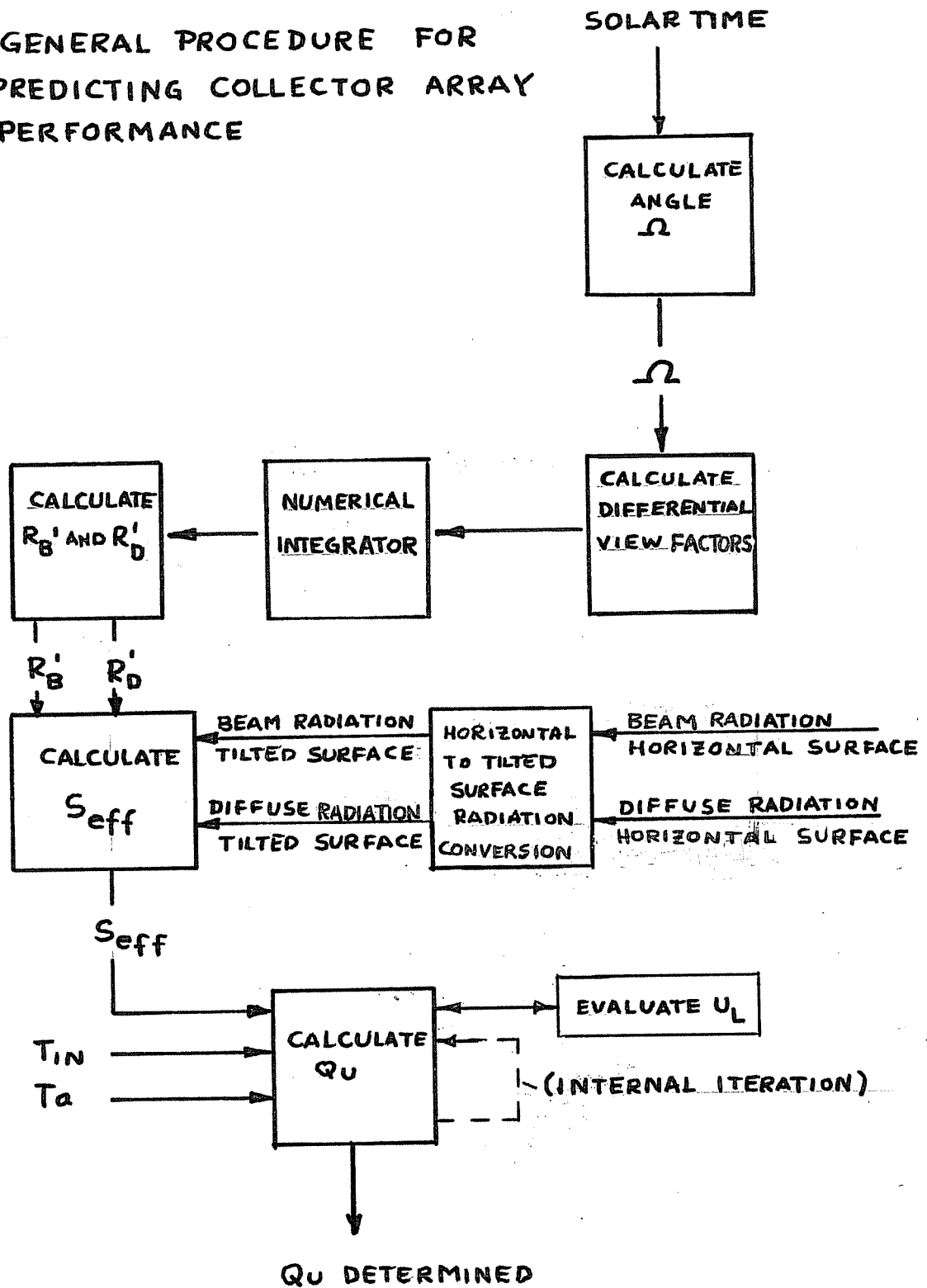


FIGURE 6.1.1

distance from the backing surface.

- b. R_B' and R_D' ; requires angle Ω , several view factors and the reflectance of the backing screen.
 - c. S_{eff} ; this requires knowing the magnitude of the beam and diffuse components of solar radiation received by the backing surface if the tubes were not present, and R_B' and R_D' .
2. When the radiation received by a single tube in an array is known, the useful energy gain for a tube (or tube pair, or an entire series-connected array) is calculated using any desired model for determining the thermal performance.

The actual model used in all TRNSYS simulations to date is shown in Figure 6.1.2. Parameters used in the collector array model that do not change during the simulation (collector tube internal geometry, tube spacing, backing surface and tube orientation and mass flow rate) are used in calculating the performance map of collector efficiency and an additional array of discrete values of R_B' as a function of Ω ; the single value of R_D' is also determined. When the useful energy output of the array is required, the following method is used.

1. Calculate angle Ω .
2. Determine R_B' by interpolation from the array of

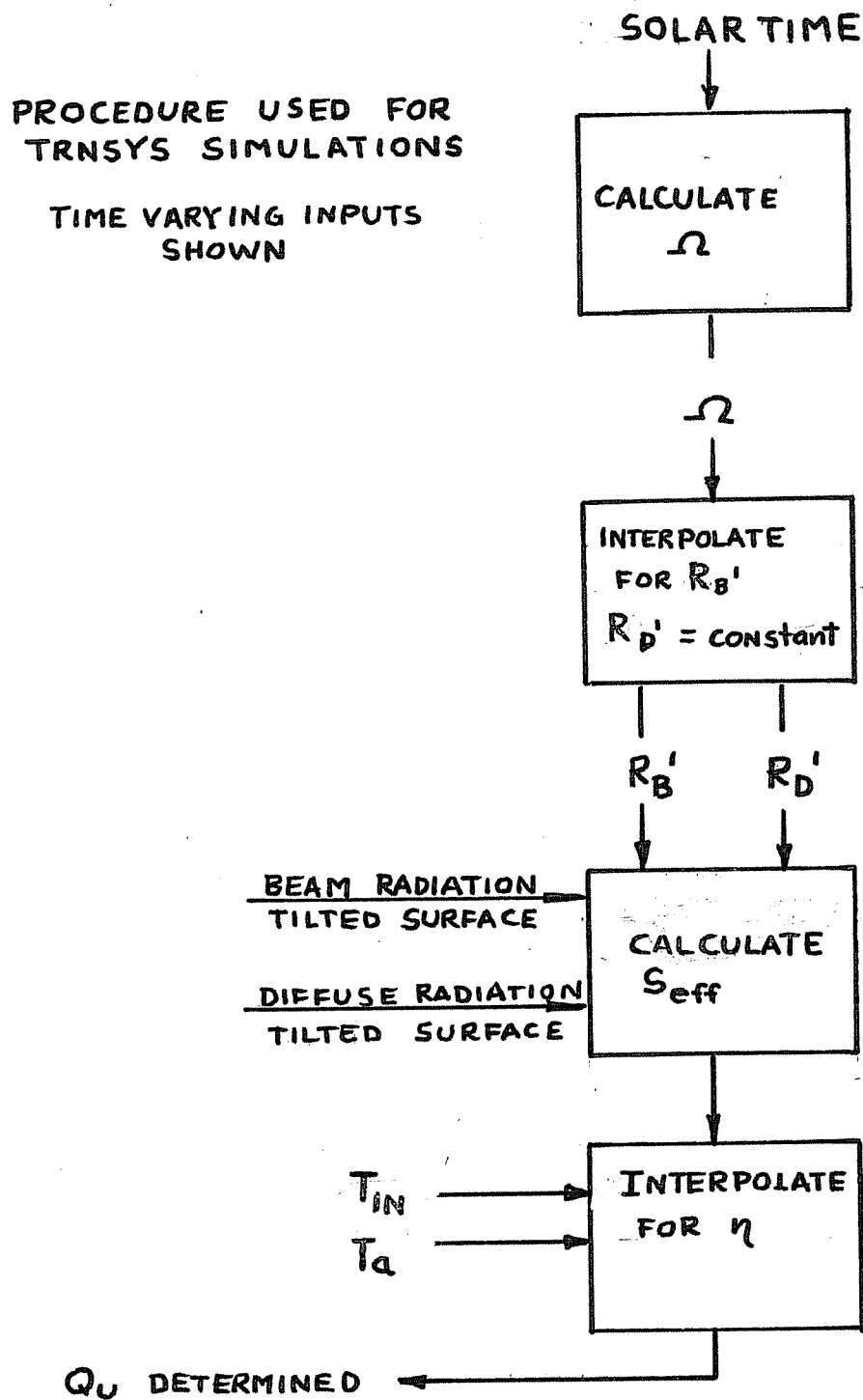


FIGURE 6.1.2

R_B' vs Ω .

3. Calculate S_{eff} .
4. Knowing the magnitudes of the inlet temperature, ambient temperature and incident solar radiation, interpolate from the performance map for the value of the tube(s) efficiency.
5. Calculate Q_u , and array outlet temperature.

By externally calculating the value of R_D' , the R_B' vs Ω array, and the collector efficiency as a function of T_{in} , T_a and S_{eff} , the collector array calculations can be done quickly.

Several models of the thermal performance of the collector tubes were tried, but the performance map approach was used most often as it gave the best compromise between computational speed and accuracy.

6.2 Description of System Configuration and Simulation

Results

The simulation program TRNSYS [14], was used to predict the performance of a typical domestic residence in the Madison, Wisconsin climate for a representative seven month heating season. These simulations were done by Hughes [8] in the design studies for the Arlington House. The evacuated tubular collector model used was the same as described in the previous section.

The general solar system configuration investigated by Hughes is shown schematically in Figure 6.2.1. For some of the system designs studied, an array of O-I collector tubes, with air as the working fluid, is used in conjunction with a gravel bed thermal storage unit. The air flow through the solar system is provided by fans, with the flow modes controlled by a central controller which operates motorized dampers. When the collector array is operating, it will operate in one of two possible ways: the heated air will circulate either from the collector to the living space, or will circulate from the collector to the storage unit. Service hot water is supplied by including an air-to-water heat exchanger in the collector-storage unit flow circuit. The space heating load not supplied by the solar system is supplied by an auxillary energy source. The auxillary energy source can be either a conventional furnace, an additional gravel bed storage unit heated by an electric auxillary furnace during off-peak hours, or a single gravel bed that combines both the functions of the solar system storage unit and the auxillary furnace. This multipurpose gravel bed is heated sufficiently at night to supply the heating load of the residence for the following day. The gravel bed, usually at an elevated temperature level, is also used as the storage unit when the collector array is operated

TYPICAL AIR HEATED SOLAR SYSTEM

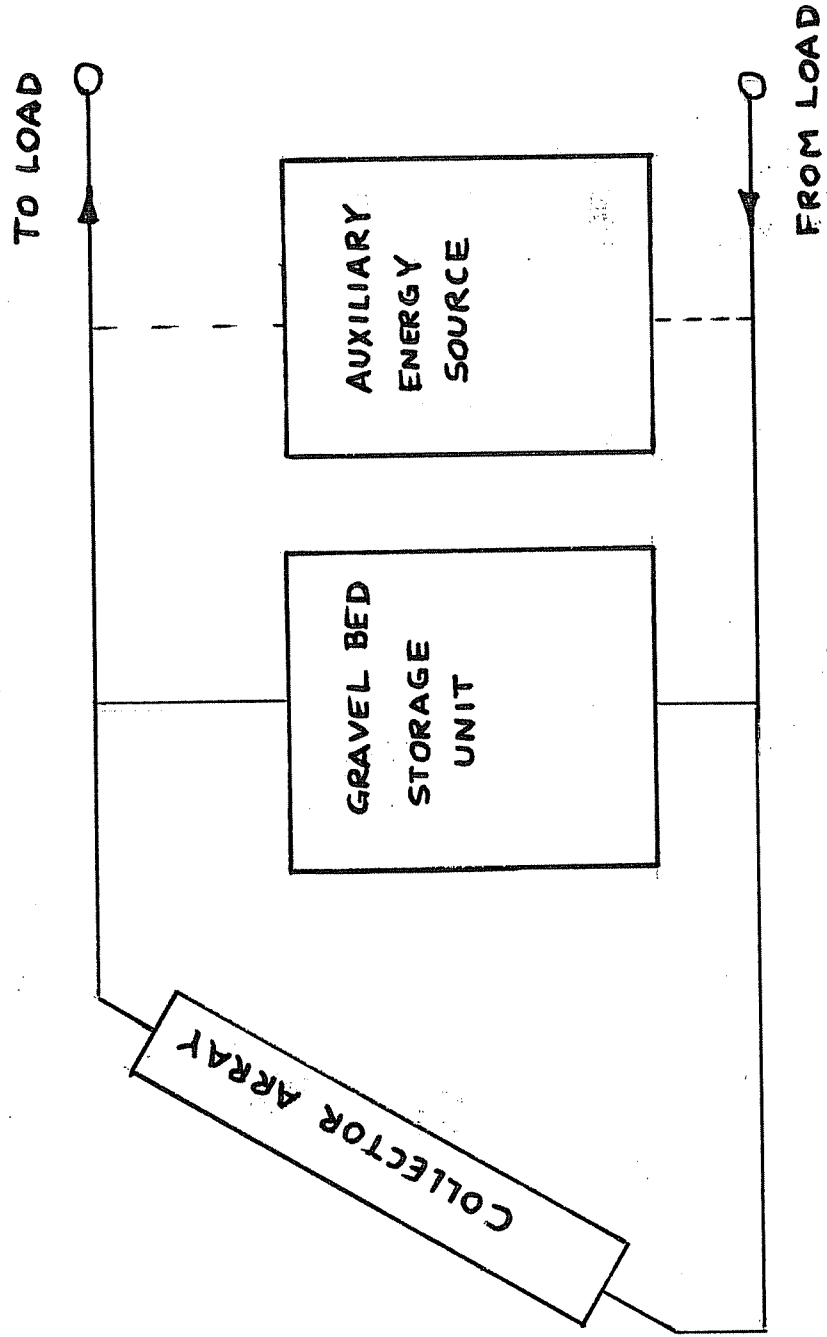


FIGURE 6.2.1

during the day.

Some of the design parameters investigated by Hughes that influenced the performance of the collector array (and the entire solar system) were the collector tubes center-to-center separation, the mass flow rate through the tubes, and the inclusion of the single off-peak heated gravel bed, which forced up the average operating temperature of the collector array. Comparisons were made between flat plate air heaters of conventional design and arrays of the O-I collector tubes. The O-I collector arrays performed significantly better than the flat plate air collectors when the off-peak heated rockpile was used. The performance decrease because of increased collector inlet temperatures was not as pronounced for the O-I collector tubes because the selective surface and evacuated cover tubes kept the losses to an extremely low level, and made the collectors reasonably insensitive to inlet temperature when compared to a non-selectively-coated flat plate type air collector operating under identical conditions.

The other changes in system performance observed by Hughes because of the changes in flow rate and tube spacing were as expected. The thermal performance per tube increased as the flow rate through the tube increased, and the overall system performance increased slightly as the number of tubes installed on the fixed roof area

increased. A detailed description of the Arlington House design and the other models used in the Arlington House simulations can be found in reference 8.

7. CONCLUSIONS AND RECOMMENDATIONS

The evacuated collector tubes currently being manufactured by Owens-Illinois, Inc. are extremely efficient in converting solar radiation to useful energy for many types of applications. The theoretical performance of a collector array has been broken into two separate topics: solar radiation received by a single tube in a collector array, and the thermal performance of the single tubes. Different models have been developed for each topic with considerable effort spent in attempting to identify the important design parameters that might affect the array performance.

Simplifications for use in predicting collector array output have also been developed, and approximate error bounds have been calculated, when possible, that indicate the error that these simplifying assumptions will have on the predicted performance of the collector array.

The collector tubes have a very low loss coefficient because of the combination of a low emittance selective surface, and the evacuated cover system. Because of the low losses from the tubes, the collector tubes are expected to be useful for system applications involving high collector inlet temperatures or low solar insolation levels. The radiation received by a single collector tube can be adjusted by changing the tube separation and the distance

from the backing surface. This offers additional flexibility in matching the collector array output to the requirements of the system application.

The theoretical performance of the collector array using air as the heat transfer medium is not expected to be much less than the performance of an array using a liquid when operated under identical conditions.

The collector array model is deficient in several important respects. No provisions have been made to include the effects of air leakage and losses from exposed manifolds, and no method for turning the collectors on or off has been proposed. Air leakage will depend upon the particular manifold design that is used to distribute the air to the collector tubes and the care with which the manifolds and duct-work are assembled and sealed. The heat losses from the manifolds will depend upon the surface area of the manifolds, the amount of insulation used, the temperatures and velocities of the air within the ducts and whether most of the duct-work is exposed to the ambient air or is contained within the heated living space. Meaningful estimates cannot be made without some idea of the specific manifold design to be used. Because these factors can have a significant effect upon the total collector array output, and the magnitudes of these losses will, in general, be experimentally established, no speci-

fic method of collector array control is recommended in this work. Possible control schemes that could be used to start and stop the air flow through the collector are the use of a single differential temperature controller, a single solar radiation sensor, or two sequentially operating controllers: either a combination of a radiation sensor and a differential temperature controller or two differential temperature devices. The use of two separate controllers can always account for the effects of air leakage and heat losses from the exposed duct-work. One controller is used to start the flow through the collector, either by sensing the incident solar radiation level or by measuring the temperature difference between a collector tube interior and some other reference temperature (possibly the room temperature or the gravel bed temperature). When the temperature difference (or radiation level) is above some minimum value, the air is circulated through the collector array. The additional differential temperature measuring device is used to measure the temperature difference between the air leaving the living space and going to the collector array and the air returning to the living space. This temperature difference will include the effects of heat losses from the duct-work and any air leakage from the ducts or collector array, and will reflect the amount of energy actually being delivered to the house. When the

temperature difference is below some minimum acceptable level, the flow through the collector array is stopped.

The optimum control strategy is unclear at this time, and will probably be determined experimentally.

Because the collector tubes are commercially available, it is recommended that experimental tests on single tubes and tube arrays be done to verify (or to point out the need for modification of) the mathematical models of the collector tube thermal performance and the radiation received by a single tube in an array. Although the theoretical performance of the collector tubes appears quite good, actual experimental testing is needed to evaluate the feasibility of using the evacuated tubular collectors with air as the working fluid. It is quite possible that the flow distribution problem and the air leakage problem may require special (and expensive) construction methods and materials that will offset any performance increase that would result from using these collector arrays instead of conventional flat plate air heaters.

Appendix 1. Derivation of Angular Relationships and Angle Ω for an Array of Tubular Collectors

The following section shows how the relationships for angle Ω , presented in Section 2.1, were derived. In the discussion below it is assumed that the collector array consists of an array of tubes, each tube parallel to all the other tubes, parallel to the backing screen, and spaced a constant distance above the backing screen. A line normal to the backing screen is, by implication, also normal to the longitudinal axis of the tubes.

It is convenient to visualize the earth-sun system as a sphere of unit radius with the earth as the center about which the sun moves. (The eccentricity of the earth's orbit around the sun is ignored.) Figure A-1.1 shows this celestial sphere with the earth at the center. Figure A-1.2 shows the apparent daily path taken by the sun as seen by an observer looking down from the celestial north pole. For the case of a collector tube axis pointing north-south, it is also helpful to set up a cartesian coordinate system. Figure A-1.3 shows the coordinate system used: the positive x direction is east, positive z direction is the south projection on the plane of the tilted collector array, the y direction is normal to the backing surface of the tilted collector. The collector array is at latitude ϕ

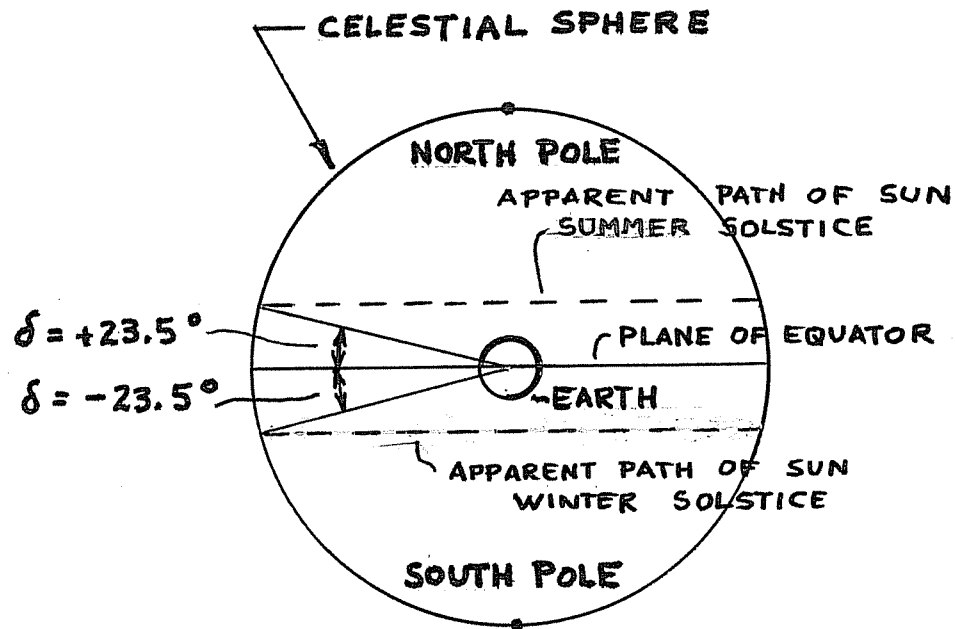


FIGURE A-1.1

CELESTIAL SPHERE AS SEEN BY OBSERVER AT NORTH POLE

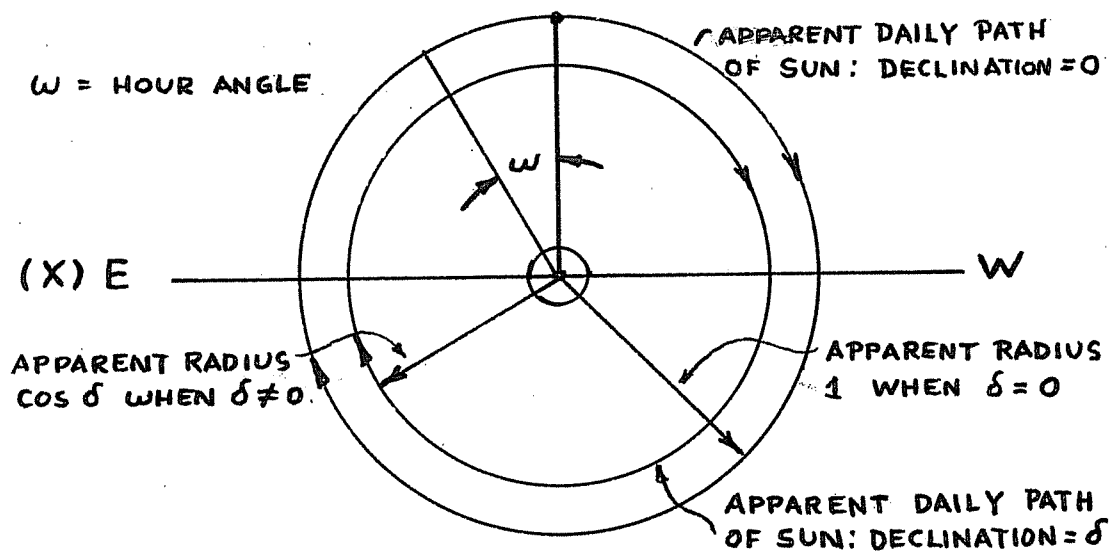


FIGURE A-1.2

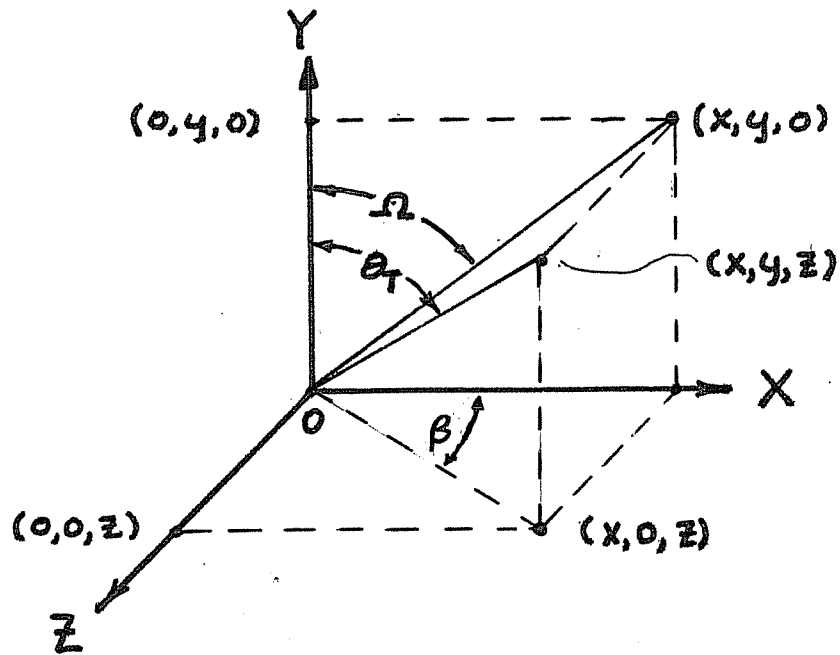


FIGURE A-1.3

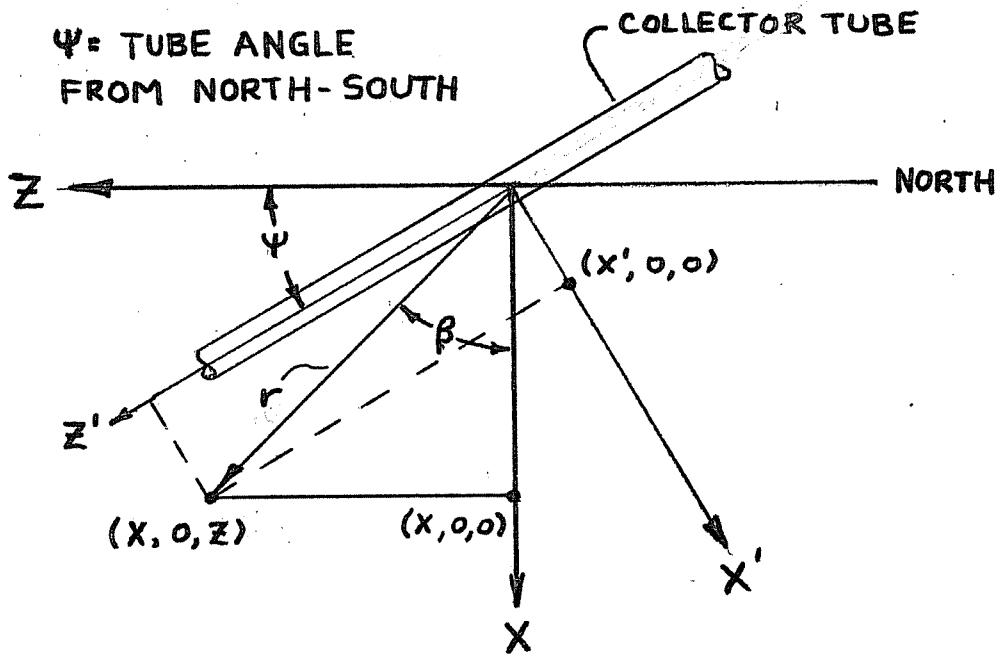


FIGURE A-1.4

and has a tilt from the horizontal, s . Because the sun is always considered to be at a unit radius distance from the earth with general position coordinates (x,y,z) , we can write:

$$\sqrt{x^2+y^2+z^2} = 1 \quad \text{and} \quad \Omega = \tan^{-1}\left(\frac{x}{y}\right) \quad \text{A-1.1}$$

Figures A-1.5a and A-1.5b are modifications of a drawing taken from Tabor [13]. They show the projected path of the sun taken during different times of the year. Because surfaces with slope s to the north or south have the same angular relationship to beam radiation as a horizontal surface at an artificial latitude of $(\phi-s)$, figures A-1.5a and b are applicable for either horizontal or tilted surfaces of latitude ϕ , slope s , with declination of the sun, δ . Angle $(\phi-s)$ is the incidence angle of beam radiation on the collector backing surface at solar noon when the declination of the sun is zero. Angle $(\phi-s-\delta)$ is the beam radiation incidence angle at solar noon for other declinations. By referring to figure A-1.5b it can be seen that

$$z_{\phi-s} \Big|_{\substack{\omega=0 \\ \delta=0}} = \sin(\phi-s)$$

where $z_{\phi-s} \Big|_{\substack{\omega=0 \\ \delta=0}}$ indicates the value of the projection of the sun's position on the z axis when the hour angle, ω , is zero and the declination is zero. $(\phi-s)$ refers to the projected path taken by

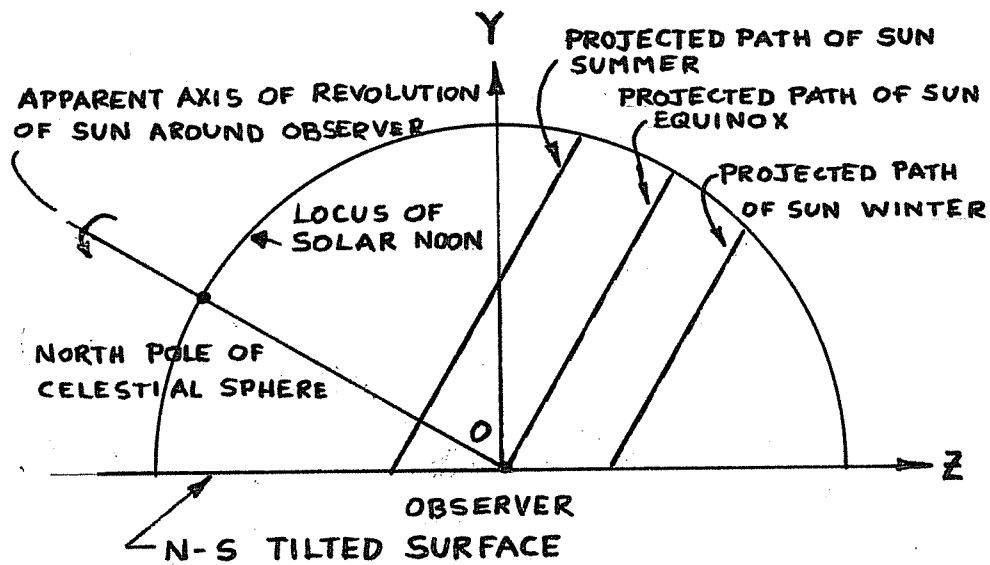


FIGURE A-1.5a

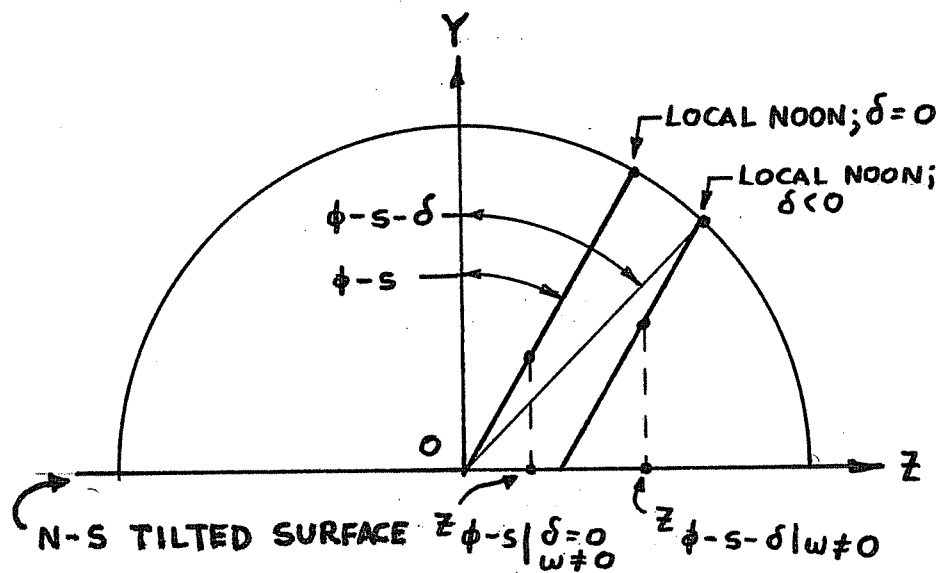


FIGURE A-1.5b

the sun. $(\phi-s)$ is the incidence angle at solar noon along this path.

Referring to Figure A-1.2 and A-1.5b it can be seen that:

$$z_{\phi-s} \Big|_{\substack{\omega \neq 0 \\ \delta \neq 0}} = \sin(\phi-s) \cos \omega$$

and

$$x_{\phi-s} \Big|_{\substack{\omega \neq 0 \\ \delta = 0}} = \sin \omega$$

$$y_{\phi-s} \Big|_{\substack{\omega \neq 0 \\ \delta = 0}} = \cos(\phi-s) \cos \omega$$

It can also be seen from Figure A-1.2 that the radius of the apparent daily path of the sun is 1 when the declination is zero. Similarly it is seen that the radius of the sun's apparent path is $\cos \delta$ for any other declination. For declinations other than zero, at solar noon (Figure A-1.5b):

$$z_{\phi-s-\delta} \Big|_{\omega=0} = \sin(\phi-s-\delta)$$

$$y_{\phi-s-\delta} \Big|_{\omega=0} = \cos(\phi-s-\delta)$$

By comparing the movement along the projected path of the sun for any arbitrary declination to the movement along the projected path of the sun when the declination is zero, it can be shown that for any latitude, slope, declination, and hour angle:

$$x = \cos\delta\sin\omega \quad \text{A-1.2}$$

$$y = \cos(\phi-s-\delta) - \cos\delta[\cos(\phi-s)(1-\cos\omega)]$$

$$z = \sin(\phi-s-\delta) - \cos\delta[\sin(\phi-s)(1-\cos\omega)]$$

upon rearrangement:

$$y = \cos(\phi-s)\cos\delta\cos\omega + \sin(\phi-s)\sin\delta \quad \text{A-1.3}$$

$$z = \sin(\phi-s)\cos\delta\cos\omega - \cos(\phi-s)\sin\delta \quad \text{A-1.4}$$

It should be noted that the above expression for y is the same as that for $\cos \theta_T$, the cosine of the angle of incidence of beam radiation on a tilted surface, as given by Duffie and Beckman [3].

For the more general tube axis orientation, with longitudinal tube axis other than along a north-south projection, the coordinate system shown in Figure A-1.4 is used. ψ is the tube rotation angle measured counter-clockwise from the north-south meridian projection in the plane of the backing surface. The z' axis is parallel to the longitudinal axis of the tubes. The y axis is unchanged. The x axis is perpendicular to the y and z' axis. Angle Ω is now:

$$\Omega = \tan^{-1}\left(\frac{x'}{y}\right)$$

referring to Figures A-1.3 and A-1.4,

$$y = \cos\theta_T$$

$$r = \sin\theta_T$$

$$\cos\beta = \frac{x}{r} = \frac{\cos\delta\sin\omega}{\sin\theta_T}$$

$$\sin\beta = \frac{z}{r} = \frac{\cos\delta\sin(\phi-s)\cos\omega - \cos(\phi-s)\sin\delta}{\sin\theta_T}$$

$$\frac{x'}{x} = \frac{\cos(\beta+\Psi)}{\cos\beta}$$

$$x' = x \left[\frac{\cos\beta\cos\Psi - \sin\beta\sin\Psi}{\cos\beta} \right]$$

After substituting in $x = \cos\delta\sin\omega$ and eliminating angle β

$$x' = \cos\delta\sin\omega\cos\Psi - \sin\Psi[\cos\delta\sin(\phi-s)\cos\omega - \cos(\phi-s)\sin\delta]$$

A-1.6

In summary:

$$\Omega = \tan^{-1} \left[\frac{x'}{y} \right]$$

A-1.7

where $x' = \cos\delta\sin\omega\cos\Psi - \sin\Psi[\cos\delta\sin(\phi-s)\cos\omega - \cos(\phi-s)\sin\delta]$

A-1.6

$$y = \cos(\phi-s)\cos\delta\cos\omega + \sin(\phi-s)\sin\delta$$

A-1.3

ϕ = latitude (north positive)

δ = declination (north positive)

ω = hour angle of sun (solar noon = 0, mornings positive, afternoons negative)

s = slope of collector array from horizontal

Ψ = tube rotation angle measured counter-clockwise from local meridian projection on plane of collector array.

It should be noted that this expression for Ω is valid only for those collector orientations where the backing surface azimuth angle, γ , is zero. γ , as defined in Duffie and Beckman [3], is the deviation of the normal to the backing surface from the local meridian, the zero point being due south, east positive, and west negative.

Appendix 2

2.1 Reduction of Differential and Algebraic Equations
for General Analytic Method

The four equations for Case 1 developed in Section 3.3 are repeated:

$$1. \quad \alpha \tau S_{\text{eff}} + U_L(T_a - T_3) + h_3(T_2 - T_3) + h_{r3}(T_w - T_3) = 0 \quad 3.3.1$$

$$2. \quad h_2(T_2 - T_w) + h_{rw}(T_3 - T_w) + U_1(T_1 - T_w) = 0 \quad 3.3.2$$

$$3. \quad -\dot{m}c_p \frac{dT_1}{dx} + U_1 P_1(T_1 - T_w) = 0 \quad 3.3.3$$

$$4. \quad \dot{m}c_p \frac{dT_2}{dx} + h_3 P_3(T_2 - T_3) + h_2 P_1(T_2 - T_w) = 0 \quad 3.3.4$$

because the air temperature distribution with length is desired, it is necessary to eliminate T_w and T_3 from the differential equations 3.3.3 and 3.3.4

Solving 2 for T_w

$$T_w = C_2 T_2 + C_3 T_3 + C_1 T_1 \quad A2.1.1$$

where

$$C_1 = \frac{U_1}{h_2 + h_{rw} + U_1} \quad A2.1.1a$$

$$C_2 = \frac{h_2}{h_2 + h_{rw} + U_1} \quad A2.1.1b$$

$$C_3 = \frac{h_{rw}}{h_2 + h_{rw} + U_1} \quad A2.1.1c$$

Solving 1 for T_3 gives

$$T_3 = b_0 + b_1 T_1 + b_2 T_2 \quad \text{A2.1.2}$$

$$b_0 = \frac{\alpha r S_{\text{eff}} + U_L T_a}{U_L + h_3 + h_{r3}(1 - C_3)} \quad \text{A2.1.2a}$$

$$b_1 = \frac{h_{r3} C_1}{U_L + h_3 + h_{r3}(1 - C_3)} \quad \text{A2.1.2b}$$

$$b_2 = \frac{h_3 + h_{r3} C_2}{U_L + h_2 + h_{r3}(1 - C_3)} \quad \text{A2.1.2c}$$

eliminating T_w and T_3 from 3 gives

$$\frac{dT_1}{dx} + e_1 T_1 - e_2 T_3 - e_3 = 0 \quad \text{A2.1.3}$$

$$e_1 = \frac{U_1 P_1}{m c_p} (C_3 b_1 + C_1 - 1) \quad \text{A2.1.3a}$$

$$e_2 = \frac{-U_1 P_1 (C_2 + C_3 b_2)}{m c_p} \quad \text{A2.1.3b}$$

$$e_3 = \frac{-U_1 P_1 C_3 b_0}{m c_p} \quad \text{A2.1.3c}$$

eliminating T_w and T_3 from 4 gives

$$\frac{dT_2}{dx} + f_1 T_1 + f_2 T_2 + f_3 = 0 \quad \text{A2.1.4}$$

where

$$f_1 = \frac{h_2 P_1 (-C_1 - C_3 b_1) - h_3 P_3 b_1}{\dot{m} c_p} \quad \text{A2.1.4a}$$

$$f_2 = \frac{h_2 P_1 (1 - C_2 - C_3 b_2) + h_3 P_3 (1 - b_2)}{\dot{m} c_p} \quad \text{A2.1.4b}$$

$$f_3 = \frac{-h_3 P_3 b_o - h_2 P_1 C_3 b_o}{\dot{m} c_p} \quad \text{A2.1.4c}$$

The same process is repeated for Case 2 when the flow path is reversed:

$$T_w = C_1 T_1 + C_2 T_2 + C_3 T_3$$

where

$$C_1 = C_2 \text{ for case 1}$$

$$C_2 = C_1 \text{ for case 1}$$

$$C_3 = C_3 \text{ for case 1}$$

$$T_3 = b_o + b_1 T_1 + b_2 T_2$$

where

$$b_o = b_o \text{ for case 1}$$

$$b_1 = b_2 \text{ for case 1}$$

$$b_2 = b_1 \text{ for case 1}$$

The two equations for the air temperatures for case 2 are the same as before

$$\frac{dT_1}{dx} + e_1 T_1 - e_2 T_2 - e_3 = 0 \quad \text{A2.1.3}$$

$$\frac{dT_2}{dx} + f_1 T_1 + f_2 T_2 + f_3 = 0 \quad \text{A2.1.4}$$

where

$$e_1 = - \left[\frac{h_3 P_3 (1-b_1) + h_1 P_1 (1-C_1 - C_3 b_1)}{\dot{m} c_p} \right] \quad \text{A2.1.3d}$$

$$e_2 = \frac{h_2 P_1 (-C_2 - C_3 b_2) - h_2 P_1 C_3 b_o}{\dot{m} c_p} \quad \text{A2.1.3e}$$

$$e_3 = \frac{-h_3 P_3 b_o - h_2 P_1 C_3 b_o}{\dot{m} c_p} \quad \text{A2.1.3f}$$

and

$$f_1 = \frac{-U_1 P_1 [C_1 + C_3 b_1]}{\dot{m} c_p} \quad \text{A2.1.4d}$$

$$f_2 = \frac{U_1 P_1}{\dot{m} c_p} [1 - C_2 - C_3 b_2] \quad \text{A2.1.4e}$$

$$f_3 = \frac{-U_1 P_1 C_3 b_o}{\dot{m} c_p} \quad \text{A2.1.4f}$$

2.2 Solutions to Reduced Differential Equations for Different Sets of Boundary Conditions

For both cases 1 and 2 the general form of the simultaneous differential equations are:

$$\frac{dT_1}{dx} + e_1 T_1 - e_2 T_2 - e_3 = 0 \quad \text{A2.1.3}$$

$$\frac{dT_2}{dx} + f_1 T_1 + f_2 T_2 + f_3 = 0 \quad \text{A2.1.4}$$

The solutions to these equations for the two sets of boundary conditions of interest are:

$$T_1 = M_1 e^{m_1 x} + M_2 e^{m_2 x} + g_1 \quad \text{A2.2.1}$$

and

$$T_2 = \frac{M_1 (m_1 + e_1)}{e_2} e^{m_1 x} + M_2 \frac{(m_2 + e_1)}{e_2} e^{m_2 x} + g_2 \quad \text{A2.2.2}$$

m_1 and m_2 are the roots to the second order characteristic equations obtained when A2.1.3 and A2.1.4 are uncoupled.

For all cases of interest where the mass flow rate, \dot{m} , and the effective solar radiation, S_{eff} , are non-zero, the roots m_1 and m_2 are real and unequal.

$$m_1 = \frac{-(e_1+f_2) + \sqrt{(e_1+f_2)^2 - 4(e_2f_1+f_2e_1)}}{2} \quad \text{A2.2.3}$$

$$m_2 = \frac{-(e_1+f_2) - \sqrt{(e_1+f_2)^2 - 4(e_2f_1+f_2e_1)}}{2} \quad \text{A2.2.4}$$

$$g_1 = \frac{f_2e_3 - e_2f_3}{e_2f_1 + f_2e_1} \quad \text{A2.2.5}$$

$$g_2 = -\left(\frac{e_1f_3 + e_3f_1}{e_2f_1 + f_2e_1}\right) \quad \text{A2.2.6}$$

The coefficients M_1 and M_2 are determined by the sets of boundary conditions used. For the flow situations where the entire collector length is being considered (see Figure A2.2a), the set of boundary conditions for both case 1 and case 2 are:

1. at $x=0$, $T_1=T_2$
2. at $x=L$, $T_1=T_{in}$ where T_{in} is the inlet air temperature to the collector.

Solving for M_1 and M_2 gives:

$$M_1 = \frac{T_{in} - g_1 + (g_2 - g_1) \left[\frac{e^{m_1 L}}{(m_1 + e_1 - e_2)} \right]}{e^{m_2 L} - \frac{(m_2 + e_1 - e_2)}{(m_1 + e_1 - e_2)} e^{m_1 L}} \quad \text{A2.2.7}$$

TEMPERATURE DISTRIBUTIONS
FOR DIFFERENT SETS
OF BOUNDARY CONDITIONS

$L =$ ENTIRE TUBE LENGTH

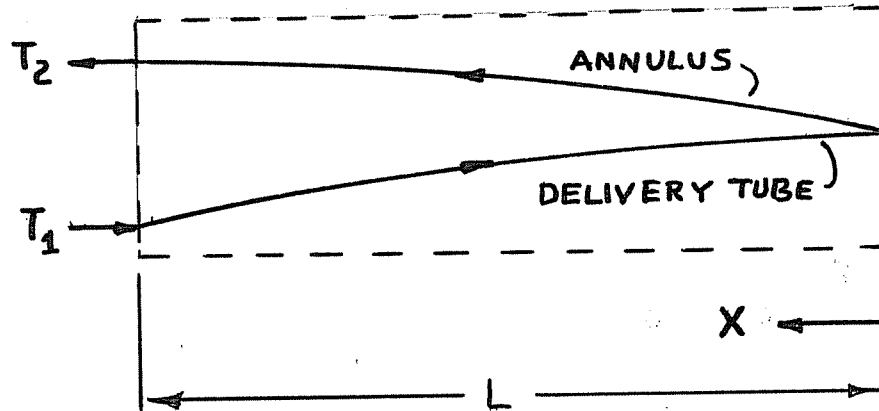


FIGURE A-2.2a

$L =$ TUBE SEGMENT LENGTH

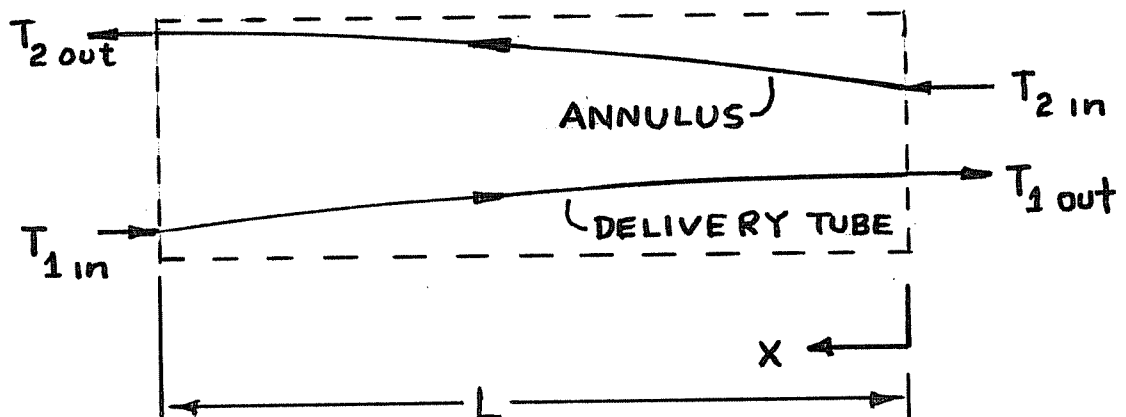


FIGURE A-2.2b

$$M_2 = - \frac{([M_1 \frac{(m_2 + e_1 - e_2)}{e_2}] + g_2 - g_1)}{(\frac{m_1 + e_1 - e_2}{e_2})} \quad \text{A2.2.8}$$

For situations where it is desirable to investigate only a section of the absorber tube length (i.e., investigating length dependent convection coefficients), the general temperature distribution shown in Figure A2.2b applies. Here the temperature at $x=0$ of the hot stream, and $x=L$ of the cold stream are known. The length L is now the length of the collector tube section of interest. The figure shows a temperature distribution for case 1, where the cold air enters the delivery tube, but the equations apply for case 2, also.

For this situation, the boundary conditions are:

1. at $x=0$, $T_2 = T_{2 \text{ in}}$
2. at $x=L$, $T_1 = T_{1 \text{ in}}$

the temperature distribution is the same as given in Eqs. A2.2.1-A2.2.6 but the coefficients M_1 and M_2 are now:

$$M_1 = \frac{T_{1 \text{ in}} - g_1 - M_2 e^{m_2 L}}{e^{m_1 L}} \quad \text{A2.2.9}$$

$$M_2 = \frac{T_2 \text{ in } - g_2 - \frac{m_1 + e_1}{m_2 + e_1} \left[\frac{T_{\text{in}} - g_1}{e^{m_1 L}} \right]}{1 - \frac{(m_1 + e_1)}{(m_2 + e_1)} (e^{(m_2 - m_1)L})} \quad \text{A2.2.10}$$

2.3 Convection and Radiation Conductances

To eliminate the need for solving for the inside surface temperature of the delivery tube, an overall heat transfer coefficient U_1 from the outside of the delivery tube to the air inside the delivery tube is defined:

$$U_1 A_{1o} = \frac{1}{\frac{\ln(R_1/R_{1i})}{2\pi kL} + \frac{1}{h_1 A_{1i}}} \quad \text{A2.3.1}$$

where

$$A_{1o} = \pi D_1 L$$

$$A_{1i} = \pi D_{1i} L$$

where D_{1i} is the inside diameter of the delivery tube then

$$U_1 = \frac{1}{\frac{D_1 \ln(D_1/D_{1i})}{2K} + \frac{D_1}{h_1 D_{1i}}} \quad \text{A2.3.2}$$

Duffie and Beckman [3] show that the radiation heat transfer between two coaxial cylindrical surfaces at constant temperatures T_w and T_3 can be expressed as:

$$Q_w = -Q_3 = \epsilon_w \epsilon_3 A_1 \hat{F}_{w3} \sigma (T_3^4 - T_w^4) \quad A2.3.4$$

where \hat{F}_{w3} is the total exchange factor from the surface at temperature T_w to the surface at temperature T_3 . For the case of two coaxial cylinders with inner cylinder at T_w

$$\hat{F}_{w3} = \frac{1}{1 - F_{33} \rho_3 - \rho_3 F_{3w} \rho_w} \quad A2.3.5$$

For surfaces that are not at uniform temperatures, but have temperatures varying with length, eq. A2.3.4 can be approximated by writing:

$$Q_w = \epsilon_w \epsilon_3 A_1 \hat{F}_{w3} \sigma (\hat{T}_3^4 - \hat{T}_w^4) \quad A2.3.6$$

where

$$\hat{T}_3^4 \equiv \frac{1}{L} \int_0^L T_3^4 dx \quad A2.3.7a$$

$$\hat{T}_w^4 \equiv \frac{1}{L} \int_0^L T_w^4 dx \quad A2.3.7b$$

\hat{T}_3 and \hat{T}_w are the fourth roots of the mean fourth power absolute temperatures of the inner and outer surfaces, respectively. Unless the temperature gradients are very steep with length, \hat{T}_3 and \hat{T}_w are usually close to the mean first power absolute temperatures of the absorber tube and delivery tube.

The radiation heat transfer can also be expressed as:

$$Q_w = h_{rw} A_1 (\hat{T}_3 - \hat{T}_w) \quad A2.3.8$$

then

$$h_{rw} = \epsilon_w \epsilon_3 \hat{F}_{w3} \sigma [(\hat{T}_3)^2 + (\hat{T}_w)^2] (\hat{T}_3 + \hat{T}_w) \quad A2.3.9$$

and

$$h_{r3} = \frac{h_{rw} A_1}{A_{3i}} = \frac{h_{rw} D_1}{D_{3i}} \quad A2.3.10$$

BIBLIOGRAPHY

1. Beekley, D.C. and G.R. Mather, "Analysis and Experimental Tests of a High Performance Evacuated Tubular Collector", submitted for publication in Solar Energy, (1975).
2. Simon, F., "Solar Collector Performance Evaluation with the NASA-Lewis Solar Simulator - Results for an All Glass-Evacuated-Tubular Selectively--Coated Collector with Diffuse Reflector," NASA TM X-71695, Cleveland, Ohio, Apr. 1975.
3. Duffie, J.A. and Beckman, W.A., Solar Energy Thermal Processes, Wiley-Interscience, N.Y., (1974).
4. Hottel, H.C. and A.F. Sarofim, Radiative Transfer, McGraw-Hill, Inc., New York (1967).
5. Kays, W.M., Convective Heat and Mass Transfer, McGraw-Hill, Inc., New York (1966).
6. Kreith, F., Principles of Heat Transfer, 3rd ed., International Textbook Co., Scranton, Pa., (1973).
7. Grunes, H., M.S. Thesis in Mechanical Engineering, U. of Wisconsin-Madison. To be completed in 1976.
8. Hughes, P.J., M.S. Thesis, University of Wisconsin, 1975 "The Design and Predicted Performance of Arlington House"
9. Kays, W.M. and A.L. London, Compact Heat Exchangers, 2nd Edition, McGraw-Hill, Inc., New York, (1964).

10. Lundberg, R.E., W.C. Reynolds, and W.M. Kays, NASA TN D-1972, Washington, D.C., Aug. 1963.
11. Kays, W.M. and E.Y. Leung, Intern. J. Heat Mass Transfer Vol. 6, pp. 537-557, 1963.
12. Klein, S.A., M.S. Thesis, University of Wisconsin, 1973. "The Effects of Thermal Capacitance Upon the Thermal Performance of Flat-Plate Solar Collectors".
13. Tabor, H., "Stationary Mirror Systems for Solar Collectors", Solar Energy, 2, 27 (1958).
14. "TRNSYS, A Transient Simulation Program," Engineering Experiment Station Report 38, Solar Energy Laboratory, University of Wisconsin, Madison, Wisconsin.